EUROPEAN ORGANIZATION FOR NUCLEAR RESEARCH
ORGANISATION EUROPEENNE POUR LA RECHERCHE NUCLEAIRE

CERN - PS DIVISION

PS/ DI/ Note 98-16

NEUTRALIZATION OF THE ELECTRON-BEAM SPACE CHARGE

Report of the CERN-PS/JINR/ITEP 1994-95 Collaboration

Edited by
I. Meskov, D. Möhl, E. Syresin, G. Tranquille

This report presents the results of the experimental and theoretical studies, performed in 1994 - 1995 by the collaboration of the CERN, JINR and ITEP groups, aimed at studying the problems of generation of an intense electron beam, whose space charge is neutralized with residual gas ions. The studies concerned the development of the electron cooling method. The experimental studies on the neutralization were carried out on the LEAR electron cooling device (ECOOL) and Test Bench of CAPT INP/JINR.

Geneva, Switzerland
23 September 1998

Participants of the Collaboration

J.Bosser[1](convenor), M.Chanel[1], Yu.V.Korotaev[2], A.Yu.Lavrentjev[2], R.Ley[1], S.Maury[1], R.Maccaferri[1], I.N.Meshkov[2](convenor), D.Möhl[1], G.Molinari[1], E.R.Mustafin[3], V.N.Polyakov[2], A.V.Smirnov[2], E.M.Syresin[2], F.Varenne[1], G.Tranquille[1], P.R.Zenkevich[3].

[1]CERN, [2]JINR, [3]ITEP

Preface

This report presents the results of the experimental and theoretical studies, performed in 1994 - 1995 by the collaboration of the CERN, JINR and ITEP groups, aimed at studying the problems of generation of an intense electron beam, whose space charge is neutralized with residual gas ions. The studies concerned the development of the electron cooling method.
The experimental studies on the neutralization were carried out on the LEAR electron cooling device (ECOOL) and Test Bench of CAPT INP/JINR.

1. GENERAL DESCRIPTION

1.1. Space-charge effects of an electron beam

The electromagnetic field of a cooling electron beam influences the value of electron velocities and their variation across the electron beam. So, in an electron beam with uniform density and beam intensity I_e the potential is given by the formula

$$U_e(r) = -\frac{I_e}{4\pi\varepsilon_0 v_e}\begin{cases} 1-\dfrac{r^2}{a^2}+2\ln\dfrac{b}{a} & 0<r<a, \\ 2\ln\dfrac{b}{r} & 0<r<b. \end{cases} \qquad (1.1)$$

Here v_e is the average electron velocity, r the radial coordinate, a, b the beam and vacuum chamber radii.

If the electron beam is accelerated by a cathode potential U_0, the kinetic energy ε_e of an electron at radius r will be

$$\varepsilon_e(r) = (\gamma - 1)mc^2 = -e(U_0 - U_e(r)),$$
$$\gamma = (1-\beta^2)^{-1/2}, \beta = v_e/c, \qquad (1.2)$$

showing that electrons at different radius will have different velocities. In the ***particle rest frame*** it gives the corresponding values of electron longitudinal velocities:

$$\Delta v = v_e(r) - v_e(0), \quad \Delta v(r) = v_e\frac{\Delta p_1}{p_e} \approx \frac{e(U_e(r)-U_e(0))}{\gamma m v_e^2}. \qquad (1.3)$$

This electron velocity variation across the beam produces the main effect reducing the electron cooling efficiency.

The second effect is related to the electron drift in crossed fields - the proper electric and magnetic fields of the electron beam

$$E_r(r) = \frac{I_e}{2\pi\varepsilon_0 v_e}\cdot\frac{r}{a^2}, \qquad (1.4)$$

$$B_\varphi(r) = v_e E_r(r) \qquad (1.5)$$

and the external longitudinal field of the electron cooling system . The drift velocity is given by:

$$v_d = \frac{I_e}{2\pi\varepsilon_0 v_e\ \gamma^2 B}\cdot\frac{r}{a^2}, \qquad (1.6)$$

Table 1.1 gives a numerical example for LEAR.

Table 1.1 Characteristics of the electron beam electric field

Electron energy, keV	30	2.5
Velocity factor β	0.328	0.1
Beam current, A	3	0.5
Magnetic field, T	0.06	0.06
Potential difference between beam boundary and axis, V	274	136
Relative longitudinal velocity difference $(\Delta v(a) - \Delta v(0))/\beta c$	$4.5 \cdot 10^{-3}$	$2.7 \cdot 10^{-2}$
Radial electric field on the beam boundary, kV/m	21.9	12
The ratio of the drift velocity to the average longitudinal one $v_d(a) / v_e 10^{-3}$	3.9	5.3

Because of the space charge effect the intense electron beam shows a large variation of the longitudinal and drift velocity in the transverse plane. Both can be significantly reduced if the neutralization of electron beam space charge by residual gas ions is applied. As a result, one can expect the generation of an intense electron beam with small electron velocity (energy) variation.

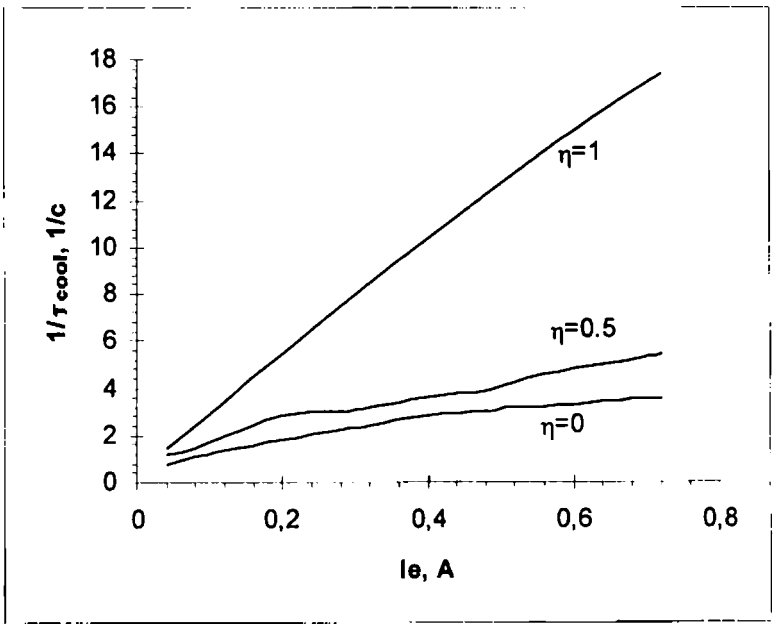

Fig. 1.1 Simulated dependence of inversed cooling time on electron current: Lead 54^+, E_p = 4.2 MeV/u, neutralization factor η = 1, 0.5, 0.

The space charge of the electron beam in an electron cooling device has an influence on the efficiency of the cooling process [1]. Actually this effect can completely annihilate the gain resulting from an increase of the electron beam

current. The computer simulations of electron cooling of the lead-ion beam in LEAR [2,3] show that in this case the increase of the electron current from 0.2 A up to 0.6 A leads to a decrease in the cooling time (Fig.1.1) by less than a factors of 2, when the space charge is not neutralized (see below). Neutralization of space charge makes electron cooling significantly faster in computer simulations [3] (Fig. 1.1).

1.2. Principle of neutralization

The neutralization of the space charge of the electron beam by storing ions, generated in collisions of the beam electrons with residual gas molecules and atoms, seems to be the most straight forward method [4,1].

For the purpose of neutralization, so-called "Parkhomchuk traps" [4] are used: two neutralization electrodes, consisting of two metallic half-cylinders separated by high-resistive-glass insulator (Fig.1.2), are installed at the gun output and the collector entrance. They are polarized by independent power supplies named U_{el1} and U_{el2} ($0 \le U_{el} \le 6$ kV). Usually, the voltages on opposite electrodes are not equal so that a transverse E - field also exists.

The energetic primary electrons will ionize the residual gas molecules. The ionized, low-energy ions and electrons will be submitted to the space charge and to the longitudinal magnetic field forces. They will move towards the cathode or the collector. At the level of the neutralization electrodes the ions will be reflected, and therefore stored, whilst the low-energy electrons which drift in the crossed electric and magnetic fields will be collected on the glass insulators. Consequently, the ion density n_i will increase with time.

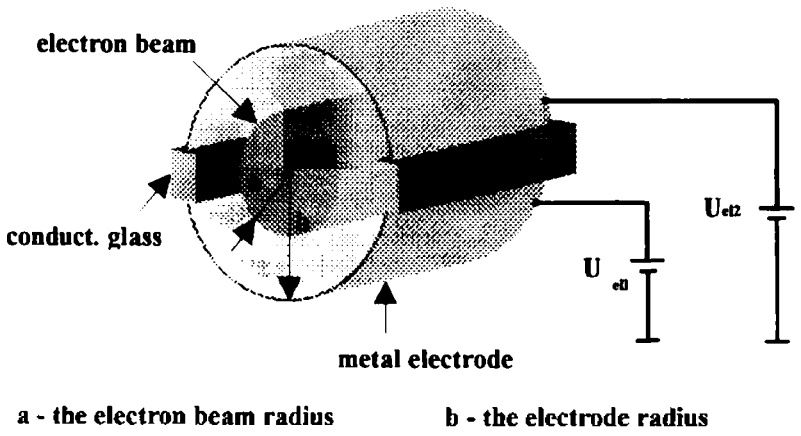

Fig. 1.2. Schematics of the neutralization electrodes

It should be mentioned that a variation of drift chamber radius (from b_1 to b_2 value, $b_1 > b_2$) will induce a "natural neutralization" due to a potential well, produced by the electron beam space charge (Eq. 1.1):

$$U_e^{(1)}(r) - U_e^{(2)}(r) = -\frac{I_e}{2\pi\varepsilon_0 v_e} \cdot \ln\frac{b_1}{b_2} \tag{1.7}$$

One can introduce the neutralization factor as

$$\eta = \frac{Z_i n_i}{n_b}\ , \tag{1.8}$$

Z_i being the ion charge number. Then in formulae (1.1) and (1.4) one has to substitute instead of the beam current I_e the parameter

$$I_e \to (1-\eta)\cdot I_e \tag{1.9}$$

However, the beam magnetic field does not change with neutralization, and because of this the electron drift velocity (1.6) in the neutralized electron beam (***NEB***) is still perceptible:

$$v_d = \frac{I_e}{2\pi\varepsilon_0\beta c\gamma^2 B}\cdot\frac{r}{a^2}(1-\eta\gamma^2) \tag{1.10}$$

In a similar manner, formulae (1.7) and (1.8) give for the natural neutralization:

$$\eta_{natural} = \frac{\Delta U}{U_e(0)} = \frac{\ln b_1/b_2}{1+2\ln b_2/a}, \qquad b_1 > b_2 \tag{1.11}$$

The value of the electrode potential is determined by followings requirements:

1. Ion reflection and storage;
2. effective secondary (ionization) electron removal;
3. small disturbance of primary electrons.

The potential distribution in the middle plane of the neutralization electrodes as a function of azimuthal ψ and radial r coordinates is given by the following formula (Fig. 1.3):

$$\varphi(r,\psi) \approx \frac{U_{el2}-U_{el1}}{2}\left(1-\frac{2}{\pi}arctg\frac{b_{tr}r\cos\psi}{b_{tr}^2-r^2}\right)+U_{el1}-U_e(r)\ , \tag{1.12}$$

where U_{el1r}, U_{el2} are the electrode potentials of the trap, b_{tr} the trap electrode radius, $U_e(r)$ the radial potential distribution inside the trap due to the beam space charge [(Eq. (1.1)].

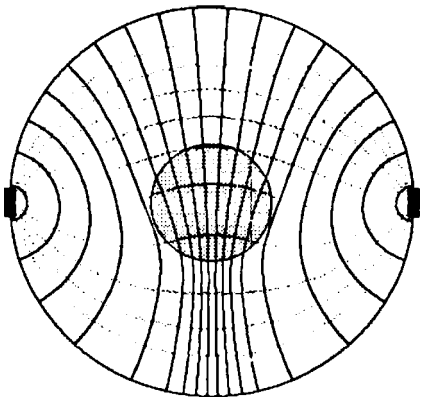

Fig. 1.3. Results of simulation of the potential distribution and the transverse electric field in the middle plane of the trap with an electron beam.

$\varepsilon_e = 2.5$ keV, $I_e = 0.3$A, $U_{el1} = 5$ kV, $U_{el2} = 0$.

The radial and azimuthal electric field between trap electrodes is equal to

$$E_r \cong \frac{U_{el2} - U_{el1}}{\pi b} \frac{\left(b_{tr}^2 + r^2\right) b_{tr}^2 \cos\psi}{\left(b_{tr}^2 - r^2\right)^2 + \left(b_{tr} r \cos\psi\right)^2} + E_e(r),$$

$$E_\psi \cong -\frac{U_{el2} - U_{el1}}{\pi b} \frac{\left(b_{tr}^2 - r^2\right) b_{tr}^2 \sin\psi}{\left(b_{tr}^2 - r^2\right)^2 + \left(b_{tr} r \cos\psi\right)^2}, \qquad (1.13)$$

$$E_e(r) \cong \frac{I_e}{2\pi\varepsilon_0 v_e} \begin{cases} \dfrac{r}{a^2} & 0 < r < a \\ \dfrac{1}{r} & 0 < r < b_{tr} \end{cases}$$

At certain conditions, the electric fields of the beam and the electrodes form closed shells in the space inside of the trap, where secondary electrons can be stored. The increase of the electrode potential difference allows this problem to be arrived.

1.3. Ion accumulation. Neutralization dynamics

The kinematics of the ion accumulation is defined by processes, which can be divided into four main groups:

1. inelastic collisions,
2. elastic processes,
3. heating processes,
4. ion losses.

Inelastic processes include: electron impact ionization, charge exchange, electron recombination. Estimates show that for our set of parameters the most important process is the electron impact ionization. Elastic processes include: intrabeam scattering, collisions with reflecting fields of the neutralization electrodes. The rate of elastic scattering of different ion components is defined as the ion-ion collision frequency. Owing to ion-ion collisions the temperature

of the different ion components is equalized, and the system is characterised by one mean energy, which is common for all ion components. Intrabeam Scattering (IBS) does not change the over all energy of the ions, but this process can result in a cooling of the highly charged ions and in a heating of the lowly charged ions.

Collisions of the ions with reflecting fields of the neutralization electrodes do not change the over all energy of the ions; however, they lead to "equipartitioning" of energy between the transverse and longitudinal degrees of freedom.

Heating processes include: ion heating due to Coulomb scattering of the primary electrons on the ions; ion heating due to "external devices"; the ion density increases with time due to the ionization by primary electrons of residual gas atoms, and the balance equation is:

$$\frac{dn_i}{dt} = n_e N \sigma_i \beta c - \frac{n_i}{\tau_{es}} = \frac{n_e}{\tau_{neutr}} - \frac{n_i}{\tau_{es}} \qquad (1.14)$$

where n_e is the density of primary electrons, N the density of residual gas atoms, σ_i the ionization cross-section, n_i the ion density, and τ_{es} the ion escape time. The neutralization time τ_{neutr} corresponds to the time needed to reach a stored ion charge density which is equal to the electron beam charge density, when τ_{es} is infinitely large. Then it follows from Eq. (1.14):

$$\tau_{neutr} = \frac{1}{Z_i \sigma_i v_e N}, \qquad (1.15)$$

where Z_i is the average ion charge state. The normalized ionization cross section is typically $\sigma_i \beta \approx 3 \cdot 10^{-18} cm^{-2}$. The neutralization time changes slightly with electron energy and is inversely proportional to vacuum pressure. At stationary conditions and a high neutralization level, when $\eta \approx 1$, the neutralization time is equal to the ion escape time

$$\tau_{neutr} = \tau_{es}. \qquad (1.16)$$

Let us consider the neutralization process. Just after the electron beam is turned on, its space charge potential $U_e(r)$ is negative. Because of ion storage the potential difference $U_e(a) - U_e(0)$ reduces until it reaches the value U_{st}. During this time ions are heated up to some temperature T_{st}. In the stationary state the potential well does not prevent an ion escape from the beam, if the ion temperature

$$T_{st} \geq -Z_i e U_{st}, \qquad (1.17)$$

when $U_{st} < 0$. Such a situation is typical for high vacuum (P < 0.1 nTorr).

At low vacuum (P > 10 μTorr) the state with positively charged beam can take place, when intensive ionization generates such an intense ion density, that the ion flux escaping the beam is limited by its own space charge (as in the Child-Langmuir diode). The beam potential is defined in this case by the value which is necessary to "push out" the ion flux. This regime is not typical for electron cooling devices operating at ultrahigh vacuum (P ~ 0.1 nTorr – 1 pTorr).

The ion temperature in the stationary state defines the beam neutralization level. It follows from Eqs. (1.16), (1.1), (1.8), (1.9):

$$1-\eta \approx \frac{U_{st}}{U_e(0)} \sim -\frac{T_i}{Z_i e U_e(0)}. \qquad (1.18)$$

It is useful to remember that the real distribution of the ion density may be far from uniform, and therefore this expression has only qualitative character.

The straight heating of ions in collision with the beam electrons is described by the well-known formula

$$\frac{dT_i}{dt} = 4\pi \frac{Z^2 e^4}{M v_e} n_e L = 4\pi \frac{Z^2}{A} n_e \frac{L}{v_e} r_p^2 m_p c^4 \quad , \qquad (1.19)$$

where Z, A are the atomic charge and mass numbers of the ion, M its mass, m_e, m_p the electron and proton masses, n_e the electron density in the beam, $L \sim 10$ the Coulomb logarithm, r_p the proton classical radius. This heating is very slow, as can be demonstrated with the numerical application:

$$\left.\begin{array}{l} A = 14 \\ Z = 7 \\ n_e = 1 \cdot 10^{14}\, m^{-3} \\ \beta = 0.1 \end{array}\right| \frac{dT_i}{dt} \approx 0.3 eV/s$$

In experiments described below the ion temperature reached a much higher magnitude. This phenomenon relates also to the main problem of the neutralization method - stability of the **Neutralized Electron Beam** (**NEB**). The problem is that an electron beam, neutralised with stored ions, behaves as a two-component plasma system with all its characteristic instabilities [1, 4, 5, 6, 7].

1.4. Transverse electron-ion oscillations in a NEB

When an electron beam is (partially) neutralized with ions, as described above, the transverse oscillations of the particles can occur just like in any plasma system. Both components, ions and electrons, can oscillate as a whole, one around the other, like two charged "columns". Actually, any displacements of electrons ξ_e or ions ξ_i lead to the electron drift in the electric field of the ion column (Fig. 1.4) and longitudinal magnetic field B, with the drift velocity

$$V_d = \frac{d\vec{\xi}_e}{dt} = \frac{\vec{E}_i}{B}, \quad \vec{E}_i = \frac{Z_i e n_i}{2\varepsilon_0}\left(\vec{\xi}_e - \vec{\xi}_i\right), \quad Z_i n_i = \eta n_e \quad . \qquad (1.20)$$

In its turn the ion column moves (oscillates) in the electric field of the electron beam:

$$\vec{E}_e = -\frac{e n_e\left(\vec{\xi}_i - \vec{\xi}_e\right)}{2\varepsilon_0} \quad . \qquad (1.21)$$

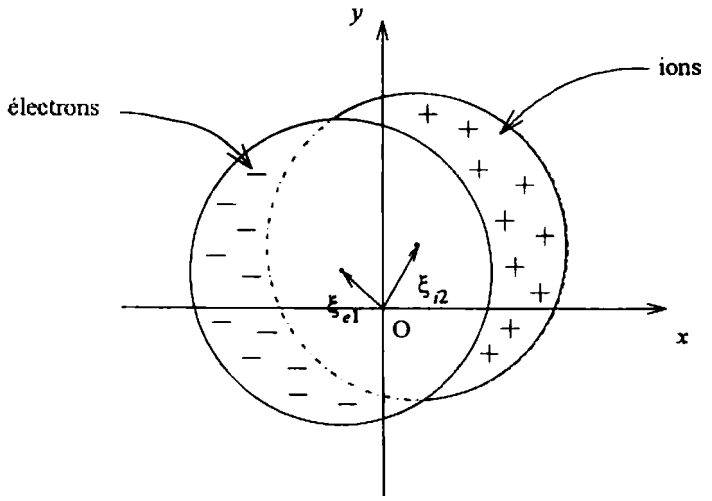

Fig.1.4. Schematics of electron-ion oscillations

The equation of the motion of the ion column can be written as follows

$$M\frac{d\vec{V}_i}{dt} = Z_i e\vec{E}_e + Z_i e\left[\vec{V}_i \times \vec{B}\right] - \nu\vec{V}_i \quad , \tag{1.22}$$

where ν is some "friction" coefficient, representing the presence of a damping mechanism - Landau damping, due to nonlinearity of the ion incoherent oscillations. It is necessary to underline that such a model has an internal contradiction: an ion beam with nonlinear spread of the ion frequencies does not oscillate as a column and therefore this model should be considered as a phenomenological one. Introducing the complex variables

$$\xi_{e,i} = \xi_x + i\xi_y \quad , \tag{1.23}$$

one can rewrite this equation in the form

$$\begin{aligned} &\frac{d^2\xi_i}{dt^2} + (i\omega_B + 2\gamma_L)\frac{d\xi_i}{dt} + \omega_i^2(\xi_i - \xi_e) = 0, \\ &\frac{d\xi_e}{dt} = \eta\omega_d(\xi_e - \xi_i), \quad \omega_B = \frac{Z_i eB}{M}, \quad \gamma_L = \frac{\nu}{2M}, \quad \omega_i^2 = \frac{Z_i e^2 n_e}{2\varepsilon_0 M}, \end{aligned} \tag{1.24}$$

where ω_B is the Larmor ion frequency, $\omega_d = \dfrac{Z_i e n_e}{2\varepsilon_0 B}$ the ion drift frequency in the electrical field of the electron beam and the external longitudinal magnetic field, γ_L is the damping coefficient. The system of equations (1.24) is to be solved with an initial condition for the ion position $\xi_i(z)|_{t=0}$ and a boundary condition for the electron beam position $\xi_e(t)|_{z=0}$. We shall look for the solution for harmonic dependence of the entrance displacement on time

$$\xi_e(0,t) = \xi_0 e^{-i\omega t} \tag{1.25}$$

in the form of travelling waves:

$$\xi_{e,i}(z,t) = A_{e,i}e^{i(kz-\omega t)} \tag{1.26}$$

We give here a simplified description assuming the electrons to be monoenergetic, with the velocity v_e, and the ion longitudinal velocity equal to zero. Substituting the functions (1.26) into the equations (1.24), one should take into account, that for electrons

$$\frac{d}{dt} = \frac{\partial}{\partial z} + v_e \frac{\partial}{\partial t} \quad . \tag{1.27}$$

Then finding the determinant of two algebraic uniform equations, we obtain the dispersion equation for the function $k(\omega)$:

$$kv_e = \omega + \eta \frac{\omega_d}{\varepsilon_\perp(\omega)} \quad , \tag{1.28}$$

$$\varepsilon_\perp = 1 - \frac{\omega_i^2}{\omega(\omega - \omega_B + i\gamma_L)} \quad . \tag{1.29}$$

Knowing for the function $k(\omega)$ we can write the solution for the electron beam coherent oscillations:

$$\xi_e(z,t) = \xi_0 e^{i(kz-\omega t)} \quad . \tag{1.30}$$

The dissipation parameter γ_L leads to complex magnitudes of the parameters $\varepsilon_\perp$ and $k(\omega)$:

$$\varepsilon_\perp = \varepsilon_\perp' + i\varepsilon_\perp'', \quad k = k' + ik'' \quad . \tag{1.31}$$

It gives an amplification of the function $\xi_e(z,t)$ with the coordinate z:

$$\xi_e(z,t) = \xi_0 e^{k''z} e^{i(k'z-\omega t)} \quad . \tag{1.32}$$

Substituting formulae (1.31) into the equations (1.28), (1.29), we find

$$\begin{aligned} k' &= \frac{\omega}{v_e} + \eta \frac{\omega_d}{v_e \varepsilon'(\omega)}, \quad k'' = \frac{\omega_d \eta \varepsilon_\perp''}{v_e(\varepsilon_\perp'^2 + \varepsilon_\perp''^2)}, \\ \varepsilon_\perp' &= 1 - \frac{\omega_i^2}{\omega(\omega - \omega_B)}, \quad \varepsilon_\perp'' = \frac{\omega_i^2 \gamma_L}{\omega(\omega - \omega_B)^2} \quad . \end{aligned} \tag{1.33}$$

The increment of the instability growth k'' has a maximum, when $\varepsilon' = 0$, or

$$\omega_{1,2,3,4} = \pm\frac{\omega_B}{2} \pm \sqrt{\frac{\omega_B^2}{4} + \omega_i^2} \quad .$$

This frequency corresponds to coherent oscillations of the ion column in the electric field of a strongly magnetized electron beam. The coherent frequency does not depend on the neutralization factor. For these frequencies the ion coherent oscillations are damped with the damping coefficient γ_L. We see that $Im\ k < 0$, if the coherent frequency has a positive value.

$$\omega_1 = \sqrt{\frac{\omega_B^2}{4} + \omega_i^2} - \frac{\omega_B}{2} \quad . \tag{1.34}$$

It means, that wave propagating in the z-direction is amplified.

The maximal value of the increments at the **coherent frequency ω_1** is equal to

$$k''(\omega_1) = \eta \frac{\omega_d \omega_i^2}{v_e \gamma \omega_1} . \tag{1.35}$$

The module of the wave amplification coefficient is

$$K_0 = e^{k''L} \quad , \tag{1.36}$$

where L is the NEB length.

The transverse waves have a circular polarisation, whose direction of rotation either coincides with that of the electron beam or is just opposite to it. The amplification is maximal in the first case.

An instability development depends essentially on a feedback in the system. Let us introduce the module of the feedback coefficient, which is the module of the ratio of the oscillating electric field induced at the system entrance to the field at the exit which induces the entrance field:

$$\chi = \left| \frac{E_e^{\max}(z=0)}{E_e^{\max}(z=L)} \right| \quad . \tag{1.37}$$

The condition of the oscillation stability leads to the requirement:

$$\chi K_{max} < 1 \quad , \tag{1.38}$$

which gives a limitation of the amplification coefficient. For the following threshold estimations one can admit

$$\chi K_{max} = 1$$

and, as a consequence, the threshold current density of this so-called ***beam-drift instability*** [see formulae (1.36) and (1.35)] is:

$$j_{th} = \frac{2\varepsilon_0}{k} \frac{\nu_e^{\,2} B}{L}, \qquad k = \eta (\varepsilon_\perp'' \ln K_{\max})^{-1} \quad . \tag{1.39}$$

The feedback can be provided by fast electrons, escaping the collector or reflected from it [7-9], by longitudinal motion of ions, and by longitudinal waves. The question of the - magnitude χ is rather uncertain.

The parameter $\varepsilon'_\perp$ is connected with the oscillation spectrum width through the amplification coefficient. This can be found, by using formulae (1.33) and representing $\varepsilon'_\perp$ near resonance in the form

$$\varepsilon'_\perp \cong \frac{2\Delta\omega}{\omega_{Res}} . \tag{1.40}$$

Then, substituting it for k'' in (1.35), we find the dependence

$$k''(\Delta\omega) = \frac{\eta \omega_d \varepsilon'_\perp}{\left(\frac{2\Delta\omega}{\omega_{Res}}\right)^2 + (\varepsilon'_\perp)^2} \frac{1}{\nu_e} \quad . \tag{1.41}$$

The amplification coefficient $K_0(\omega_1 \pm \Delta\omega)$ [see Formula (1.36)] decreases by half from the resonant value $K_0(\omega_1)$ to the value at a distance $\Delta\omega$ from the resonance, given by

$$\frac{2\Delta\omega}{\omega} = \frac{\varepsilon''_\perp}{\sqrt{\frac{\ln(K_{Res}/2)}{\ln 2}}} \quad . \tag{1.42}$$

When the beam is partially neutralized, the ions oscillate in transverse directions under the influence of the beam electric field and the longitudinal magnetic field of the cooling system. The ***frequency*** of these ***incoherent oscillations*** is equal (see Appendix 1, Formula A 1.4) to

$$\omega_{1,2} = \sqrt{\omega_i^2 (1-\eta) + \frac{\omega_\beta^2}{4}} \pm \frac{\omega_\beta}{2} \quad . \tag{1.43}$$

A crucial point of the theory is an estimation of ε_1'' (imaginary part of dielectric permeability of the plasma). In Ref.[5] the following expression is derived:

$$\varepsilon_1'' = \frac{4}{\sqrt{\pi}} \frac{r_D}{a} = \sqrt{\frac{4T_i}{\pi Z_i e \Delta U_e}} \tag{1.44}$$

Here r_D is the beam Debye radius, T_i is the ion transverse temperature, ΔU_e is a potential difference between the centre and the boundary of the unneutralised electron beam. This formula is valid only, if

$$r_D << \rho_L << a \quad , \tag{1.45}$$

where ρ_L is the Larmor radius of the ion.

For the derivation the authors assumed that Landau damping (LD) is connected with a strong nonlinearity of the ion incoherent oscillations. Let us devide all the ions into two groups: "core" ions moving inside the electron beam and "tail" particles, whose amplitude of radial oscillations is larger than the electron beam radius. If "tail" particles are absent, the LD coefficient is zero. This is connected with the following fundamental theorem; in a linear external field the internal field (in our case, the ion field) does not influence the oscillations of the beams centre of gravity.

Thus for a uniform electron beam the theoretical derivation, performed in Ref. [5], is wrong. However, these results were confirmed by the experiment, and we can consider this expression as a phenomenological one.

Let us mention that there is another possible reason for the LD: the longitudinal velocity spread of the ions which appears due to intra beam scattering (IBS) and "collision" with an inclined field of the traps. In Ref. [6] the following simple model is considered: both beams (electron and ion) have uniform density and equal sizes, and the LD appears due to longitudinal velocity spread (LVS). The LVS model is self-consistent and has no internal contradictions. However, estimations have shown an increment for the LVS model which is too large compared with experiments.

In conclusion let us note that amplification of the travelling wave and the presence of feedback result in amplification of the transverse Schottky noise of the ion beam. A rate of heating from this effect can be written as :

$$\frac{dT_i}{dt} \approx T_i \frac{\omega_i}{N_e} \frac{\omega_d L}{v_e} (K_f)^2 , \tag{1.46}$$

here N_e is the total number of electrons in the primary electron beam, and a module of the amplification factor K_f takes into account an influence of the feedback:

$$K_f \approx \frac{K_0}{1 - \chi K_0} \quad , \tag{1.47}$$

χ is the module of the feedback coefficient.

1.5 Stationary state

The simulations of the parameters of neutralised electron beams in the electron cooling device are given in Refs.[5,10]. For the stationary state a self-consistent transverse potential of the ions U in the central region of the ion column (i.e. for from the neutralising electrodes) is determined by the Poisson equation:

$$\frac{1}{r}\frac{d}{dr}\left(r\frac{dU_i}{dr}\right) = -\sum_i \rho_i(r) Z_i e / \varepsilon_0, \tag{1.48}$$

$$\rho_i(r) = \int d^3 v_i F_{ik}(v_i, r).$$

Here v_i is the ion velocity, $F_i(v_i, r)$ is the ion distribution function in a phase space, Z_i is the ion charge number.

Let us introduce the following simplifying assumptions:

1. there is only one ion species;
2. the effects of the longitudinal magnetic field are negligible;
3. $F(v_i, r)$ is the Maxwell-Boltzmann distribution function (MBD), i.e.

$$F(v_i, r) = F_0 \exp(-H / H_0). \tag{1.49}$$

Here F_0 is the some normalizing constant, and H_0 is the ion energy

$$H = \frac{m\vec{v}_i^{\,2}}{2} + eZ_i U(r), \tag{1.50}$$

$$U(r) = U_i(r) + U_e(r). \tag{1.51}$$

In Eq. (1.51) $U_e(r)$ is the potential of the electron beam [see Eq. (1.1)].

Let us discuss the last assumption in more detail. We know that a stationary distribution function should depend on the integrals of motion. For a beam with a radial symmetry we have two integrals of motion: H and $P_\varphi = mr^2\dot{\varphi}$ (the azimuthal momentum). However, in our case there are two processes which destroy conservation of the last integral: 1) interaction with the inclined field of the neutralising electrodes; 2) intrabeam scattering (IBS). Both processes result in uniform distribution of the ion kinetic energy on all degrees of freedom, i.e. to the "ergodization". The estimations show that for the high vacuum case

$$\tau_{erg} << \tau_{es}. \tag{1.52}$$

Here τ_{erg} is the ergodization time, τ_{es} is the ion escape time. Besides the ergodization, IBS results in "Maxwellization" of the beam, i.e. appearance of the exponential tail. It is known that for infinite maximal energy the beam distribution becomes MBD. However, in our case there is a border due to the final radius of the vacuum chamber. It is clear that MBD may be considered as a reasonable model only if

$$\frac{H_m}{H_0} >> 1. \tag{1.53}$$

Here $H_m = eZ_i U(b)$, b is the radius of the chamber wall.

Substituting Eqs. (1.49) - (1.51) into (1.48) we obtain:

$$\frac{1}{r}\frac{d}{dr}\left(r\frac{dU_i}{dr}\right) = -\frac{Z_i e n_i^0}{\varepsilon_0} exp\left[-\frac{Z_i e(U_i + U_e)}{H_0}\right], \qquad (1.54)$$

here n_i^0 is the ion density at the beam centre. Let us introduce new dimensionless variables:

$$\tilde{Z} = eZ_i\frac{U_i + U_e}{H_0}, \qquad \tau = \kappa r, \qquad \kappa^2 = \frac{Z_i^2 e^2 n_e}{H_0 \varepsilon_0} = \frac{1}{r_D^2}. \qquad (1.55)$$

Here r_D is the beam Debye radius. In these variables Eq.(1.54) may be rewritten as

$$\frac{1}{\tau}\frac{d}{d\tau}\left(\tau\frac{d\tilde{Z}}{d\tau}\right) = -\eta_0 \exp(-\tilde{Z}) + \begin{cases} 1 \text{ for } \tau \le \kappa a \\ 0 \text{ for } \tau \ge \kappa a \end{cases} \qquad (1.56)$$

Here $\eta_0 = Z_i n_i / n_e \ (\eta_0 < 1)$ is a local neutralization factor at the beam centre (r = 0).

We have solved Eq. (1.56) for the following initial conditions:

$$\tilde{Z}(0) = 0; \qquad \tilde{Z}'(0) = 0. \qquad (1.57)$$

The numerical solution of Eq. (1.56) with initial conditions (1.57) depends on the following parameters:

1. $\kappa a = a / r_D$,
2. η_0,
3. $\tau_{max} = \kappa a \frac{b}{a}$.

We can express through these three parameters all the parameters of interest:

1. the effective neutralization factor $\eta_{eff} = \tilde{Z}N_i / N_e$, N_e is the linear density of the electrons, N_i is the linear density of the ions inside the electron beam:

$$\eta_{eff} = \frac{2\eta_0}{(\kappa a)^2}\int_0^{\kappa a} \exp[-\tilde{Z}(\tau)]\tau d\tau, \qquad (1.58)$$

2. the neutralization factor $\eta = Z_i N_i^{ch} / N_e$, N_i^{ch} is the linear density of the ions inside the vacuum chamber:

$$\eta = \frac{2\eta_0}{(\kappa a)^2}\int_0^{\tau_{max}} \exp[-\tilde{Z}(\tau)]\tau d\tau, \qquad (1.59)$$

3. the normalized (normalization means division by $eZ_i U_e(a)$, i.e. potential energy of the ion in the field of the electron beam at $r = a$) maximal energy of the ion:

$$\tilde{H}_{max} = \frac{4}{(ka)^2}\tilde{Z}(\tau_{max}), \qquad (1.60)$$

4. the normalized transverse temperature of the ions:

$$\tilde{H}_0 = \tilde{T}_\perp = \frac{4}{(\kappa a)^2}, \qquad (1.61)$$

5. the normalized mean potential energy of the electrons (for electrons normalization corresponds to division by $eU_e(a)$ without Z) or of the newly born ions:

$$\tilde{V}_e = \frac{8}{(\kappa a)^4}\int_0^{\kappa a}\tilde{Z}(\tau)\tau d\tau . \qquad (1.62)$$

The number of free parameters may be reduced by use of the conservation law for a number of particles. Taking into account that diffusion losses of the ions are forced by IBS, we obtain the following estimation:

$$\tilde{Z}(\tau_{max}) = \frac{H_{max}}{T_\perp} \approx \ln(\nu_{ii}\tau_i) . \qquad (1.63)$$

Dependence of these parameters on κa for $\tilde{Z}_{max} = 5$ is represented in Fig. 1.4.

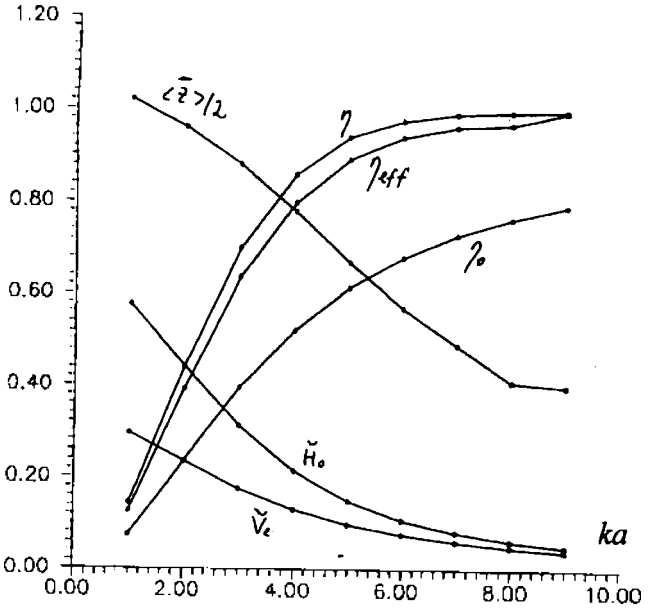

Fig.1.4 The integral neutralization factor η, local neutralization factor in the centre η_0, effective neutralization factor η_{eff}, normalised maximum energy, normalised electron and ion potential energy dependence on the factor *ka* for $b/a = 3$.

The intrabeam scattering diminishes the number of ions in the core (inside the electron beam) and especially in the tail of the ion beam.

However, one can not find parameters of the beam stationary state from these pictures if the ion temperature $\tilde{T}_\perp = 4/(\kappa a)^2$ is unknown. In order to find $\tilde{T}_\perp$ one may apply the conservation law for the energy of the ions. Let us write it in the following form:

$$H_{max} = eZ_i V_0 + \Delta H_{inc} + T_\perp \Lambda K_f^2 . \qquad (1.64)$$

Here $eZ_i V_0$ is the energy at which the ion is born due to the ionization process, ΔH_{inc} is an increase of the ion energy during its lifetime due to incoherent heating and it may be estimated from the mean rate of the incoherent heating $< \frac{dH_{inc}}{dt} >$ [Eq. (1.19)] as

$$\Delta H_{inc} = \tau_{es} < \frac{dH_{inc}}{dt} > . \qquad (1.65)$$

And the last term in Eq. (1.64) describes the coherent heating due to the ion Schottky noise which excites in the system the dipole ion-electron travelling

wave (in the absence of absolute instability). Parameters Λ and K_f [see. Eq. (1.47)] are defined by following formulae:

$$\Lambda = \frac{\omega_1 \tau_i}{N_e L}\lambda, \qquad \lambda = \frac{\omega_d L}{v_e}, \tag{1.66}$$

$$K_f = \frac{K_0}{1 - K_0 \chi}.$$

Dividing all the terms in (1.64) by $eZ_i U_e(a)$, neglecting $\tilde{V}_0$ in comparison to $\tilde{H}_m$ and using (1.63) we obtain

$$\tilde{T}_\perp [\tilde{Z}(\tau_{max}) - \Lambda K_f^2] = \Delta\tilde{H}_{inc} \tag{1.67}$$

In order to solve (1.67) we have to know the dependence of K_f on $\tilde{T}_\perp$. Let us apply a simple model, which was checked experimentally in the MOSOL device (the question of the validity of this model for LEAR is open). Guided by the results from MOSOL we assume:

$$K_0 = exp[\eta\lambda\sqrt{\pi/(2\tilde{T}_\perp)}]. \tag{1.68}$$

The system of equations (1.66), (1.67) may then be solved for two extreme cases:

- <u>No coherent heating</u>: $\tilde{T}_\perp = \Delta\tilde{H}_{inc} / \tilde{Z}(\tau_{max})$. If we consider that the only source of incoherent heating is the Coulomb interaction of the ions with the electron beam, then $\Delta\tilde{H}_{inc}$ may be estimated as [Eq. (1.19)]

  $\Delta\tilde{H}_{inc} \approx 8.34 * 10^{-3}(Z_i^2 n_e \tau_i / A_i \beta)[eV]$. Here n_e should be expressed in units of $10^8\,cm^{-3}$ and A_i is the mass number of the ion.
- <u>No incoherent heating</u>: In this case the amplification factor of the travelling wave is $K_0 = 1/[\chi + \sqrt{\Lambda / \tilde{Z}(\tau_{max})}]$. Substitution in Eq. (1.68) gives us the necessary dependence $\tilde{T}_\perp / \eta(\tilde{T}_\perp) = (\pi/2)[\lambda / ln(K_0)]^2$.

Let us underline that the correct value of $\tilde{T}_\perp$ can be found with good accuracy from the condition:

$$\tilde{T}_\perp = \max[(\tilde{T}_\perp)_{inc}; (\tilde{T}_\perp)_{coh}]. \tag{1.69}$$

Here coherent and incoherent temperatures within parentheses are roots of equations corresponding to two extreme cases considered above. A set of parameters for typical experiments in LEAR are given in Table 1.2 (for $\tilde{Z}(\tau_{max}) = 5$). We see from Table 1.2, that values of $\varepsilon_\perp^{"}$ do not contradict the estimations of this value, obtained from results of the measurements (see Table 5.1); however, $\tilde{T}_\perp$ is, perhaps, underestimated. The values of κa from the table correspond to a very high neutralization degree ($\eta \cong 1$), which does not fit the experimental data at LEAR ($\eta \cong 0.7$ - 0.9). And we may conclude that the simple model [5] is not valid for LEAR electron cooling device conditions. Nevertheless we may assume that the dependence of K_0 on the beam parameters is the same as in Eq. (1.68), but in order to fit the experimental data for LEAR we have to multiply the argument of the exponent by a factor 4. To get the more reasonable phenomenological model for LEAR we need more detailed measurements of the beam parameters (the ion density, composition of ion species and so on).

Table 1.2 Theoretical estimations of the parameters of the stationary neutralised beams at LEAR

The ratio of the electron velocity to the light velocity, β	0.103	
Neutralisation time, [s]	3	
Beam radius, [cm]	2.5	
Vacuum chamber radius, [cm]	7.5	
Atomic mass number of the ion, A	14	
Charge number of the ion, Z_i	3	
Length of neutralized electron beam, [m]	3.2	
Beam current, I_e, [A]	0.13	
Potential difference between beam boundary and axis, [V]	83	
Longitudinal magnetic field, [G]	600	
Parameter λ	0.21	
Electron beam density, $[cm^{-3}]$	$1.34*10^6$	
Feedback coefficient, χ	0.1	0.02
Transverse temperature, [eV]	3.5	1.3
Ratio of beam radius to Debye radius, *ka*	17	27
Imaginary part of dielectric permeability, ϵ_1''	0.13	0.08

2. EXPERIMENTAL SET-UPS

2.1. LEAR electron cooler

Neutralization electrodes are used for studies of the electron beam neutralization on the LEAR electron cooling system (**ECOOL**). They are placed near the gun exit and the collector entrance. The neutralisation electrodes consist of two metallic half cylinders, separated by high-resistive-glass insulators of a width of 20 mm [1] (Fig. 2.1). The electrodes have a radius of 50 mm. The resistance of the insulators (between the half-cylinders) is of the order of 3 GOhm.

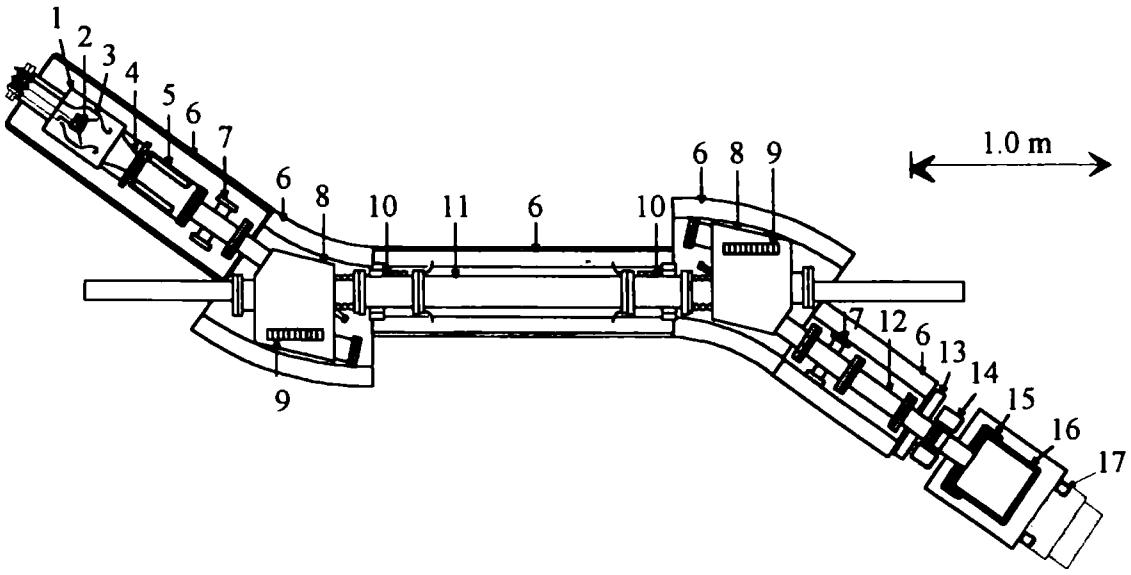

Fig. 2.1. The layout of the LEAR electron cooler:

1. Electron gun
2. Cathode
3. Grid anode
4. Anode
5. NEG pump
6. Solenoid
7. Neutralization electrode
8. Toroid chamber with pump and diagnostic ports
9. ToroidNEG pump
10. Pick-up
11. Central drift tube
12. Collector drift tube
13. Vacuum valve
14. Collector coil
15. Repeller
16. Collector
17. Collector coil

For diagnostics of the neutralization process, two position pick-ups installed in the ECOOL drift section were used (Fig. 2.1).

The experiments were performed in an electron energy and beam current range, corresponding to the LEAR standard operation regimes (Table 2.1).

Table 2.1.
ECOOL parameters.

Electron energy, keV	2.3	7	20	30
Beam current, A	0.01÷0.5	0.07÷2.93	0.35÷2.83	0.65÷2.6
Perveance, $\mu A/V^{3/2}$	0.125÷5	0.125÷5	0.125÷1.0	0.125÷0.5
Electron beam diameter, mm	50			
Vacuum pressure, pTorr	5-15			
Grid anode potential, referred to the cathode electrode, kV	-1.45÷+8.1	-4.3÷+25.6	-12.5÷+11.5	-18.6÷+1.7

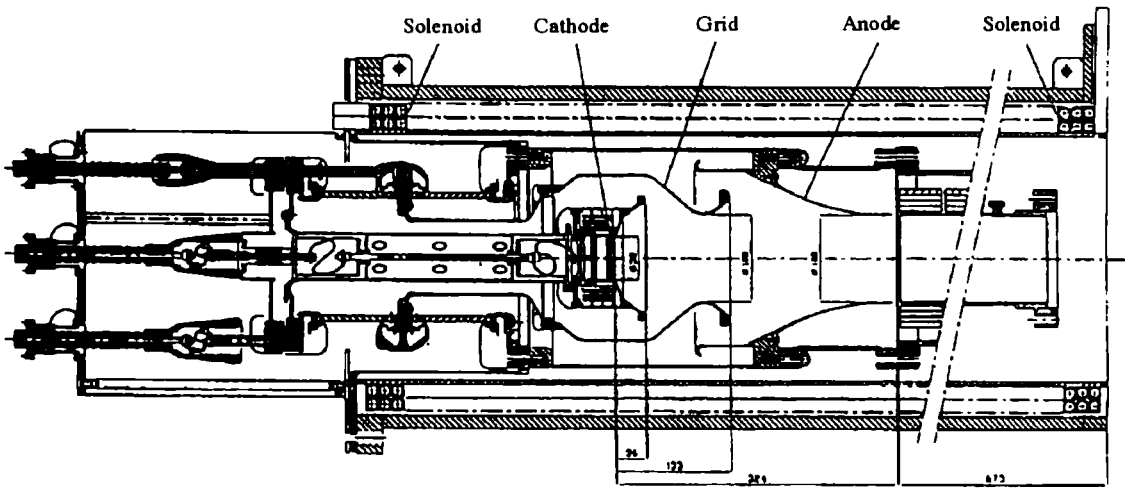

Fig. 2.2 The ECOOL electron gun mechanical layout

The gun of the ECOOL has three sets of electrodes: the cathode, the grid and the anode (Fig. 2.2) [11]. The grid electrode (steering anode) has positive potential to the ground when the gun operates in a regime of high perveance. This can lead to the storage of secondary electrons, generated in collisions of primary beam electrons with residual gas atoms. This leads to a limitation of the beam current generated by the gun. To avoid this effect a special technique is used: a pulsed generator (called "blower") that creates a short (1 μs) pulse which

brings the steering anode potential periodically to the ground. This opens the electron trap and cleans the space inside the steering electrode. The current limitation vanishes. The "blower" repetition period depends on the vacuum, and at LEAR pressure (10 pTorr) it is about a minutes.

2.2. JINR Test Bench

The JINR Test Bench constructed at Lipetsk CAPT INP during a previous collaboration for design and construction of the LEAR gun and the collector [11, 12,13] was developed for studies of neutralized electron beams.

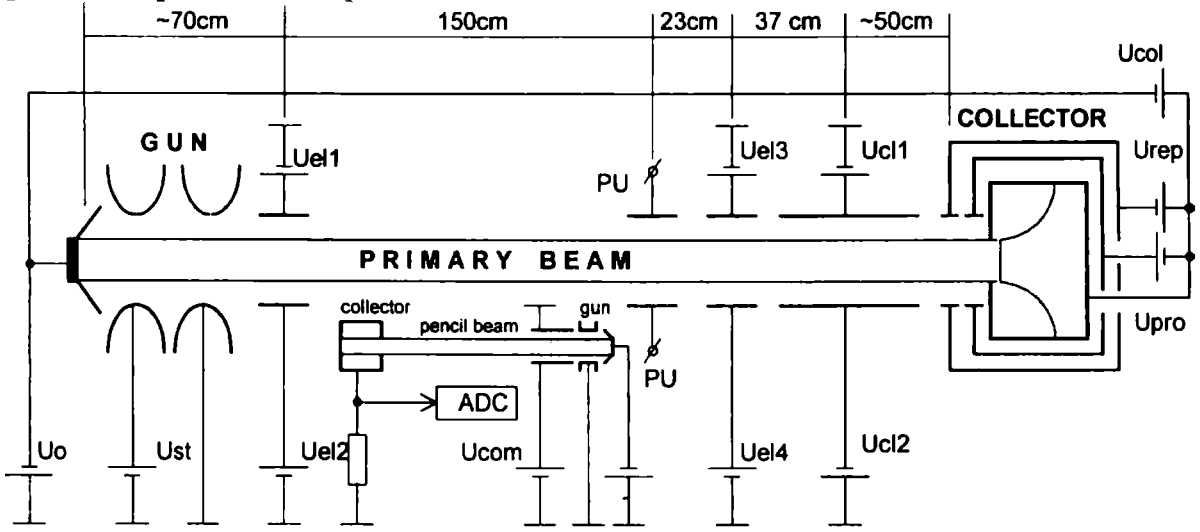

Fig. 2.3. Scheme of the Test Bench

The Test Bench consists of (Fig.2.3) the electron gun, collector, neutralisation electrodes ($U_{el1}..U_{el4}$), pick-up electrodes, clearing electrodes (U_{cl1}, U_{cl2}) [14] and the diagnostic pencil beam [13]. The length of the Test Bench is about 4 m. The vacuum chamber diameter varies from 10 cm to 30 cm. Diaphragms with diameters of 60 mm are placed at the entrances and exits of the neutralisation electrodes, pick-up electrodes and clearing electrodes. Neutralisations and pick-up electrodes have 10 cm diameter and 10 cm length. The vacuum chamber diameter is equal to 30 cm in the pencil beam area. The distances between the Test Bench elements are shown on Fig. 2.3. The Test Bench electron beam is immersed in the longitudinal magnetic field, which can be chosen from 300 to 600 G.

The electron gun used in the Test Bench has optics similar to that of the LEAR ECOOL (Sec. 2.1), i.e. it also contains three electrodes. It differs mainly in terms of the cathode diameter, which is equal to 3 cm. The gun generates the electron beam with parameters providing the necessary experimental conditions (Table 2.2).

The electron beam collector has one additional electrode, which makes it different it from that of the LEAR ECOOL [15]. During Test Bench operation this electrode did not play any significant role and was finally connected to the collector receiving surface. The efficiency of the collector was sufficient, and the ratio of the beam current losses to the beam current did not exceed $2*10^{-4}$ normally.

Table 2.2.
Test Bench parameters

Electron energy, keV	2.3	7	20	30
Beam current, A	0.01÷0.7	0.07÷1.8	0.35÷2.0	0.65÷2.0
Electron beam diameter, mm	30			
Vacuum pressure, nTorr	1-5			

The traps are copies of the LEAR ECOOL traps. The design of the clearing electrodes is similar to that of the neutralization electrodes [14], however, they are much longer (40 cm). An additional transverse magnetic field is used in the system with clearing electrodes

Test Bench and ECOOL have some fundamental differences:

1. The pressure in the vacuum chamber of the Test Bench (10^{-9} Torr) is higher then in ECOOL (10^{-11} Torr).
2. The Test Bench has no toroid bending magnets.
3. The diameter of the Test Bench vacuum chamber varies along the propagating beam. The neutralisation and clearing electrodes have screening diaphragms.
4. The diameters of the beam and the vacuum chamber are different for the Test Bench and ECOOL.

3. DIAGNOSTICS

Both set-ups are equipped with various diagnostics instruments, which can be separated into two groups - the conventional methods and the special ones.

The conventional diagnostics include the measurements of the following parameters (see Figs .2.1 and 2.3):
-all electrode potential,
-the electron beam current,
-the electron beam loss current,
-the signal of particle oscillations - coherent ones and noise of the beam. They are measured with pick-up electrodes and analysed with oscilloscopes and network analysers.

The special methods, described in details below, were used for measurement of the neutralisation factor η [Formula (1.8)]. They include:
-time-of-flight method [1, 5, 11, 16, 13-17],
-use of a Pencil Beam [1, 16, 13-17],
-use of electron cooling [4, 16, 17].

3.1. Time-of-flight method

The electron velocity is dependent on the beam space charge as described above, because electron kinetic energy is in general a function of radius [see Formulae (1.1), (1.2) and (1.7)].

Let us consider a longitudinal velocity modulation of the electron beam at high frequency ω_{mod} by applying a voltage $U_{mod}(t)=U_{\omega}\cos\omega_{mod}t$ on both half-cylinders of the neutralisation electrode 1 at the gun exit (Fig. 3.1).

This provides electron velocity modulation and, as a result, electron density modulation. Measuring the modulation signal with the second pick-up placed downstream of the beam and producing correlation analysis, one can obtain the phase shift between the exciting and modulation signals. This phase shift is equal to

$$\Delta\varphi = \frac{\omega_{mod} L_{ps}}{v_e(\eta)} \quad , \tag{3.1}$$

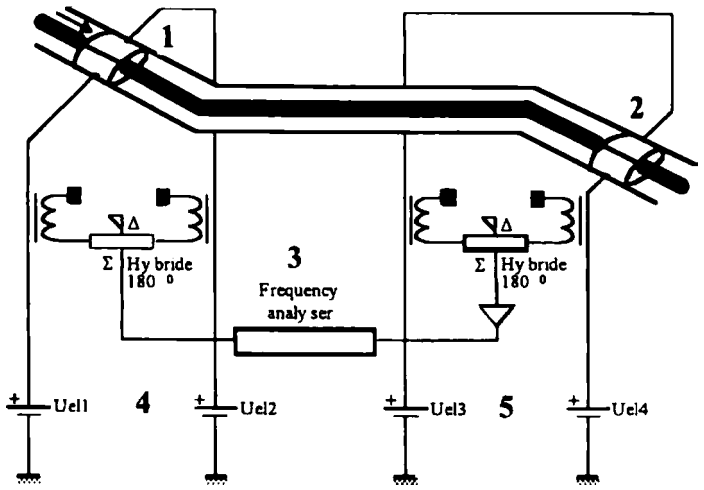

Fig. 3.1.The principle of the time-of-flight method: 1 the gun neutralisation electrode, 2 the collector neutralization electrode, 3 the network analyser, 4 the power supply of the gun neutralization electrode, 5 the power supply of the collector neutralization electrode.

where L_{pu} is the distance between two pick-ups. This allows the neutralization factor to be measured. Indeed, the average velocity variation due to the beam neutralization is about [see Formulae (1.1), (1.2) and (1.7)]

$$\frac{\delta v_e}{v_e} \approx \frac{1}{2}\cdot\frac{U(r=0,\eta=0)-U(r=0,\eta\neq 0)}{U_0} = \\ = -\eta\frac{eI}{4\pi\varepsilon_0 m v_e^3}\left(1+2\ln\frac{b}{a}\right). \tag{3.2}$$

Correspondingly, the phase shift variation related to neutralization is equal to

$$\delta\varphi = -\frac{\omega L_{pu}}{v_e}\frac{\delta v_e}{v_e} = -\Delta\varphi\frac{\delta v_e}{v_e} \quad . \tag{3.3}$$

$$\delta\varphi = \Delta\varphi(1-\eta)\frac{eI}{4\pi\varepsilon_0 m v_e^3}\cdot\left(1+2\ln\frac{b}{a}\right).$$

The phase shift measurement was performed using a network analyser to determine "the time of flight of the signal" between the gun and collector neutralization electrode. A special circuit allowed insertion and reading of the signal from neutralisation electrodes, which have high voltage potential. Attention was given to the problem of the spectral characteristics of the signal. For correct measurements one needs to choose the working frequency in the range where amplitude and phase shift vary smoothly with frequency. A typical example of such a choice is presented on Fig. 3.2.

By turning on and turning off one of the two traps, one can change the beam neutralization state and measure a change of the η factor (Fig. 3.3).

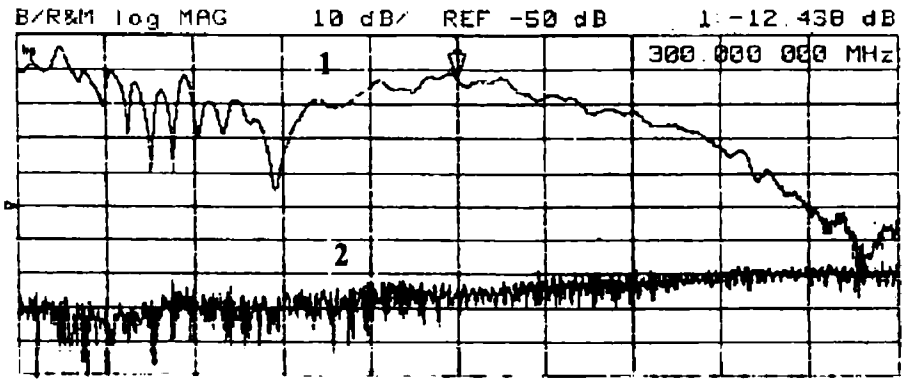

150 MHz 450 MHz

Fig. 3.2. The dependence of the phase shift of the Beam transfer function between the neutralization electrodes on the modulation frequency. 1- beam ON, 2- beam OFF.

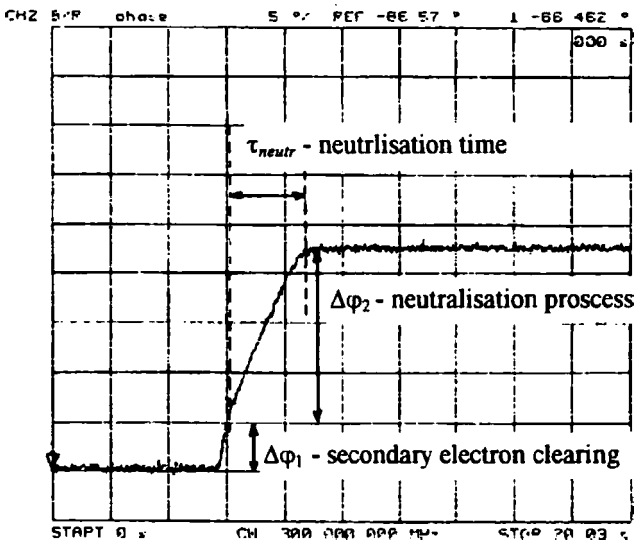

Fig. 3.3. The TOF signal for constant excitation frequency (300 MHz) when a trap is OFF and ON:

$\mathcal{E}_e = 27$ keV, $B = 600$ G, $U_{el1} = U_{el3} = 6$ keV, $U_{el2} = U_{el4} = 0$;
$I_e = 1.2$ A, the trace of secondary electron clearing and neutralization process are seen distinctly.

The calibration over a wide range of parameters (Figs. 3.4 and 3.5) demonstrates a good agreement of the experimental results with the calculated ones Eqs. (3.1), (3.3).

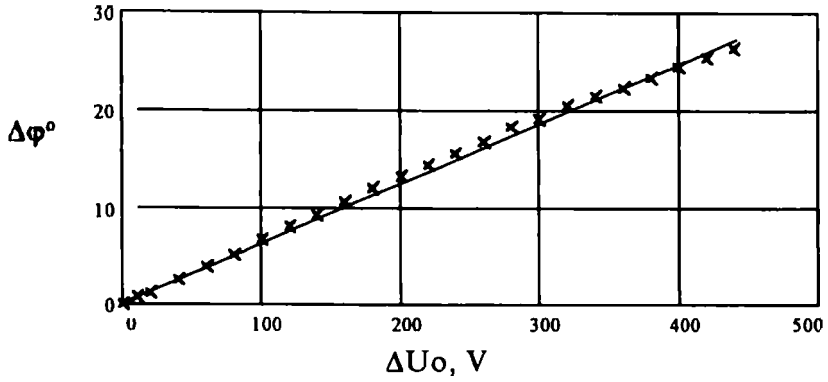

Fig. 3.4. Dependence of the phase shift on cathode potential variation ΔU_0. *** - experiment, --- - Formula (3.1)

$\mathcal{E}_e = 27.6$ keV, $I_e = 1.93$ A;

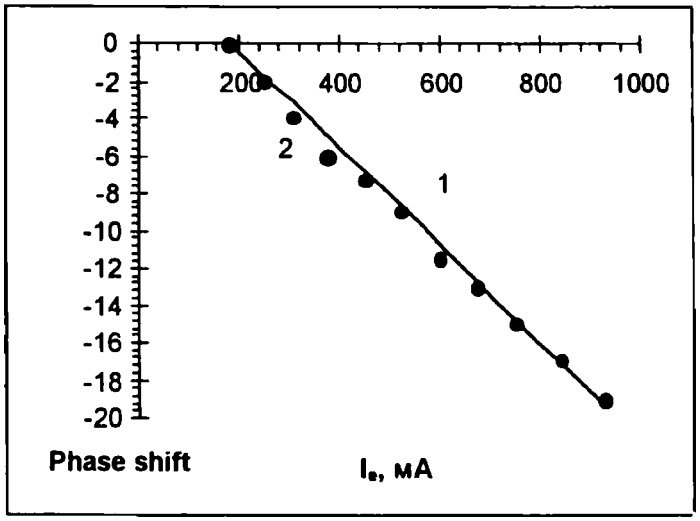

Fig. 3.5 Dependence of the phase shift on the beam current. U_0 = 11,8 kV, $\eta_n = 0{,}1$. 1- Formula (3.3); 2 •- experiment.

3.2 Pencil beam diagnostic

The the Pencil Beam (PB) method [1, 16, 13-17] is based on measurement of a displacement of a low-energy electron beam propagating in the electric and magnetic fields of the primary beam parallel to its axis and outside of it (Fig. 3.6). To increase the resolution, the well-know "null-method" is used: the PB passes through a pair of parallel plates (compensation plates), which have some voltage U_{cp} between them. The electric field $E_\perp$ of plates compensates the PB drift in the electron beam fields, if

$$E_\perp s = -(1-\beta^2)E_b L_d\,,\quad E_\perp = U_{CP}/d\,, \tag{3.4}$$

where s is the length of the compensating plates, E_b the electric field of the primary beam, L_d the distance between the plate exit and PB collector. If condition (3.4) is respected, the PB enters its collector and we have a signal which is recorded via ADC in a PC (Fig. 3.7).

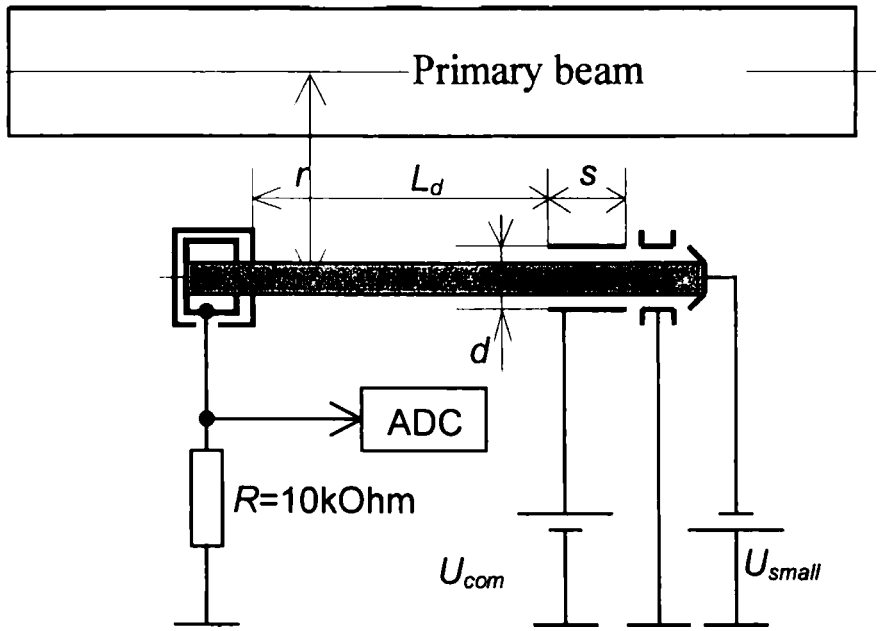

Fig. 3.6. Pencil beam method scheme.
R = 10 kΩ - the resistor for the measurement of the pencil beam current.

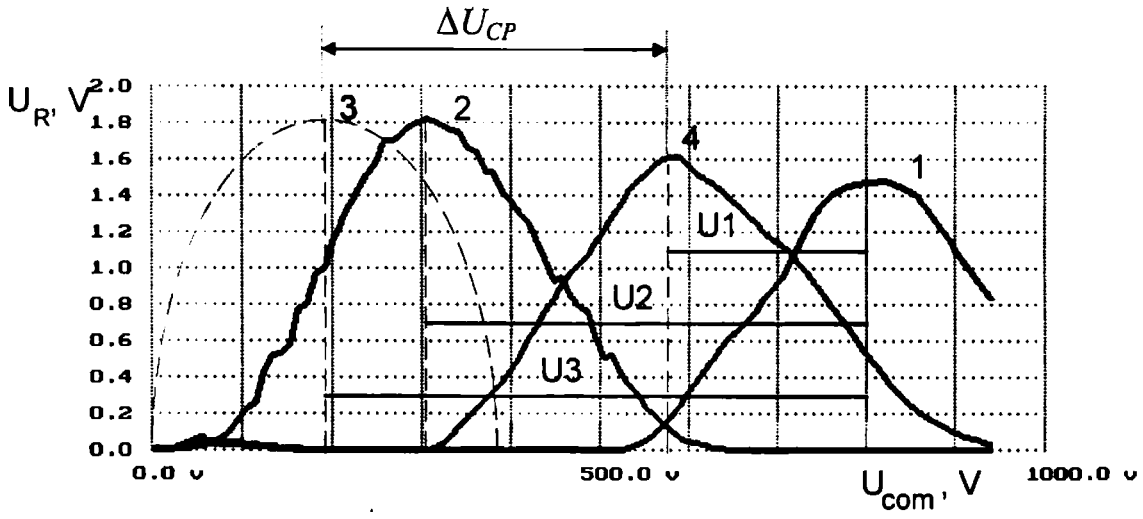

Fig. 3.7. The typical signals from the pencil beam collector
U_{com} - compensation electrode voltage,
U_R - voltage on 10 kΩ resistor at the collector output.
1 - primary beam is "OFF"; 2 - primary beam is "ON", neutralisation electrodes are "OFF"; 3 - the theoretical curve when primary beam is "ON" and neutralised electrodes are "OFF"; 4 - primary beam and neutralised electrodes are "ON".

The distance between the PB gun and the PB collector is L_d = 64.3 cm; between the primary and pencil beams axis is r = 5.3 cm; the gap between

compensated plates is $d = 2.8$ cm, the length of the compensating plates is $s = 10$ cm. The pencil beam diameter is 1.5 mm, the electron energy in the PB is 500 - 1500 eV, the PB current is 50 - 200 μA. A narrow slit of 1 mm width is used on the entrance of the PB collector to localize the PB position.

In the experiments the collector current is measured as the function of the compensating plate (CP) voltage. One proceeds in the following manner. At first the signal is recorded, when the primary beam is switched off (Fig. 3.7, curve 1). The second step is the measurement of the pencil beam current, when the primary beam is "on", but the trap voltage is "off" (curve 2). The third step is the measurement of the pencil beam current, when primary beam and trap voltage are on (curve 4).

In the presence of the electron beam, the compensation plate voltage is described by Formula (3.4) with $\eta = 0$. This corresponds to curve 3, when the PB density is supposed to be uniform and the beam form a cylindrical one. In the case when traps are "on", the neutralisation factor can be found from the formula

$$\eta = 1 - \frac{U_1}{U_3}, \tag{3.5}$$

where U_1, U_3 are the voltage shifts shown on Fig. 3.7. The shift between curves 3 and 2 shows that some "natural" neutralisation exists, even when traps are "off":

$$\eta_{natural} = 1 - \frac{U_2}{U_3} . \tag{3.6}$$

The PB method also allows one to observe the stability of the NEB. When U_{com} is kept constant, any variation of the beam electric field gives an immediate shift of the PB in an azimuthal direction. That produces a decrease of the PB current, coming to the collector. Figure 3.8 represents the dependence of the collector current on time for stable (a) and unstable (b) regimes.

The development of an instability leads to a "jump" of the collector current (Fig. 3.8b). Such a "jump" signal allows one to measure a period of the instability. The resolution of the PB method, when it is used with a "null-method", can be estimated with Formula (3.5). If the PB diameter is equal to the slit size (that is the optimal case), we find the resolution δE_b of the NEB electric field measurement

$$\frac{\Delta\eta}{\eta} \sim \frac{\delta E_b}{E_b} \sim \frac{\delta U_{com}}{\Delta U_{com}} , \tag{3.7}$$

where E_b is the electric field of the charged beam, ΔU_{com} the voltage shift of compensation plates, when the beam comes from a nonneutralized state to the neutralized one, δU_{CP} the resolution of the ΔU_{CP} measurement. Using the data from Fig. 3.7, one can estimate $\delta U_{com} \sim 10$ V, which gives the resolution $\Delta\eta/\eta \sim 0.05$ for a typical case $\Delta U_{com} \sim 200$ V.

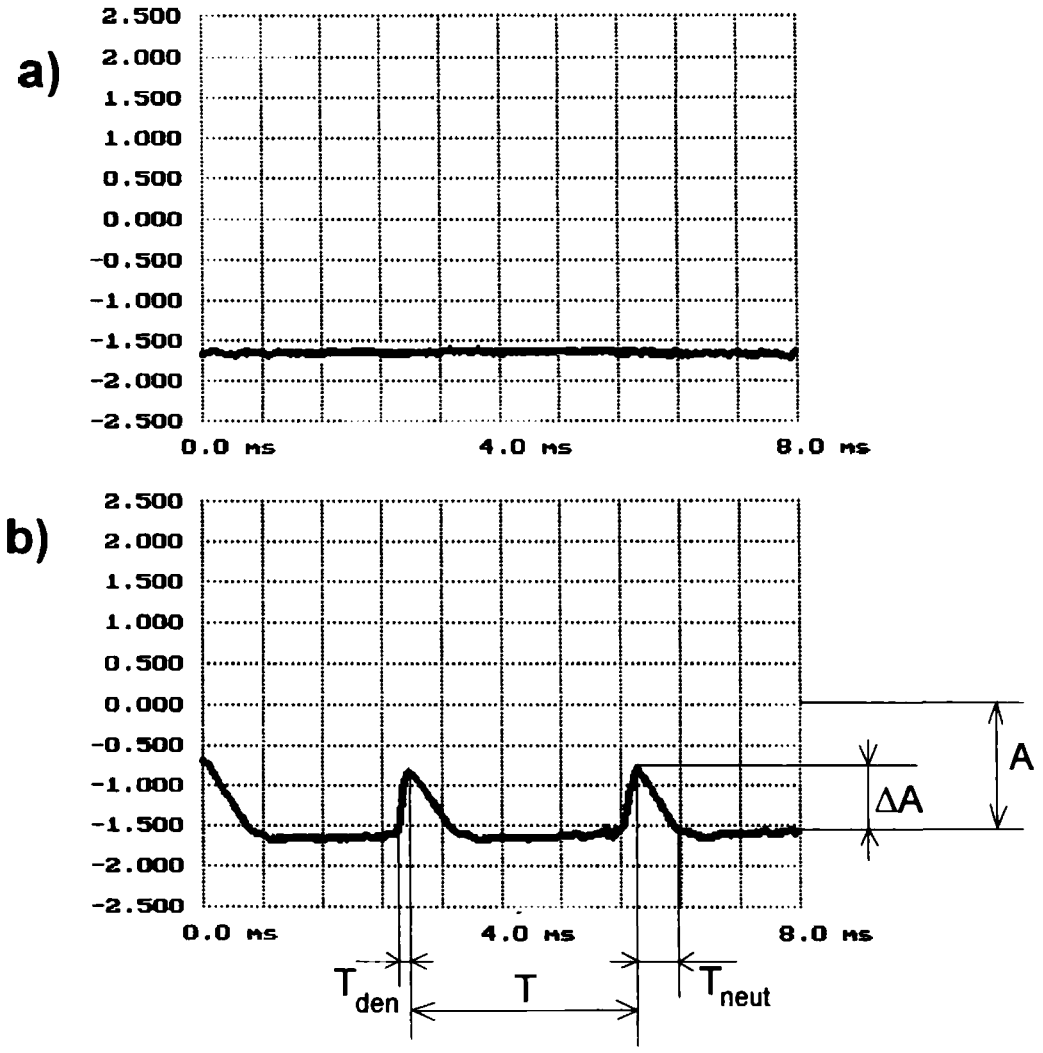

Fig. 3.8.The dependence of the pencil beam collector current on time:
a) stable regime, b) unstable regime.

We emphasise, that the magnetic field variations and the PB energy and intensity have no influence, when the "null-method" is used. However, the stability of U_{com} plays a decisive role - it limits the resolution. So, if U_{com} fluctuates with an amplitude $\overline{U}_{com}$, the resolution of η [see Formulae (3.5) and (3.7)] is not better than

$$\frac{\Delta\eta}{\eta} \sim \frac{\delta U_{com}}{\Delta U_{com}} + \frac{\overline{\overline{U}}_{com} \cdot d}{U_{com} \cdot s}, \qquad (3.8)$$

where d is distance between compensate plates, s is length of compensation plate.

3.3. Diagnostic with cooled proton beam

The use of a cooled proton (ion) beam as a probe sensitive to the electron beam potential distribution [11, 4, 16, 17], is the most precise absolute method. It can be performed in different ways.

3.3.1. Proton beam scanning across the electron beam

The proton beam at constant energy and constant magnetic field of the storage ring is scanned with correction magnets across the electron beam and the proton revolution frequency is measured. If the electron beam is perfectly neutralised its potential does not vary with proton beam co-ordinates, the proton revolution frequency does not change. If the electron beam potential varies, the proton momentum changes in accordance with requirement of the proton-electron velocities equality. The revolution frequency changes with the proton co-ordinates as follows:

$$\Delta\omega(r_p) = \omega(r_p) - \omega(0) = \eta_\omega \omega(0)\frac{\Delta p(r)}{p}, \quad \eta_\omega = \frac{1}{\gamma_{tr}^2} - \frac{1}{\gamma^2} \quad . \tag{3.9}$$

Then the formula (1.3) gives the potential variation:

$$\Delta U_b(r_p) = \beta^2\gamma \frac{mc^2}{e}\frac{1}{\eta_\omega}\frac{\Delta\omega(r_p)}{\omega(0)} \quad . \tag{3.10}$$

3.3.2. Scanning of the proton beam with electron energy variation

The second method uses again the condition of equality of electron and proton velocities and also operates in a constant magnetic field of the storage ring. Then, when the electron energy (the cathode voltage) is changed by some small value $e\Delta U_0$, the proton beam is displaced in accordance with the equations (see Fig. 3.9)

$$\Delta r_p = D\frac{\Delta p}{p} = D\frac{e}{\beta^2\gamma mc^2}\left(\Delta U_0 + \delta U_b(r_p)\right) \quad , \tag{3.11}$$

where D is the dispersion in the cooling section, $\delta U_b(r_p) = U_b(r_p) - U_b(0)$. Measuring the revolution frequency variation and the cathode voltage change, one can find the beam displacement:

$$\frac{d\omega}{dx} = \gamma_{tr}^2\eta_\omega\frac{\omega}{R_s}, \quad \Delta r_p = \frac{R_s}{\gamma_{tr}^2\eta_\omega}\frac{\Delta\omega}{\omega} \quad , \tag{3.12}$$

where $R_s = C/2\pi$ - the average radius of the storage ring. One can find Δr_p also from measurements of the proton trajectory, however, the accuracy here is lower. Using the experimental values of Δr_p and ΔU_0, one can obtain $\delta U_b(r_p)$.

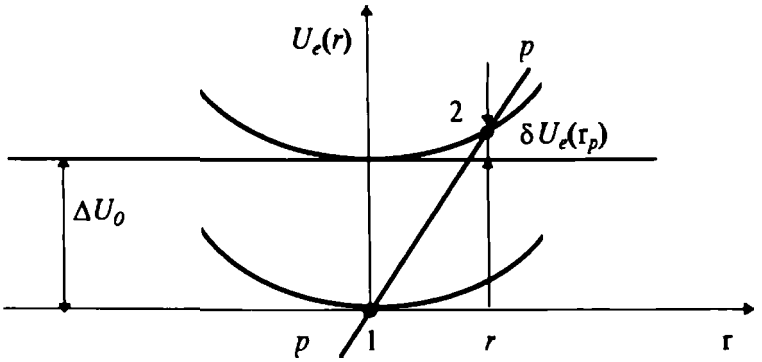

Fig. 3.9. Measurement of $U_b(r)$ with U_0 variation: pp - the proton dispersion "trajectory" in co-ordinates (U_b , r); 1, 2 are the initial and final positions of the proton beam.

The variation of the revolution frequency with U_0 and I_e was measured experimentally and used for the calibration (Fig. 3.10).

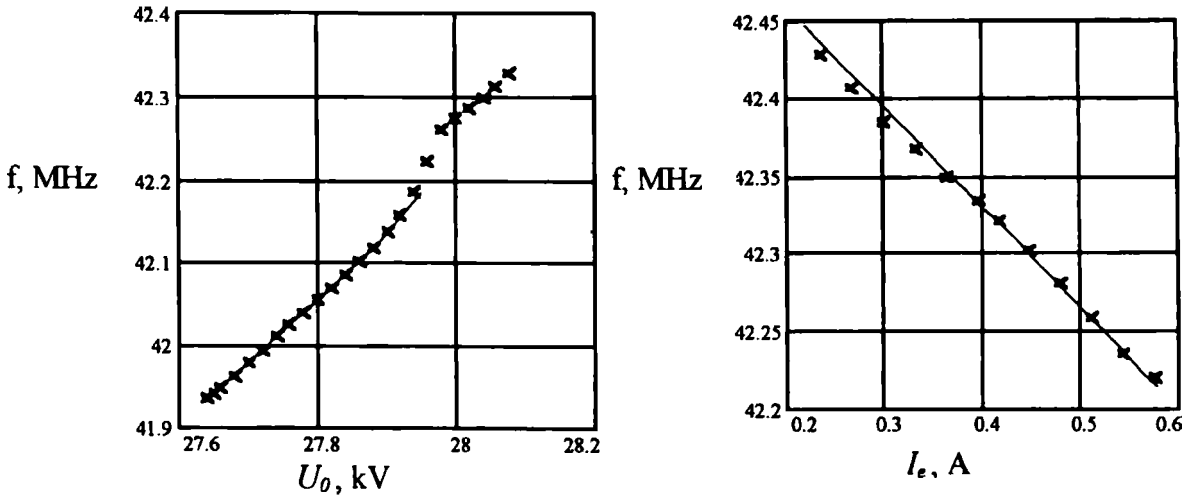

Fig. 3.10. Dependence of the revolution frequency on U_0 and I_e measured in LEAR.

4. STUDIES OF THE STABLE ELECTRON-BEAM NEUTRALIZATION

In this chapter we describe a set of experiments [18, 19, 11, 16, 17], which were designed to reach a high neutralization and to study its dependence on different parameters in the ranges presented below:

- electron energy: 2.0÷28 keV,
- beam current: 0.05÷3.0 A,
- vacuum pressure: 1÷10 pTorr on LEAR, 2-100 nTorr on Test Bench,
- ion trap voltage: 0÷6 kV,
- solenoid magnetic field: 300÷600 G.

During these measurements the problem of the neutralized beam stability received high attention.

4.1. Dependence of the neutralization factor on trap electrode potentials

The first question concerns the trap electrode potential required for an efficient ion trapping. The numerous measurements performed on LEAR ECOOL with the TOF method (Fig. 4.1) and on the Test Bench with the PB method (Fig. 4.2) demonstrate a characteristic dependence: the neutralization factor η increases with the growth of the potential reaches a saturation at certain potential values dependent on parameters of the experiment. One can estimate roughly this saturation value using formula (1.1) and the condition

$$U_b(a) + \frac{b-a}{b} U_{el1} + \frac{a}{b} U_{el2} \geq 0 \quad . \tag{4.1}$$

The comparison of experimental data and corresponding estimations shows a satisfactory agreement.

The experiments demonstrated also the presence of secondary electrons in NEB. So, when one of the traps is switched OFF and turned ON again (the regular method of stability checking), the TOF signal (see Fig. 3.5) reveals some abrupt jump, which can be interpreted as a clearing of the secondary electrons. The data, presented in Fig. 4.2, characterize a significance of the secondary electron clearing: curve 2 shows that the η-factor increases with the trap voltage even when only the collector trap is ON and ion trapping is not complete (the gun exit is open for ion escape). This can be explained as clearing of secondary electrons with the collector trap.

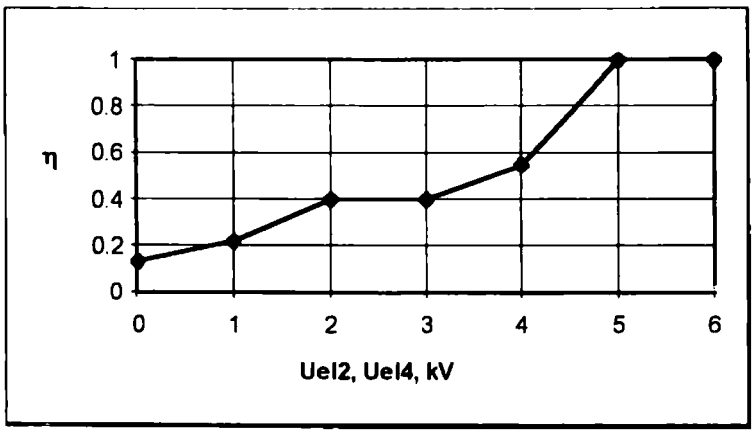

Fig. 4.1. The dependence $\eta(U_{el})$ ECOOL, TOF method,
$U_{el1} = U_{el3} = 0$, $\varepsilon_e = 27.7$ keV, $I_e = 0.14$ A, $P = 10$ pTorr

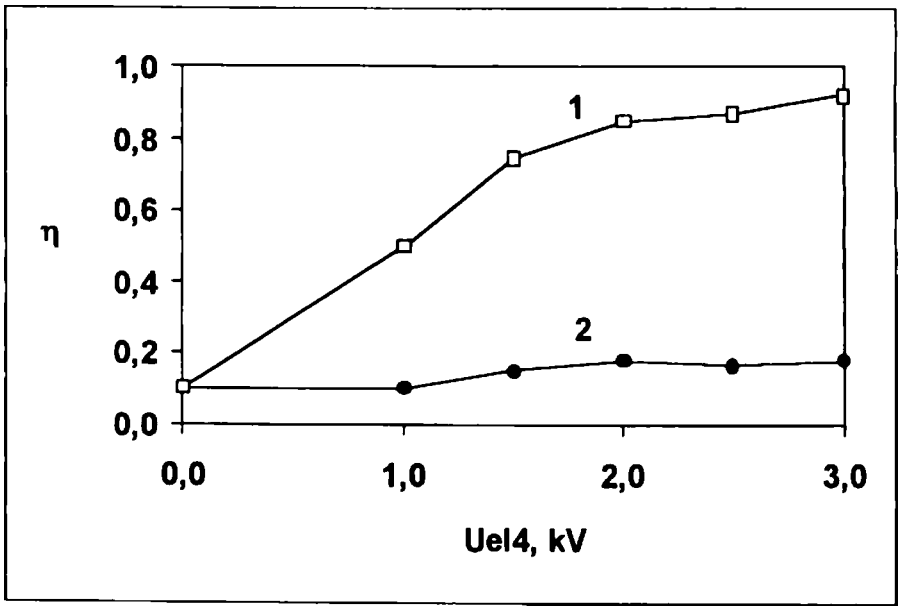

Fig. 4.2. The dependence $\eta(U_{el})$ at the Test Bench, PB method,
$\varepsilon_e = 6$ keV, $I_e = 0.5$ A, $P = 100$ nTorr
1- $U_{el1} = U_{el3} = 1/4\ U_{el2} = 1/4\ U_{el4}$ two traps on
2- $U_{el1} = U_{el2} = 0$, $U_{el3} = 1/4\ U_{el4}$ only collector trap on

When the ion traps are ON, there is an increase not only of the η factor, but also of the current losses (Fig. 4.3).

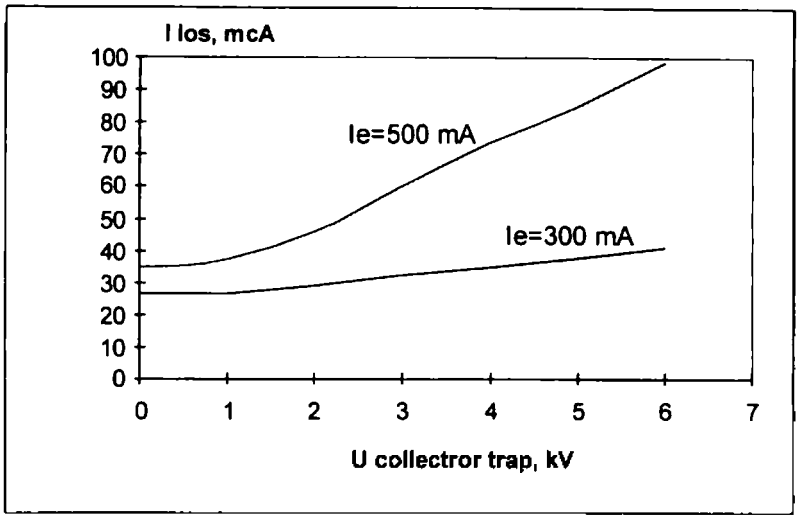

Fig. 4.3. Dependence of current losses in Test Bench on the collector trap electrode voltage:
U_0 = 2.5 keV, 1) I_e = 300 mA, P = 3 nTorr ; 2) I_e = 500 mA, P = 4 nTorr.

We must underline again that all experimental data presented in this paragraph pertain to a stable electron beam, when no "jumps" of the signal occur on TOF and PB detectors.

4.2. Measurements with the cooled beam probe

The method of the cooled proton beam probe (CBP, Sec.3.3.) was used for measurement of the radial distribution of the potential in the electron beam in LEAR ECOOL (Fig. 4.4). When the traps are "OFF", the classic parabolic dependence (1.1) was obtained (Fig. 4.4a). For traps "ON" with sufficient values of potentials of all electrodes, the distribution (Fig. 4.4b) is very peculiar: η is close to 1 in the central part of the electron beam, $r \leq 20$ mm, and a very abrupt growth of the potential takes place near the beam border, 20 mm $\leq r \leq 25$ mm. The "jump" for the parameters of experiment is about 40 V.

The measurements of the neutralization factor by the measurement of the cooled particle revolution frequency (see Sec.3.3) were performed at different electron beam parameters. Because of the high neutralization level, a variation of the NEB current did not lead to a shift of the revolution frequency (Fig. 4.5). Theoretically such an effect brings a great advantage for electron cooling: one can change the NEB current and, correspondingly, the cooling rate, without any shift in stored (cooled) particle energy.

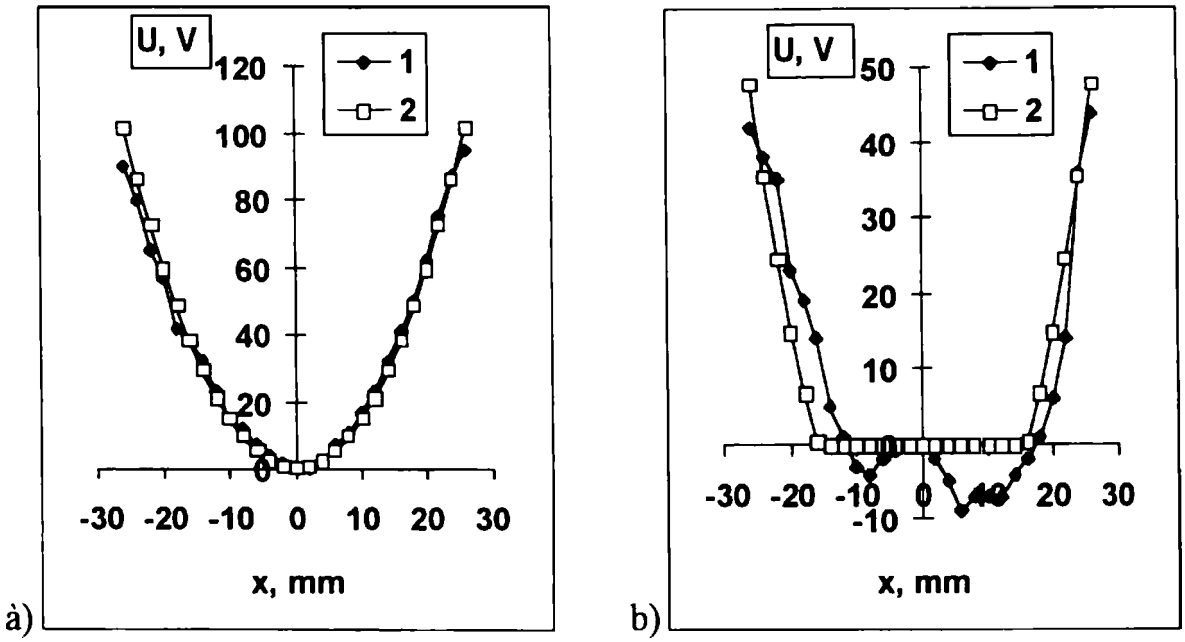

Fig. 4.4. Distribution of the electron beam potential across the beam (the method of ε_e variation), a) traps are "OFF", b) traps are "ON", $U_{el1} = U_{el3} = 6$ kV, $U_{el2} = U_{el4} = 0$, $\varepsilon_e = 27$ keV, $I_e = 1.0$ A, $P = 10$ pTorr. 1-experiments, 2-computed values.

Table 4.1.The parameters of the stable electron beam at high neutralization level

Electron energy, keV	27.5	11.5	3.2
Beam current, A	1.5	0.5	0.1
Neutralization factor, η	0.9	0.85	0.75
Beam perveance, $\mu A/V^{3/2}$	0.32	0.4	0.6

A stable and well-neutralized electron beam ($\eta \approx 1$) was obtained (Table 4.1), when the perveance did not exceed 0.6 $\mu A \cdot V^{-3/2}$.

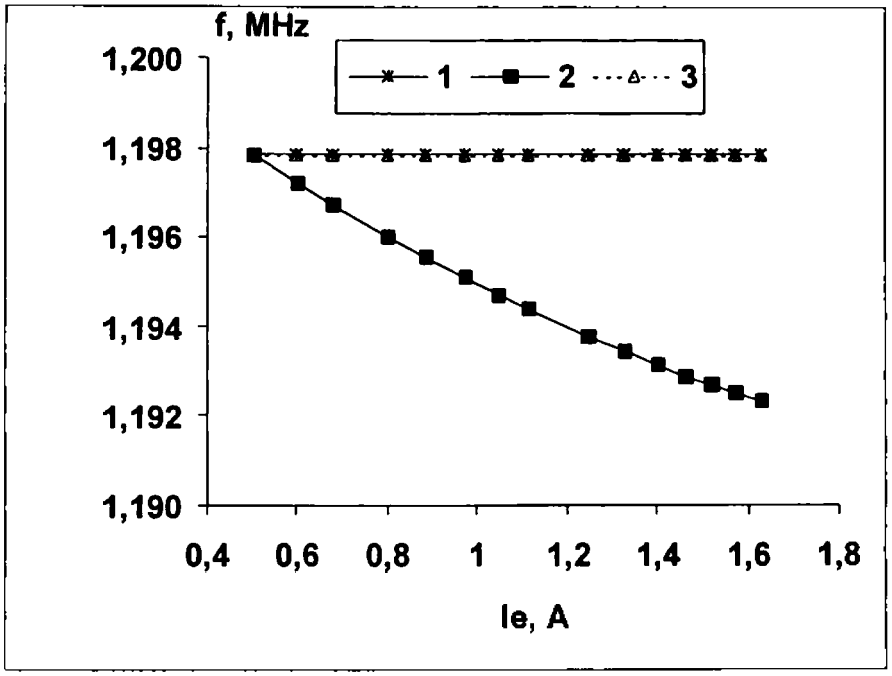

a)

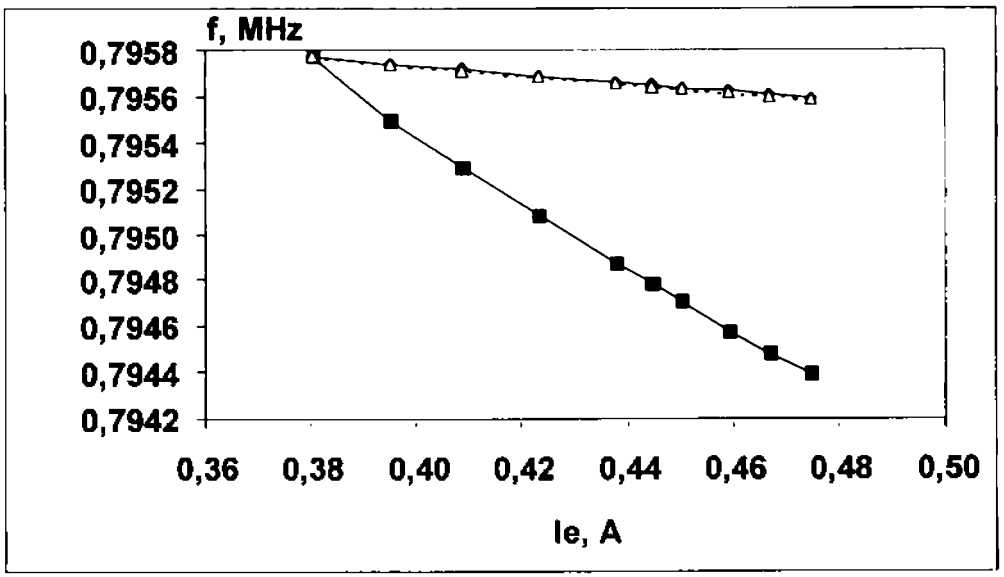

b)

Fig. 4.5. Dependence of the proton revolution frequency on the beam current

B = 600 G, $U_{el4} = U_{el2} = 6$ kV, $U_{el1} = U_{el3} = 0$. ∆, ✳ - neutralized beam, ∆-measurements, ✳-computed values, a) $\eta = 1$, b) $\eta = 0.83$; ■ -computed values for the beam with $\eta = 0$. a) $U_0 = 27.8$ kV, b) $U_0 = 11.7$ kV.

4.3.Influence of electron-beam current and magnetic field on the neutralization factor on LEAR

The experiments performed on LEAR [11, 16, 17, 18, 19] have shown that the neutralization factor can be kept constant up to a certain value of electron beam current (Fig. 4.6), when the instability threshold is not exceeded. Above the threshold one can observe with TOF abrupt "jumps" of deneutralization (see Fig. 3.5).

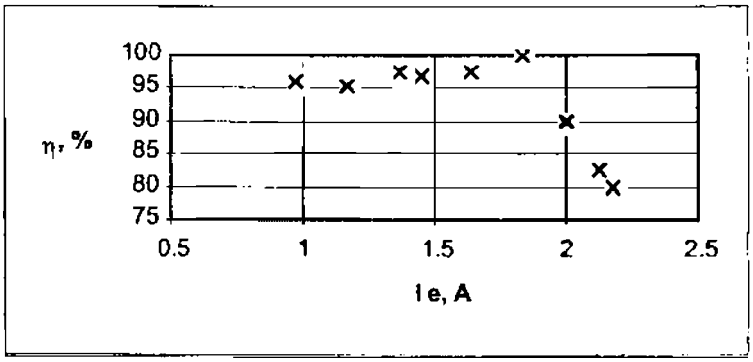

Fig. 4.6.The dependence $\eta(I_e)$ for ECOOL
ε_e= 27.5 keV, $U_{el1} = U_{el3}$= 6 kV, $U_{el2} = U_{el4}$= 0.

The influence of magnetic field on η has a quasithreshold character (Fig.4.7).

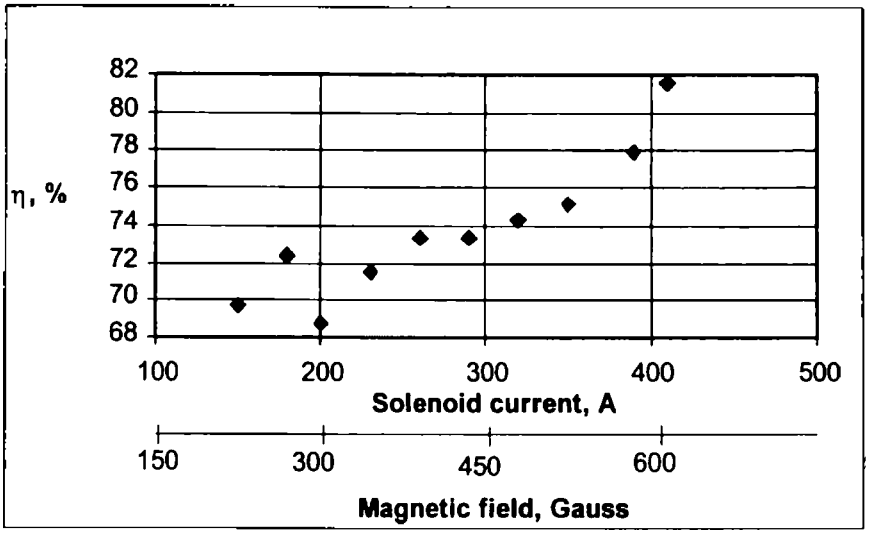

Fig. 4.7. The dependence of η-factor on *B* for ECOOL
$\mathcal{E}_e$= 12 keV, I_e= *0.375 A*, *P* = 10 pTorr. *B(Gs)* = 1.54**I*$_s$*(A)*, I_s -solenoid current.

The theoretical dependence of the neutralization factor on the beam parameters is given by the relation [16]:

$$\eta \cong \frac{1}{1+\frac{j_b L}{\Lambda \varepsilon_0 v_e^2 B}} \tag{4.2}$$

where j_b is beam current density, L the length of the neutralised beam, v_e the electron velocity, B the magnetic field, ε_0 the permeability, and $\Lambda \cong 1\text{-}2$ a numerical coefficient. Eq (4.2) reproduces the measured curve only in a qualitative manner.

4.4. Influence of electron-beam current and vacuum pressure on neutralization factor on Test Bench

The neutralization factor in Test Bench experiments [16] was reduced with increase of the beam current (Fig. 4.8).

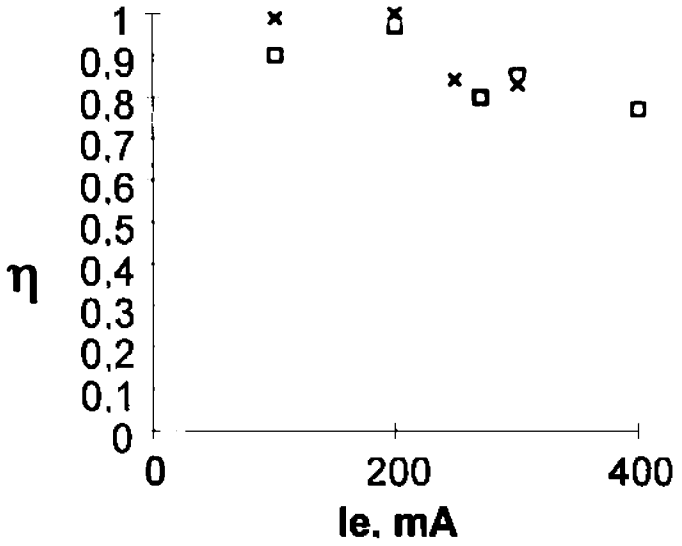

Fig.4.8. Dependence $\eta(I_e)$ for the Test Bench;
ε_e = 2 keV, B = 450 G, P = 15÷70 nTorr,
□- $U_{el1} = U_{el3}$ = 4 kV, $U_{el2} = U_{el4}$ = 1.3 kV
×- $U_{el1} = U_{el3}$ = 5 kV, $U_{el2} = U_{el4}$ = 1.8 kV

One should also underline here, that already in the early experiments on the Test Bench a very strong influence of vacuum conditions on the maximal η value obtainable under stable conditions was observed [16, 17]: η decreases when P decreases (Fig. 4.9)

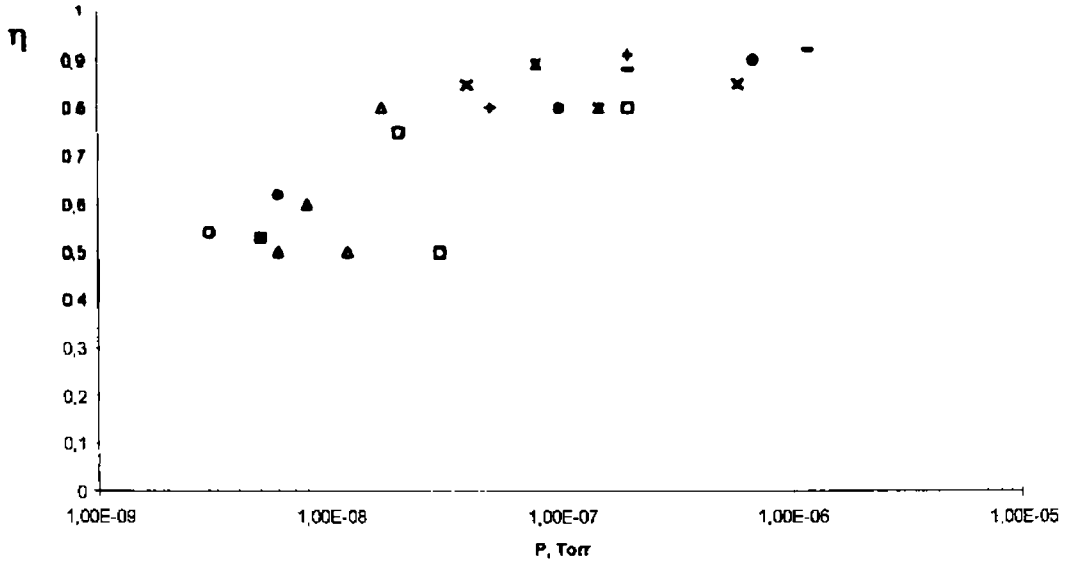

Fig. 4.9. Dependence of the η factor for the Test Bench on pressure (parameters pertaining to the different measurements are presented in the table below).

Uo,kV/Ib, mA / B,G
□ 2 / 370 / 450
△ 2,5 / 300 /500
◇ 2,5 / 100 / 500
○ 2,5 / 500 / 500
× 4 / 725 / 450
■ 5 / 820 / 500
◆ 5 / 980 / 500
▲ 5 / 1250 / 500
✳ 6 / 1250 / 450
+ 6 / 1250 / 500
● 8 / 1900 / 500
— 10 / 2300 / 500

5. WAVE PHENOMENA AND BEAM INSTABILITY

Experimental studies of transverse electron oscillations in NEB

The drift instability, which restricts the formation of a dense neutralized electron beam [1, 5, 20] [see Section 1.4 and Formula (1.39)], is intimately linked with its oscillation characteristics. Knowledge of them leads to an understanding of the possibilities to counteract the development of an instability.

In this chapter we present result of the experimental studies of the spectra of the free transverse electron-ion wave, Beam Transfer Function (BTF) of the NEB - its oscillation patterns and the threshold beam current of the drift instability [18, 19, 11, 14, 19]. The experiments were performed on the ECOOL and on the Test Bench.

5.1. Neutralization and the beam-drift instability

The beam-drift instability [20] leads to destruction of neutralization (Fig. 5.1 a). The dependence of the neutralization factor on time measured by the TOF method is shown in Fig. 5.1 a. The instability can also be observed with PU electrodes, where a signal of the transverse oscillations appears (Fig. 5.1b). There are correlation between neutralization factor "jumps" and bursts of transverse oscillations observed on the PU electrodes (Fig. 5.1 b). The neutralization jumps coincide with the jumps of the current losses (Fig. 5.2). The last ones occur due to fast ion escape after the onset of the beam-drift instability (Fig. 5.2).

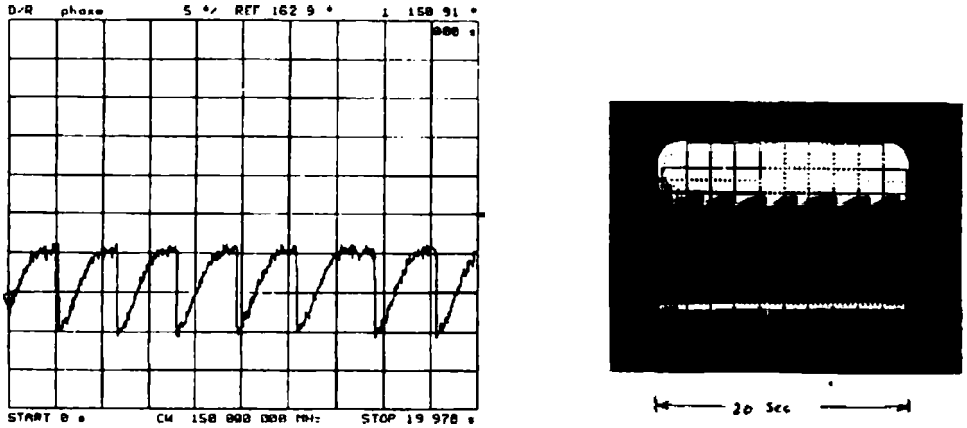

a b

Fig. 5.1. a) Neutralization factor "jumps" (TOF method). b)Correlation between neutralization factor "jumps" (upper picture) and bursts of transverse oscillations of NEB from PU electrode (lower trace).

The studies of the beam-drift instability on the Test Bench were performed using the PB method. The development of the instability was registered at constant voltage on the compensation plates (see Section 3.2 and Fig. 3.6).

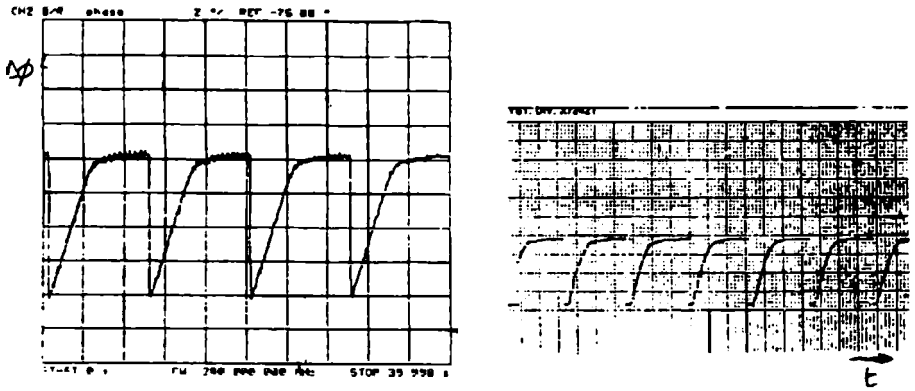

Fig. 5.2 a) Dependence of the neutralization factor on time.
b) Dependence of the current losses on time.

5.2. Free transverse electron-ion oscillations of the NEB in ECOOL

The free transverse electron-ion oscillations in ECOOL are measured with differential pick-up electrodes (see Fig. 2.1). The free transverse oscillations are due to the coherent motion of the electron-ion columns. The amplitude of free transverse oscillations increases during development of the beam-drift instability (Fig. 5.3). The recorded signal on both pickup-electrodes (gun and collector pick-ups) are equal.

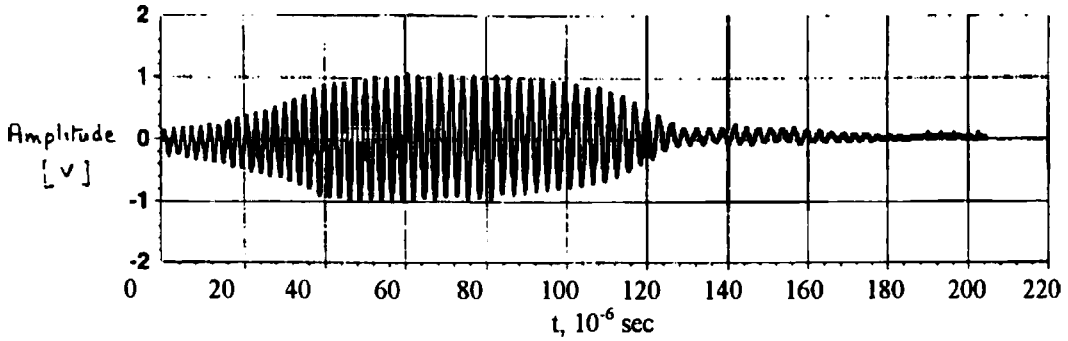

Fig. 5.3. Transverse oscillation signals from differential pick-ups at the development of the beam-drift instability.

The duration of the increase is determined by the conditions of wave amplitude saturation, when an equilibrium between the wave amplification and Landau damping occurs (see Sec. 1.4). The duration of the decay depends on the Landau damping decrement [5] [see Sec.1.4, Formulae (1.33) and (1.35)]. The resonant frequency of transverse electron-ion oscillations corresponds to coherent ion frequency f_l (see Section 1.4) (Fig. 5.4).

$$f_l = \sqrt{f_i^2 + \frac{f_B^2}{4}} - \frac{f_B}{2}, \qquad (5.1)$$

where f_B is the ion Larmor frequency, f_i the plasma frequency. The spectrum of the transverse oscillations of the NEB in ECOOL (Fig. 5.4) was obtained from

these measurements by use of spectrum analyser. It was measured for a longer time than that of the burst of the instability.

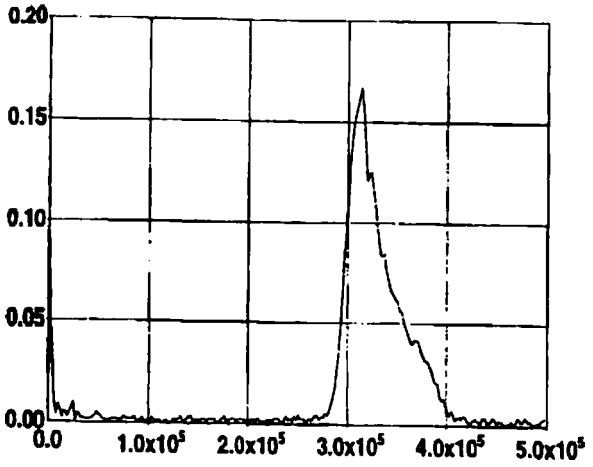

Fig. 5.4. Spectrum of the free transverse oscillations of NEB in ECOOL: $U_0 = 27$ kV, $I_e = 1.54$ A, $U_{el2} = U_{el4} = 4$ kV.

The resonant oscillation frequency reduces during the development of the beam-drift instability (Fig. 5.5). This can be explained by an escape of the lighter ions.

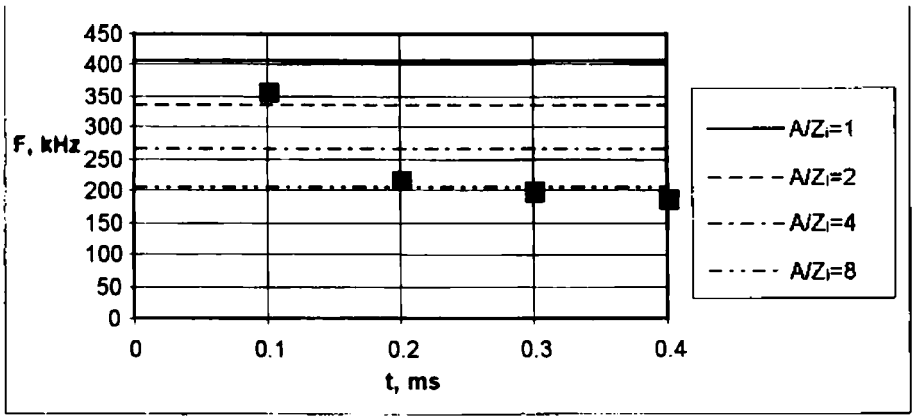

Fig. 5.5. Dependence of transverse oscillation frequency on time during the instability burst.

The measurements of these frequencies as a function of the beam current and the magnetic field magnitude were performed for a helium atmosphere created by a controlled inlet of helium into the ECOOL vacuum chamber (see Figs. 5.6 - 5.7).

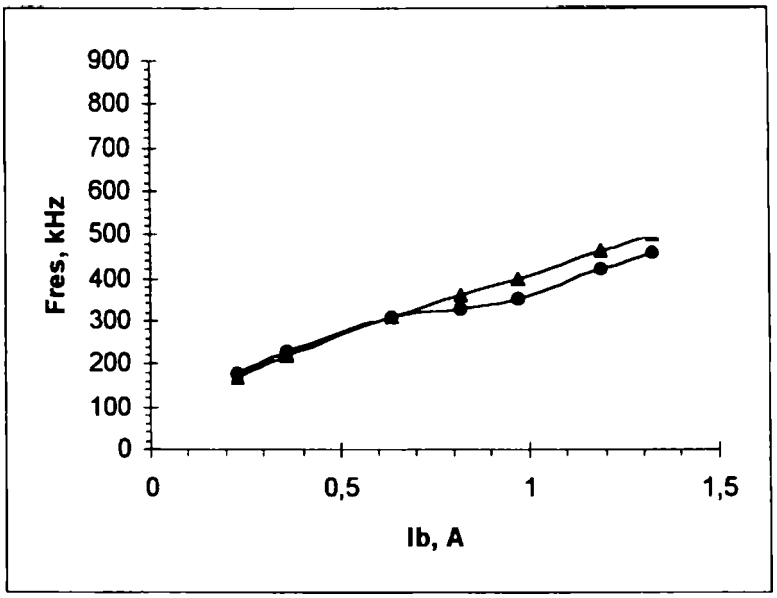

Fig. 5.6. Dependence of (●) resonant frequencies on the beam current: $U_0 = 27$ kV, $\eta = 0.15$, $A/Z_i = 4$ - He atmosphere in ECOOL vacuum chamber. (●) - experiment, ▲ - calculation with formula (5.1).

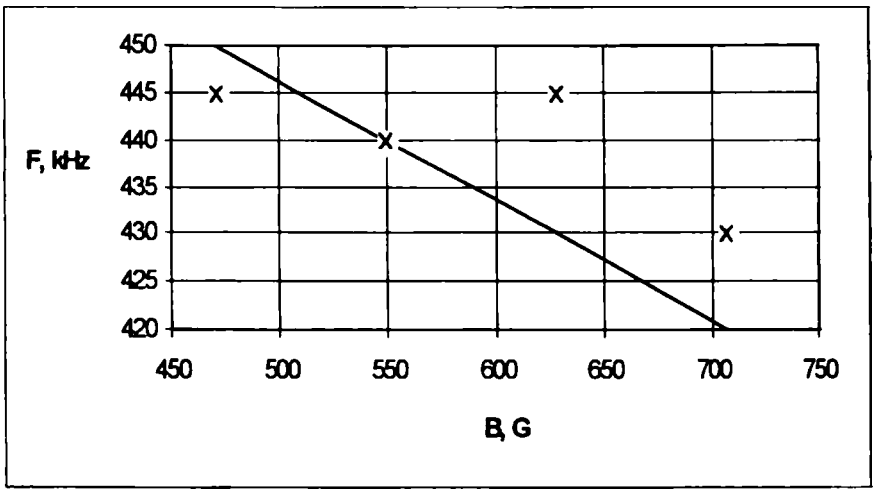

Fig. 5.7. Dependence of the resonant frequency of free transverse oscillations on the magnetic field
× - experiment, —— - calculation, $A/Z_i = 4$, He atmosphere in ECOOL vacuum chamber

The agreement of the experimental and calculated values [Formulae 5.1)] is relatively good.

Of specific interest for the understanding of the instability dynamics is the variation of transverse oscillation characteristics along the beam. For this reason the transverse oscillations and their spectra were measured with two differential pick-ups, placed at a distance 0.9 m and 2.3 m from the gun trap. The pick-up signals were registered during neutralization jump, when bursts of instability appeared (Fig. 5.8 a). Between the bursts of instability the amplitude of transverse oscillations was very low and a signal from the differential pick-ups was not registered during this time.

The conclusion from this measurement was, that the amplitudes of transverse oscillations during instability on both pick-ups were comparable. This means that in the unstable regime the wave amplification is very low or the transverse oscillation amplitude is saturated over a length less than the distance between the gun neutralization electrode and the gun pick-up one (distance 0.9 m).

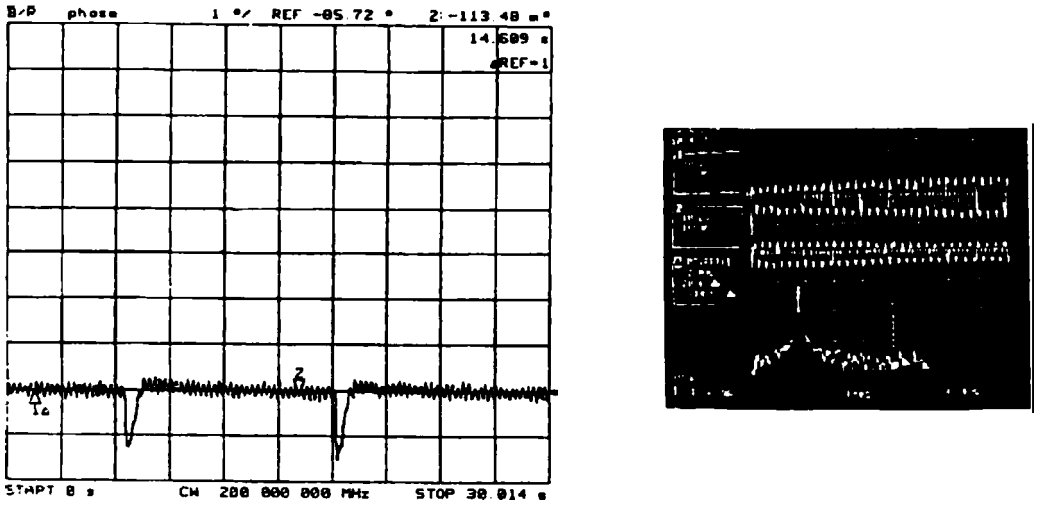

a) b)

Fig.5.8. a) Dependence of the neutralization factor on time, b) signal from gun pick-up during burst of instability, the same for the collector pick-up, the spectrum of the transverse oscillations registered with the gun pick-up.

5.3. Free transverse oscillations of the NEB in the Test Bench

The free transverse electron-ion oscillations were investigated also with the pick-ups placed before the collector trap (see Fig. 2.3). The burst of instability occurs in the system when the beam current exceeds the threshold magnitude. The amplitude of the pick-up signal during the burst of instability increases with the beam current (Fig. 5.9). It is associated not only with an increase of the beam charge, but also with the growth of the oscillation amplitude.

Typically the oscillation amplitude is of the order of 0.1 mm at $I_e = 300$ mA (the PU signal in this case is about 10 mV).

The resonant frequency of transverse oscillations registered with the pick-up electrode corresponds to the ion coherent frequency f_I with atomic number $A/Z_i \approx 12 \div 14$.

The more detailed spectral studies of transverse oscillations were done at low heating of the gun cathode, when the threshold of instability increases (Fig. 5.10).

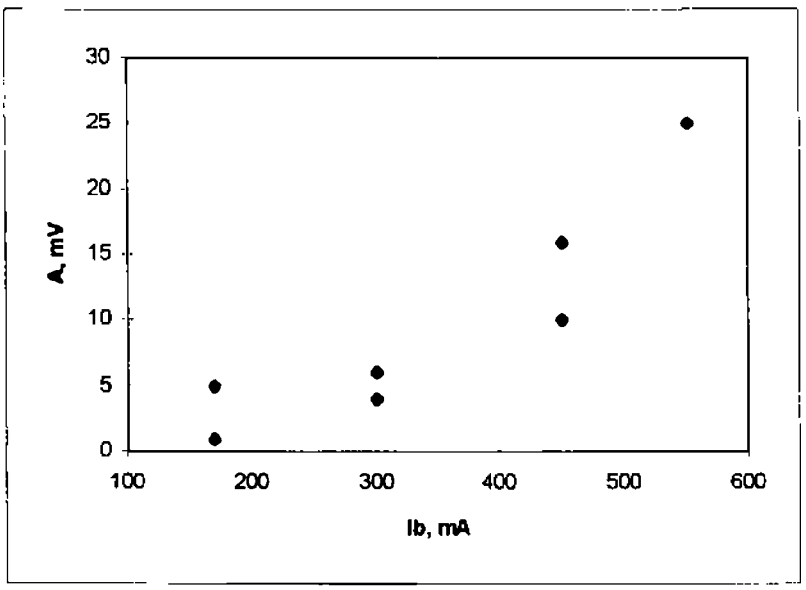

a

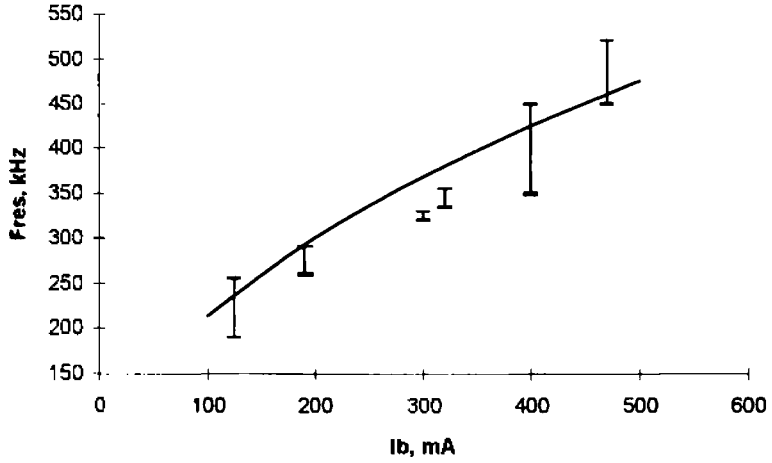

b

Fig. 5.9. Dependence of the amplitude (a) and the resonant frequency (b) of free transverse oscillations on the beam current.
The curve presents the frequency dependence calculated for $A/Z_i = 14$

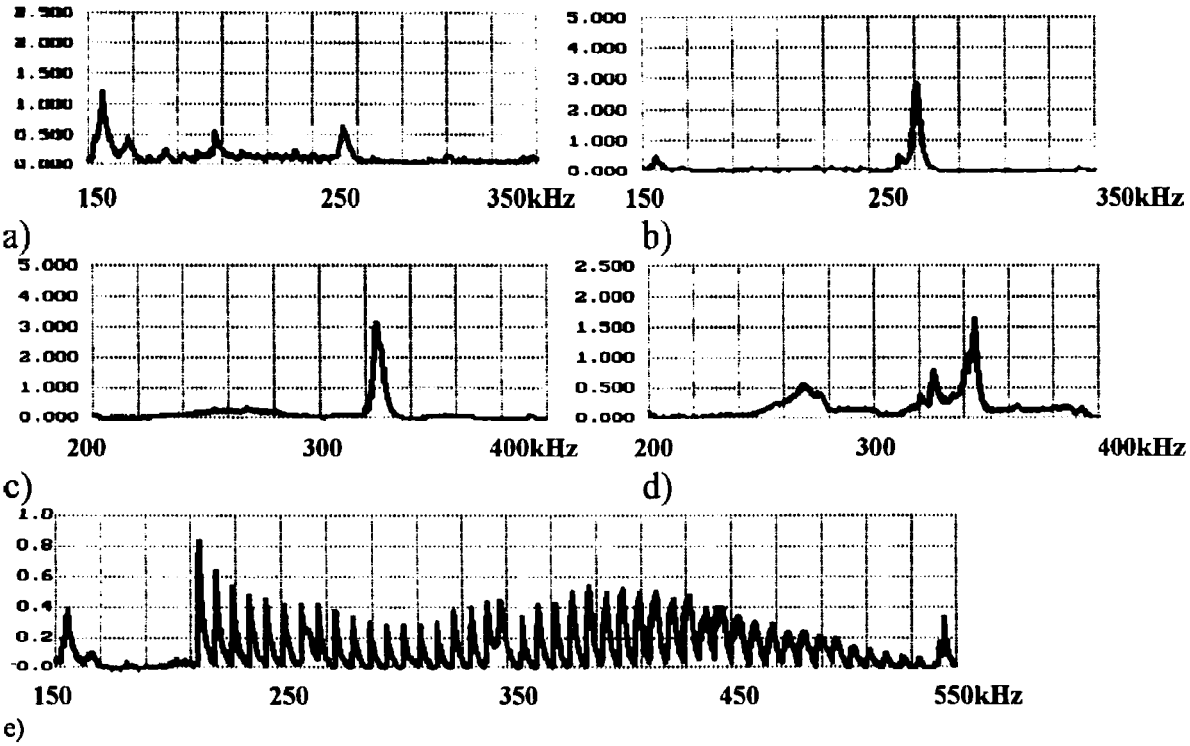

Fig. 5.10. Spectrum of the transverse oscillations at the different beam current values.

U_0 = 2.5 kV, B = 500 G, P = 2-4 nTorr

I_e(mA) = 50(a), 170(b), 230(c), 300(d), 360(e);

Y-axis:1 division = 20 μV [(a)-(d)], 60 μV (e).

The bursts of instability appeared at the beam current I_e = 130 mA. The spectral interval of these transversal oscillations is relatively wide for beam current less than 130 mA. The resonant frequency lies in the range 180 - 260 kHz (Fig. 5.10 a). The resonant oscillations occur at the ion coherent frequency for beam current 170 - 300 mA (Fig. 5.10 b-c). This spectrum has a narrow maximum. The resonant frequency increases with the beam current (Fig.5.10 b-c). The width of spectrum characterises the damping decrement [see Section 1.4 Formula (1.42)]. It is small at beam current 170 - 300 mA, i.e. $2\Delta f/f \sim 0.01$-0.05, but increases significantly, when the beam current exceeds 360 mA (Fig. 5.10 d). In this case $2\Delta f/f \sim 0.5$ (Fig. 5.10 d,e). The burst of instability with small amplitude does not lead to a neutralisation destruction, if the beam current is less than 300 mA (see Fig. 5.10 a-e). For a beam current of more than 300 mA theneutralisation is completely unstable.

When the beam current is near 360 mA, the oscillation amplitude also increases during an instability burst, but the level of this signal is lower compared to the previous case (Fig. 5.10 b and c). This corresponds to an ion escape from the beam. After the neutralization jump the amplitude of transverse oscillations reduces and the beam returns to the stable conditions.

We have to stress an effect, which can lead to a wrong interpretation of the characteristics. The point is that the spectrum analyser used in the experiments (which works in the frequency sweeping regime) has finite filter band width

δf = 3kHz and finite read-out time. The analyser reads an instantaneous value of the oscillation frequency, if it coincides with that of the analyser heterodyne frequency (which is scanned at a certain rate $\dot{f}$ ~ 40 kHz). However, during an instability burst the oscillation frequency varies in some range Δf (210-490 kHz for the parameters of Fig. 5.10, e). When the scanning time is much longer than the period T of the burst repetition, the analyser reads the corresponding frequency in the frequency variation range N times, where

$$N = \frac{\Delta f}{\dot{f} T},$$

and the width of the registered "spectrum" peak is of the order of δf (Fig. 5.11). *The real width of the spectrum* of oscillation burst is equal to the frequency range, where a " fence" of the spectral peaks appears. For instance, in the case of Fig. 5.10 e it is $\Delta f \approx 250$ kHz.

If the frequency range is small or the repetition rate is very low, the spectrum appears on the analyzer screen as a single peak (Fig. 5.10 b-d).

The oscillation amplitude distribution along the beam was studied. In these experiments the beam neutralisation was produced with steering electrode and clearing electrodes, while the electrodes of the gun and collector traps were used for measurement of transverse oscillations at two points of the neutralized beam (see Fig. 2.3).

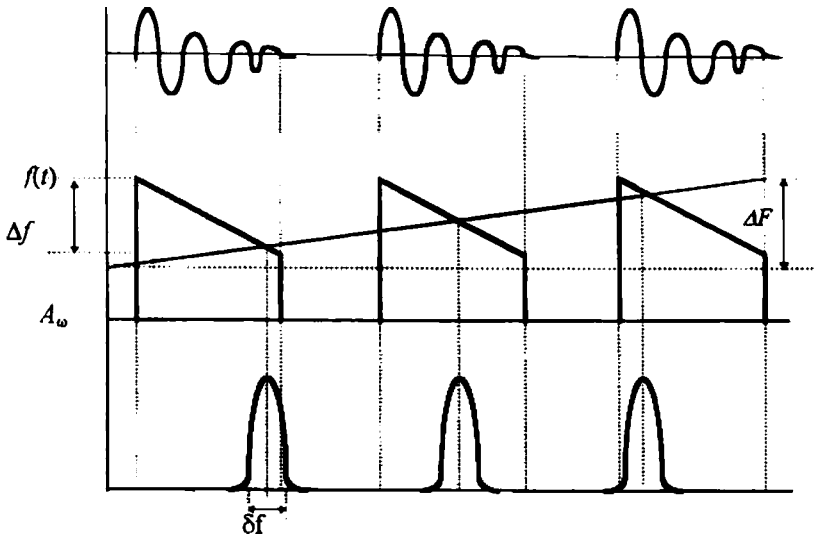

Fig. 5.11. Schematics of the oscillation burst analysis.
$U_{PU}(t)$ - the signal from PU-electrodes; $f(t)$ - the frequencies: 1 - the oscillation frequency variation during the "burst", 2 - the scanning frequency of the analyzer (f_{anal}), A_ω - the registered spectrum.

The spectra of transverse oscillations measured at the Test Bench demonstrate a distinct amplification of the oscillation amplitude along the beam (Fig. 5.12). The ratio of the gun neutralization (trap) electrodes (GT) amplitude to collector ones (CT) at the resonant frequency and the beam current 200-300 mA reaches the level K_{res}~10÷13 (remember, that the distance between GT and CT is equal to 1.7m). It decreases to 1.5-2, when beam current increases up to I_e = 360 mA. These results differ strongly from the NEB behaviour in ECOOL.

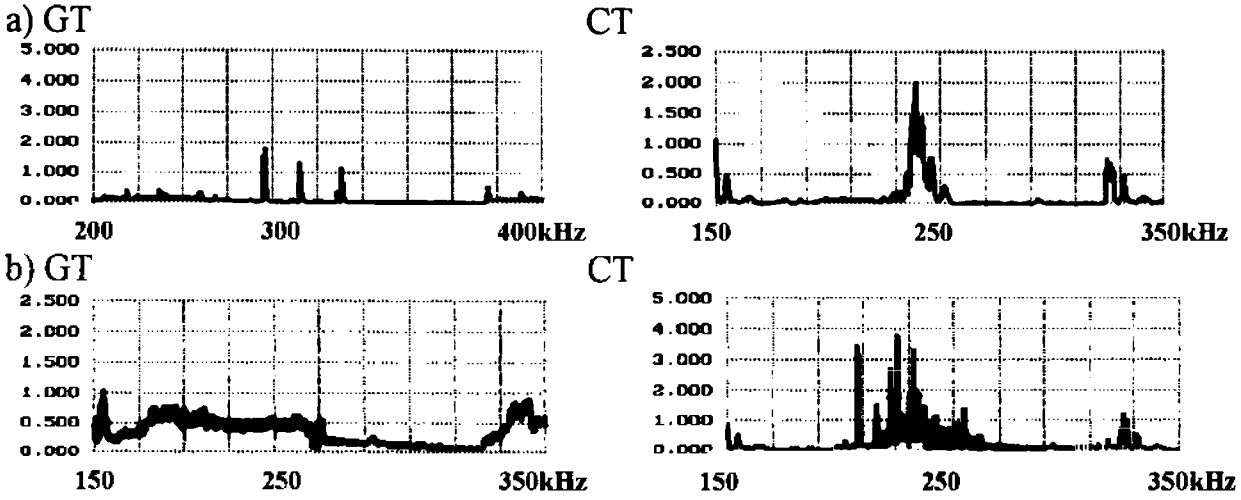

Fig. 5.12. Spectra of transverse oscillations obtained at the Test Bench, using the gun neutralization (trap) electrodes (GT) and collector ones (CT) respectively as pick-up electrodes

$U_0 = 2.5$ kV, $B = 500$ G;

I_e(mA) = 130(a), 200(b) 1 unit = 60 μV.

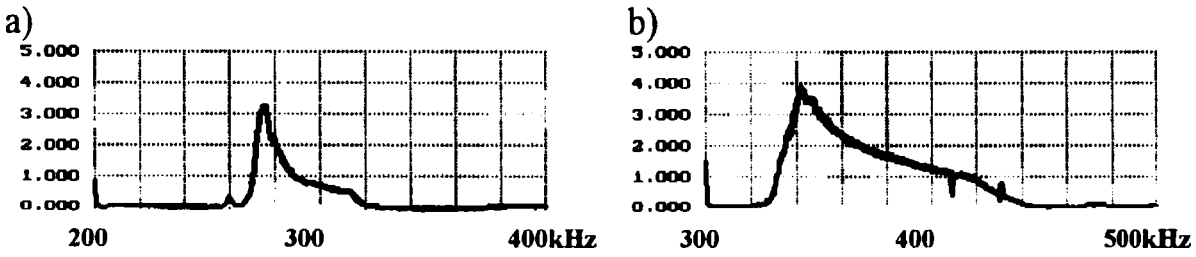

Fig.5.13. Spectra of free transverse oscillations for different magnitudes of the beam current: $I_h \sim 6$ A, $U_0 = 2.5$ kV, $B = 500$ G,

$P = 3$ nTorr; I_b(mA) = 310(a), 470(b); 1 unit = 20 μV.

One should stress that these results were obtained for low cathode heating current $I_h \sim 6$ A. In the case of the heating current, $I_h = 10$ A, the threshold of the beam instability reduces. At the same time the narrow peak at the resonant frequency transforms into a "fence" of spectral peaks, when the current is equal to 130 mA (Fig. 5.12). The PB indicates an appearance of the unstable regime, when the current exceeds 150 mA.

In some experiments oscillations were observed, where the frequency corresponds to that of coherent oscillations of ions with $A/Z_i = 26$-28 (Fig. 5.13). The spectrum is rather narrow -$2\Delta f/f \approx 0.05$-0.1 (Fig. 5.14). One has to emphasise here that two different states (different frequencies) with $A/Z_i = 14$-16 and $A/Z_i = 26$-28 were observed at the same beam current. A transition from one state to the other occurs under the influence of the shaker, which can be associated with a change of ion composition, like

$$N_2 \rightarrow N_2^+, \quad N_2^+ \rightarrow N^+$$

(see Table 6.1).

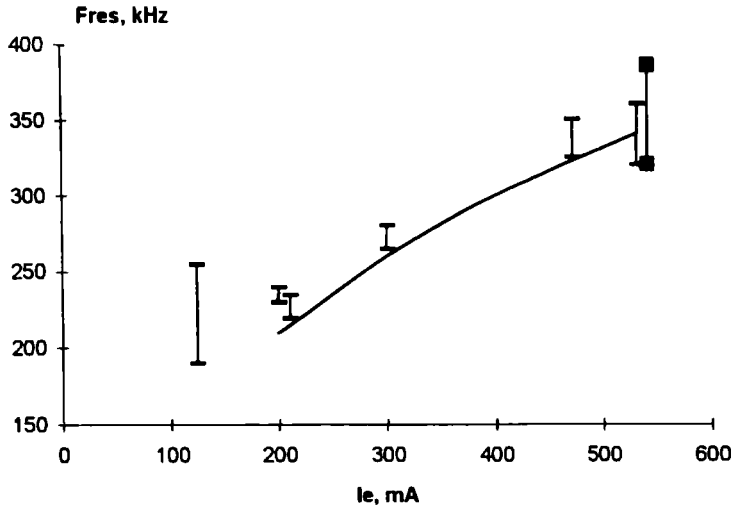

a)

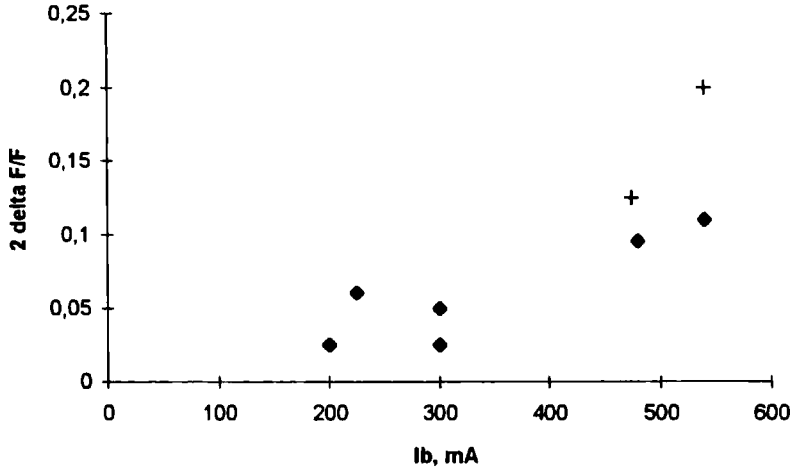

b)

Fig. 5.14. Dependence of resonant frequency (a) and frequency width (b) of free transverse oscillations on the beam current
• stable regime, + unstable regime.
The line on the Fig. 5.14a is calculated for $A/Z_i = 26$

5.4. Beam transfer function measurements on ECOOL

The experimental investigations of the transverse oscillations on ECOOL were carried out by excitation of the electron beam in the transverse direction for the stable regime of the neutralisation. This was done by applying an Rf-voltage to "pick-up electrodes" using them as a kicker. The displacement of the beam electrons under the influence of the transverse electric field generates a travelling wave on the beam. The beam response, i.e. the beam transfers

function (BTF) (Fig. 5.15), was measured by differential pick-up electrodes about 1m downstream of the kicker. The peaks of the BTF signal correspond to excitation of the transverse waves with the ion coherent frequency f_l for the ions with the different ratios A/Z_i [see Eq. (5.1)]. The resonant frequencies slowly increase with the beam current (Fig. 5.16).

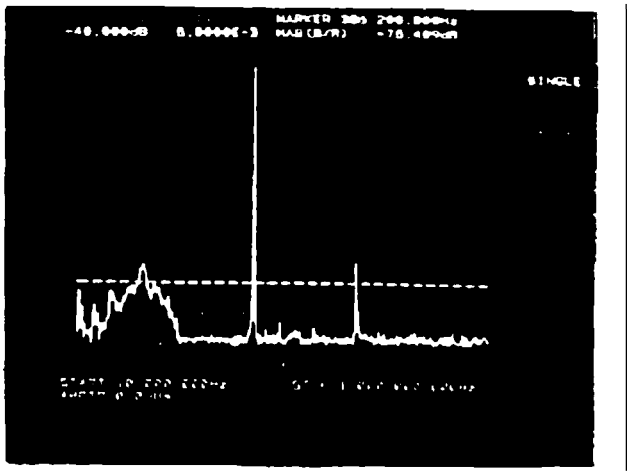

Fig. 5.15. The ECOOL BTF measurements: $U_0 = 27$ kV, $B = 600$ G, $I_b = 1.54$ A.

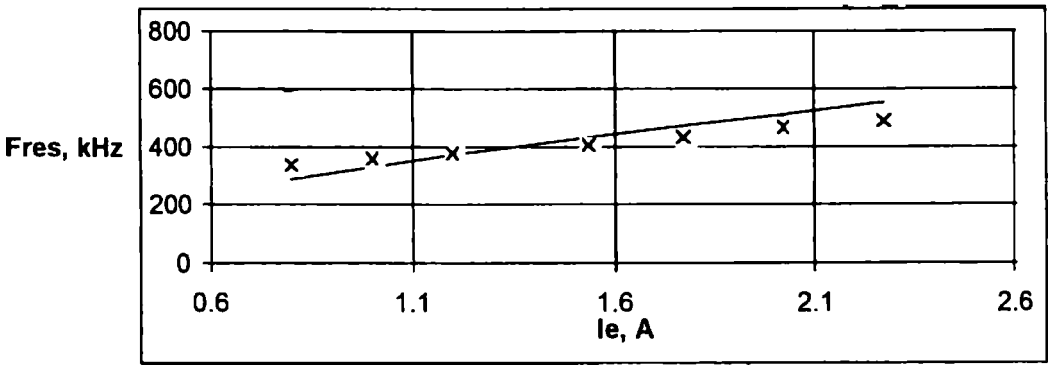

Fig. 5.16. Dependence of resonant frequency on the beam current: $U_0 = 27$ kV. Experiments, × resonance frequency. Calculations. - —— - coherent frequency (Formula (5.1) $A/Z_i = 4$).

The BTF signal in the frequency range $f < 200$ kHz vanishes when the potential of the neutralization electrodes is sufficiently increased. This effect is probably associated with the clearing of secondary electrons.

5.5. Beam current threshold of the beam-drift instability

As mentioned in Section 1, the NEB current is limited by the development of the beam-drift instability. The beam current density threshold is given by Eq. (1.39). The value of the numerical coefficient k (1.39) depends on the feedback, which can occur e.g. through the secondary electrons.

The threshold beam current increases with the electron energy for both facilities, ECOOL and Test Bench (Fig. 5.17, Fig. 5.18). For ECOOL the lower limit of the stable beam current was also observed.

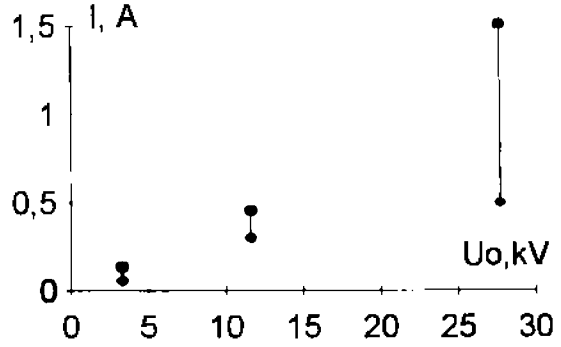

Fig. 5.17. Dependence of the upper (◆) and lower (●) current limits on the accelerating voltage for ECOOL (B = 600 G), $P=10^{-11}$ Torr.

The beam is stable between the lower and upper current limits. The neutralization factor between these limits is equal to 0.7-0.9.

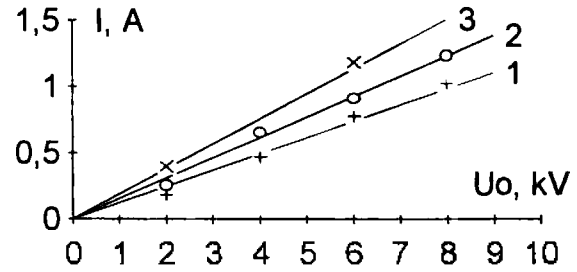

Fig. 5.18. Dependence of the threshold beam current on accelerating voltage for the Test Bench.
P (nTorr) = 3 (1), 60-80 (2), 150-400 (3), B=500 Gs.

The threshold beam current decreases with pressure increase (Fig. 5.19).

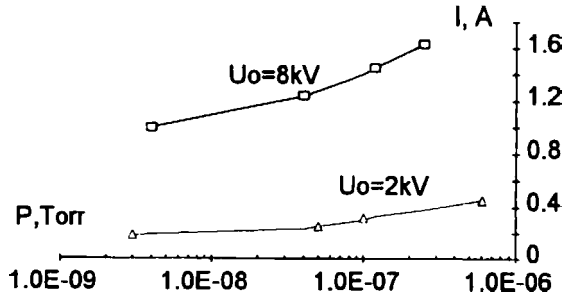

Fig. 5.19. Dependence of the upper beam current threshold on the pressure in the Test Bench

The density of the beam current near the upper threshold for pressure 1 pTorr in the ECOOL is four times less than in the Test Bench for pressure 1 nTorr (Fig. 5.20) at the electron energy of 3 keV.

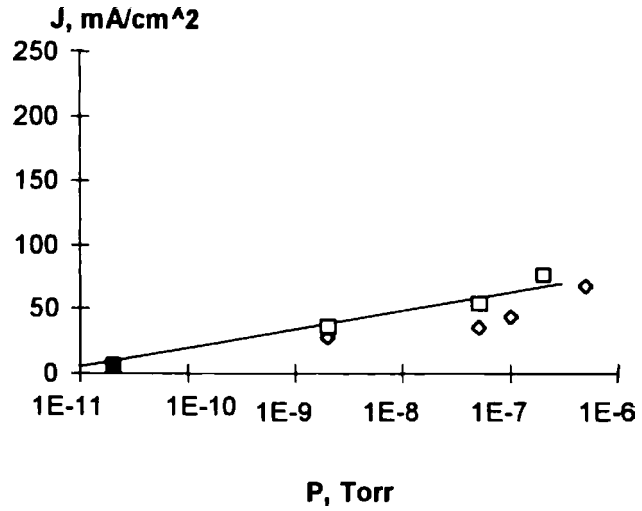

Fig. 5.20. Dependence of the threshold beam current density on pressure
■ ECOOL experiment: $B = 600$ G, $U_0 = 3$ kV, $L = 3.2$ m;
Test Bench experiment: □ - $U_0 = 3$ kV, ◇ - $U_0 = 2$ kV; $B = 450$ G, $U_{el2} = U_{el4} = 4$ kV, $U_{el3} = U_{el1} = 0$, $L = 1.9$ m.

The threshold beam current depends also on the cathode heating current (Fig. 5.21).

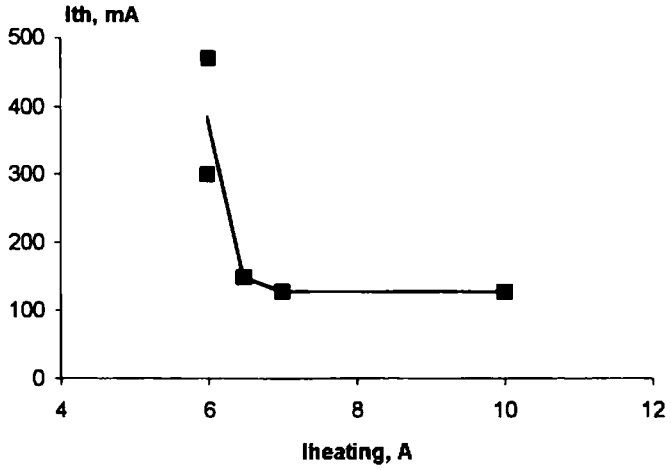

Fig. 5.21. Dependence of the beam current threshold on the cathode heating current in the Test Bench
$U_0 = 2.5$ kV, $B = 600$ G, $P = 2$ nTorr.

The beam current threshold may be increased, if special tools are used for this purpose (see Section 6).

5.6. Summary and discussion of the wave phenomena

One can summarize the main results of BTF and wave measurements on ECOOL and the Test Bench as follows.

1.When the ***NEB is stable***, its BTF in ECOOL has the resonant frequency (Figs. 5.15 and 5.16) which corresponds to the ion coherent oscillation frequencies (see Formula 5.1) at A/Z_i = 4÷6. The oscillation spectra in the TB have a resonant frequency at A/Z_i = 12-16, 26-30. The difference of the ratio A/Z_i for ECOOL and TB is related to the difference of vacuum conditions. The value of A/Z_i is determined by primary electron density n_e and neutralization time τ_{neutr}, $A/Z_i \propto (n_e \tau_{neutr})^{-1}$.

2.The spectrum width of the ***stable NEB*** state is very narrow: $2\Delta f / f_{Res} \approx \varepsilon''_{\perp} \cong 0.05 \div 0.1$ for ECOOL and 0.05÷0.15 for the Test Bench spectra (see Fig. 5.16) . Using Formula (1.42), one can find that $\varepsilon'' \cong 0.05 \div 0.15$ at I_e = 200-540 mA.

3. The module of the amplification coefficient at the resonant frequencies of the ***stable NEB*** is equal to:

ECOOL (indirect measurements) $K = 30$

Test Bench (direct measurements) K = 12÷15 (this corresponds to $\varepsilon'' \cong 0.08$ at I_e = 170÷230 mA) .

These results were extracted from the measurements of $\Delta f/f$ and the calculations of ε″ for ECOOL and TB. The direct measurements at the TB have given results that agree with indirect measurements for ECOOL.

The direct measurements of an amplification coefficient, performed in ECOOL in a regime of an ***unstable NEB*** (Fig. 5.9), did not show any amplification. That can be explained also by a saturation of the oscillation amplitude on the length less than 0.9 m.

4. The frequencies of the oscillations during an ***instability development*** ("burst") correspond to those of the ion coherent oscillations in ECOOL (A/Z_i = 4÷6) and TB (A/Z_i = 12-28).

The experimental data presented in Section 5, allow an estimate (Table 5.1) the coefficien k in Formula (1.39).

One should stress that previous research gave k equal to 1.27 [20] and 0.76 [5].

In the TB the decrease of the cathode heating current from 10 A to 6 A allows an increase in the stable NEB current from 130 mA up to 400 mA, when the pressure is 1÷2 nTorr. One can suppose that such an increase of the stable NEB current is associated with the beam inhomogeneity, which appears near its boundary.

All the results presented in Section 5, mean that a way for further development of the neutralization method and an enhancement of the NEB current can be found.

Table 5.1. Results of estimations for $\varepsilon_{\perp}''$ Eq. (1.44) and k Eq. (1.39)

Measurement method	Measured parameter	Formula	$\varepsilon_{\perp}''$ LEAR	$\varepsilon_{\perp}''$ TB	k LEAR	k TB
BTF signal, (Fig. 5.15)	$2\frac{\Delta f}{f} \approx 0.03 \div 0.1$	(1.34) (1.36) (1.42)	0.05-0.1	--	4.5	
Spectrum max. width (Fig. 5.14)	$2\frac{\Delta f}{f} \approx 0.03 \div 0.1$	(1.34) (1.36) (1.42)	--	0.05-0.15		1.8-0.7
Wave amplification (Fig. 5.12)	$K = 10 \div 15$	(1.36)	--	0.075		1.3
"Burst" pulse parameters (Fig. 5.3)	$\tau \approx 0.1\ ms$	(1.33)	0.03		4.5	
Threshold current (Figs. 5.17-5. 21)	I_{th}	(1.36) (1.39)	0.05-0.1	0.05-0.15	4.5-5.8	2.7-1.75

6. INSTABILITY SUPPRESSION AND THRESHOLD CURRENT ENHANCEMENT

The experiments, described in Sections 4, 5, as well as early experiments, performed in Budker Institute INP [4,5] for parameters, very different from present ones, suggest two main reasons for the instability development [14,17]:

- the existence of an effective feedback;
- a very low ion temperature.

The main source of the feedback, we suppose, is a flow of secondary electrons, escaping the collector and passing along the beam in the opposite direction [7-9]. In principle, these electrons can oscillate a few times back and forth before leaving the beam due to some transverse drift or any other reason.

The low heating of ions is favourable for an instability development. One can illustrate this with the following qualitive explanations. Let us suppose, that the feedback limits the stable neutralization factor to some value η_{FB}. The relation between the ion temperature T_i and η is given by the function $T_i^0(\eta)$(see Fig. 6.1), as described in Section 1.3. Then let the ions gain in temperature during the neutralization process (from some heating source), so that the temperature goes up, as ions are being stored. This heating can be represented by the functions 1-2 on Fig. 6.1. The highest η - value at a stable NEB state can be reached, evidently, as close as possible to $\eta_{unstable}$. This means that the ion heating by an external source is a delicate process, but, any way, it needs to be tested.

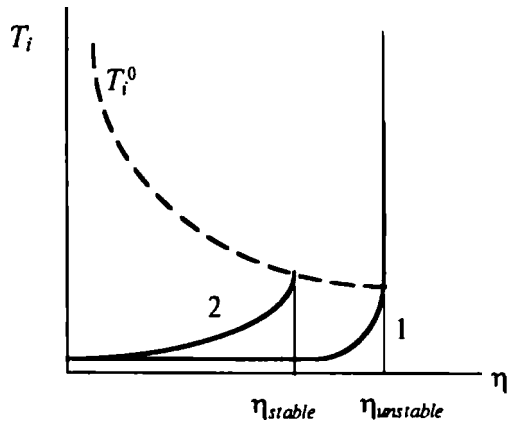

Fig. 6.1. Diagram of the neutralization process: $T_i^0(\eta)$- the relation between T_i and η values; $\eta_{unstable}$ - a limit of the neutralisation factor due to an instability developed by the feedback influence, 1- the dependence of T_i on η for the "passive" regime of the ion heating, 2 - the dependence of T_i on η, when some additional heating is present.

Such a preliminary understanding suggests three methods of further studies with NEB:

- clearing of secondary electrons or improvement of the collector efficiency [18,14,17],
- ion heating with the "shaker" [19,11,14,17]
- electron beam modulation [14,17].

These methods and experimental studies of the NEB behaviour under the action of the methods will be described in the rest of this chapter.

6.1 Secondary-electron clearing

To eliminate the feedback associated with the secondary electrons [7-9], a clearing electrode (CE) [18,14,17] was placed in the Test Bench vacuum chamber between the collector and the collector trap. The CE design is similar to that of the ion trap (Fig. 6.2): it consists of two half-cylinders 40 cm long and 10 cm diameter. Four conductive glass plates are placed between the electrodes - two on each side. The plates are 7×28×80 mm. Two coils producing a transverse magnetic field are placed outside of the vacuum chamber. Their maximal magnetic field is about 40 G. A positive potential of 4-6 kV is applied to one electrode, a negative potential of 0-2 kV is applied to the other one.

To avoid a disturbance of the primary beam by CE transverse electric field $E_\perp$, an additional transverse magnetic field $B_{\perp\perp}$, perpendicular to $E_\perp$, is applied. it compensates, in the first approximation, the primary electron drift, if

$$B_{\perp\perp} = E_\perp / v. \tag{6.1}$$

Then the secondary electron displacement after the passing clearing electrodes is

$$\Delta = 2\frac{E_\perp}{vB} L. \tag{6.2}$$

However, the space between electrodes is non-equipotential, which introduces some shift of electron velocity:

$$\frac{|\Delta v|}{v} \le \frac{eE_\perp a}{2\mathcal{E}_e}. \tag{6.3}$$

This shift leads to some deformation of the electron beam:

$$\Delta Y \sim \frac{B_{\perp\perp}}{B}\frac{\Delta v}{v} L \sim \frac{eB}{2vmc^2}\frac{\Delta^2}{L}. \tag{6.4}$$

At certain conditions this deformation can be significant.

For instance, for B = 500 G, $\mathcal{E}_e$ = 2.5 keV, L = 50 cm and Δ = 2.5 cm, Eq. (6.4) gives ΔY = 0.19 cm. The electric field, providing the displacement of 2.5 cm here is about 400 V/cm.

The detailed analyses of electron trajectories inside traps and clearing electrodes is given in Appendix 2.

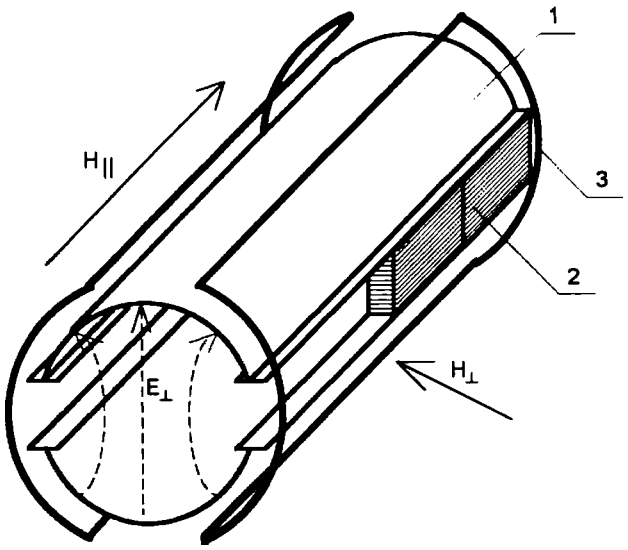

Fig. 6.2. The clearing electrodes.

6.2. Experiments with clearing electrodes

The experiments with clearing electrodes on the Test Bench were performed for the electron energy ε_e = 2.5 kV, beam current 100-600 mA in the magnetic field B = 500 G at pressure 2-8 nTorr.

The summary of the results obtained in the experiments with CE, shaker and modulation (see below, Sections 6.3 and 6.4) on the Test Bench are presented on Fig. 6.3.

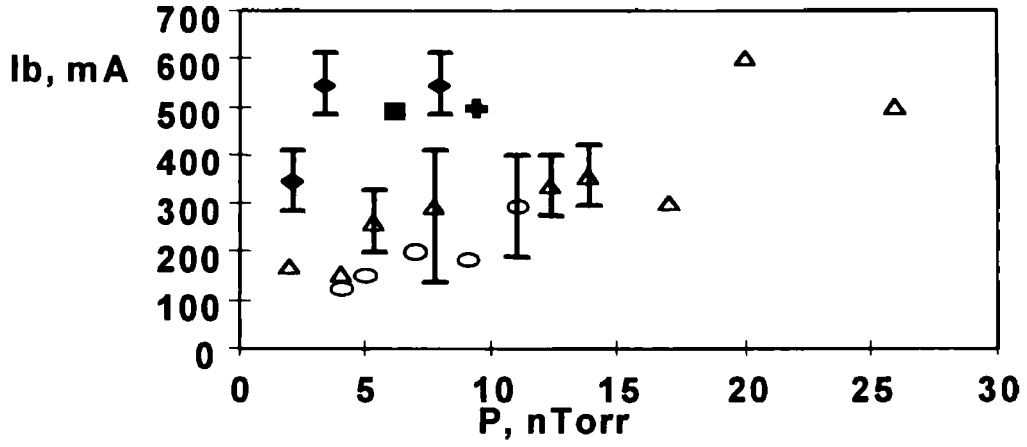

Fig.6.3. The dependence of the threshold current on the residual gas pressure:
○ - with neutralization electrodes, △ - with CE and neutralization electrodes (NE), ■ - with NE and clearing by gun electrode ◆ - with CE, NE and shaker, + - with NE, CE and longitudinal modulation.

The use of clearing electrodes allows an increase in the threshold current of approximately 1.5 times at fixed pressure.

The CE influence on the NEB stabilisation is weaker than that of the shaker (see Section 6.3 below). But their use increases the neutralization factor due to two reasons: they clear the secondary electrons and allow a reduction in the shaker voltage.

The influence of CE and traps on the current losses was investigated in more detail for two different values of the pressure. An increase of the current losses with the CE voltage of a factor 10 does not lead to an essential variation of the pressure. The pressure rises from 2 nTorr to 4-6 nTorr when the CE electrode voltage is turned on and reaches 4-6 kV. The current loss level with the clearing electrodes corresponds to that with traps, when the electrode potentials satisfy the equality

$$U_{el1} - U_{el2} = (U_{el3} - U_{el4}) \frac{L_{el}}{L_{cl}} \tag{6.5}$$

where $U_{el3,4}$ is the collector trap electrode potential, L_{el} the trap length, L_{cl} the clearing electrode length.

For the stabilisation of a neutralized electron beam, the regime when the CE electrode potentials are equal to 4/0 kV and the transverse magnetic field is "OFF" is preferable to the regime with CE potentials 7/-1.5 kV, transverse magnetic field "ON". One could not increase the CE potentials higher than 4/0 kV without the beam position correction with transverse magnetic field. The clearing electrodes were usually used in the regime (CE voltage U_{cl} = 4/0 kV) when secondary electrons were cleared between the gun and the collector. Their density is the determined by the relation [8,9]:

$$\frac{n_{sec}}{n_e} = \frac{I_{sec}}{I_e} \left(\frac{b_{cl}}{\Delta x}\right)^2 \Delta\psi \,, \tag{6.6}$$

where $\Delta\psi$ is the rotation angle of the secondary electrons produced by space charge of the primary beam, Δx is the displacement of the secondary electrons inside the clearing electrodes, b_{cl} the radius of the clearing electrodes. The increase of secondary electron displacement inside the CE leads to a reduction of the secondary electron density and simultaneously the feedback coefficient decreases. This can be obtained with a better collector efficiency.

6.3. Experiments with the shaker

To stabilise the NEB instability the method of the "shaker" was implemented [19]. It was tested in experiments on ECOOL [11,14,17,19] and later on the Test Bench [14,17].

The idea of the shaker is to use a pair of electrodes, applying the transversal RF voltage at an optimal (to be found!) frequency, to heat and, if necessary, knock out ("to shake out") the ions. The shaker mechanism is analysed in detail in Appendix 3.

The ion heating with the shaker electric field has a diffusion character because of random phase, which the field has at the moment when an ion enters the shaker. The field is transversal, but it produces the heating over all three dimensions freedom, because of thermalization in ion collisions with other ions, atoms and, most particularly due to skewed reflection on the trap fields.

The heating with the shaker stabilises the NEB state, but it increases the ion escape from the NEB, which results in an η decrease.

The heating time is estimated as (see Appendix 3) [14]

$$\tau_h \approx \tau_{\|}\left(\frac{2M\Omega\omega_{sh}a}{ZeE_{sh}}\right)^2 , \tag{6.7}$$

where $\tau_{\|}$ is the half-period of ion longitudinal oscillations, E_{sh}, ω_{sh} the electric field and the frequency of the shaker, $\Omega = \sqrt{\omega_i^2(1-\eta) + \omega_B^2/4}$. The ions can be shaken out from the system because of excessive heating, and the neutralization factor reduces because of shaking. The choice of the shaker parameters can be determined by the condition, that the heating time is equal to the neutralization time [see Eq. (1.16)]

$$\tau_h \sim \tau_{neutr} . \tag{6.8}$$

Then the shaker voltage can be estimated as follows

$$U_{sh} = E_{sh}b \cong \frac{M\Omega\omega_{sh}ab}{Ze}\left(\frac{\tau_{\|}}{\tau_{neutr}}\right)^{1/2} \tag{6.9}$$

where b = 10 cm is the diameter of the shaker PU electrodes.

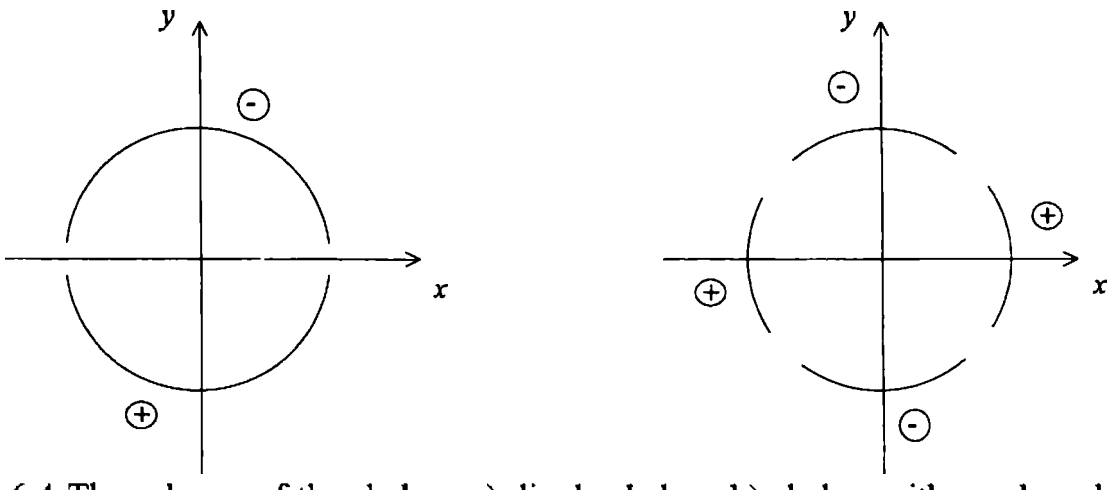

.Fig. 6.4 The scheme of the shaker. a) dipole shaker, b) shaker with quadrupolar polarisation of the transverse electric field.

6.3.1. Experiments with the shaker on ECOOL

The experiments were performed using an RF generator, whose voltage amplitude and frequency were optimised by observation, with the TOF-method, of the NEB. Such a process is illustrated in Fig. 6.5.

The optimal shaker frequency corresponds to that of the incoherent ion oscillations [see Formula (1. 43)]. It is about 100 kHz. The shaker voltage amplitude necessary to reach a stable NEB state was about 2-4V. The neutralization disappears (ions are "shaken out"), when the voltage is increased up to 12 V.

The shaker stabilises the NEB and allows one to reach a rather high η-level, when the frequency and amplitude are carefully optimized

In region 1, when traps and shaker are OFF, some natural neutralization [see Formula (1.11)] is present. This leads to NEB instability, which can be clearly seen on the picture. When the shaker is turned ON (region 2), the instability "jumps" disappear, but the η-level is low - it corresponds to a clearing of ions from NEB with the shaker. Turning ON the traps (region 3) we get stable and well neutralized beam. Finally, switching OFF the shaker at this state again provokes NEB instability.

One can observe also a very characteristic behaviour of the oscillation spectra of pick-up signals in all four regimes. At first (regime 1) the spectrum is wide, which corresponds to the frequency "jumps" during the beam neutralization. In regime 2, when all the ions are "shaken out", the spectrum becomes "quasi-monochromatic" and remains like this in regime 3, as long as the NEB is stable. In regime 4 the spectrum expands again. The stable NEB, which was obtained with the shaker at $\mathcal{E}_e$ = 2.8 kV and I_e = 0.3 A, had η = 0.4.

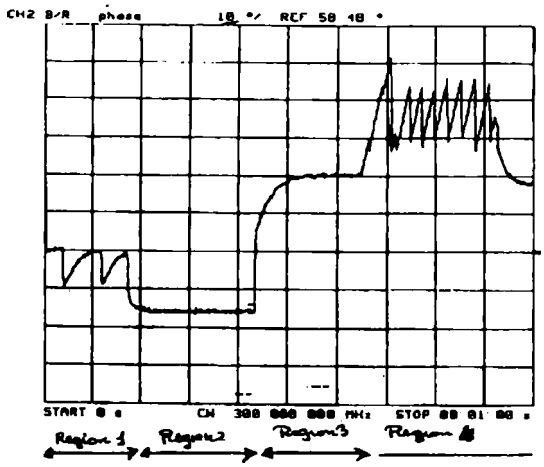

Fig. 6.5. The TOF signal at different NEB regimes at ECOOL

6.3.2. Experiments with the shaker on the Test Bench

The experiments at the Test Bench with a shaker were performed at an electron energy of

$\mathcal{E}_e$ = 2.5 keV, beam current I_e = 100-600 mA, trap voltage U_{el} = 4/0 kV, magnetic field 500 G, distance between neutralization electrodes L = 1.5 m and the pressure 2-4 nTorr.

For the Test Bench we have *the ion travelling time*

$$\tau_{\parallel} \cong \frac{L}{v_{i\parallel}} = 1.5 \cdot 10^{-4} \text{ s}, \qquad (6.10)$$

where $v_{i\parallel} = 10^6$ cm/s, and the shaker voltage can be found as

$$U_{sh} \cong 50 \text{ V}.$$

In the experiment the necessary shaker voltage was about 40 V. This voltage is applied to one shaker electrode, the other one is kept at zero potential.

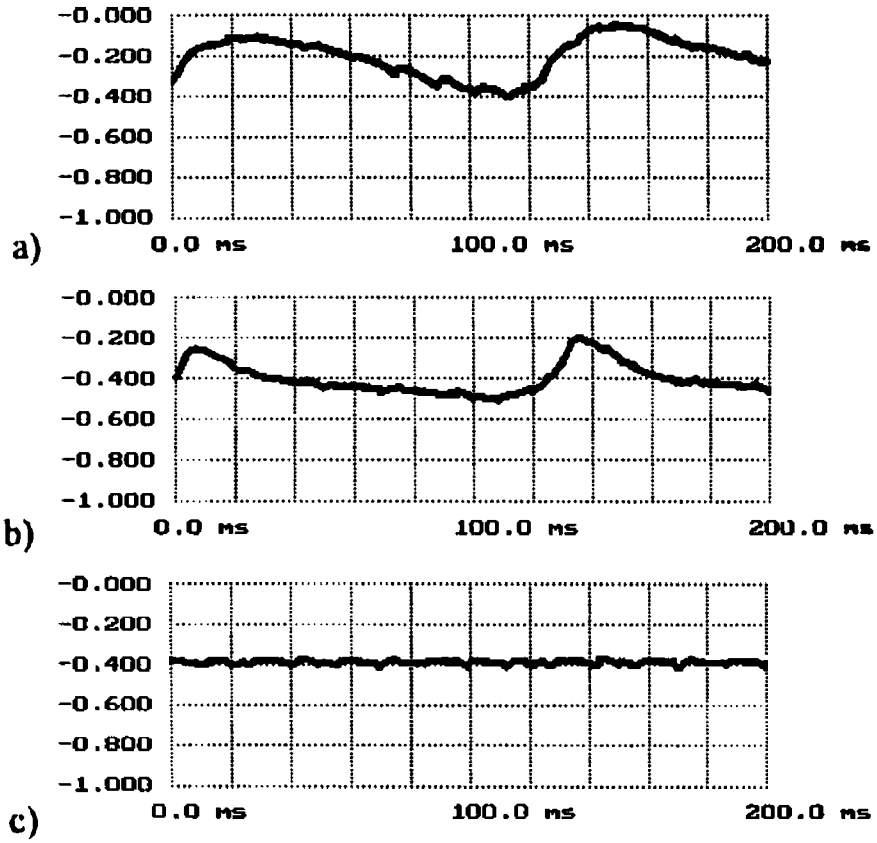

Fig. 6.6. Records of the pencil beam current.
$I_e = 400$ mA, $eU_0 = 2.5$ keV, $P = 4$ nTorr;
a) shaker and clearing are "OFF";
b) shaker "ON", clearing "OFF";
c) shaker and clearing are "ON".

The shaker voltage in these experiments is 10 times higher than for ECOOL ones, which can be explained by the value of neutralization time [see (6.9)]. This value in ECOOL is 100 times larger than in the Test Bench.

During measurements with the shaker the following parameters were investigated: frequency-amplitude characteristics of the shaker generator, neutralisation factor, frequency of the transverse electron-ion coherent oscillations in the neutralised beam.

The neutralization factor with the shaker alone is about $\eta \cong 0.5$. Without shaker the beam is stable at this pressure only if the beam current $I \leq 130$ mA. The stable regime was not reached with the shaker when beam current was higher than 400 mA (Fig. 6.6).

The use of clearing electrodes together with the shaker increases the upper current limit to 600 mA (Fig. 6.6.). The clearing electrode voltage in this experiment was equal to U_{cl} = 4/0 kV, (one electrode has the potential of 4 kV, the other one - zero). The neutralization factor was equal to 0.4.

The ion behaviour, observed is more important for stabilisation than the secondary electron influence. The clearing electrodes amplify the shaker stabilising effect. They help to increase the threshold current by 1.5 approximately. The clearing electrodes allow a reduction in the shaker electrode voltage as well and increase of the stable neutralization factor. The beam can be stabilised when the shaker frequency is placed near the ion incoherent frequency [Formula (1.43)].

The optimal shaker frequency increases with the beam current (Fig. 6.7.) [Eq. (1.43)].

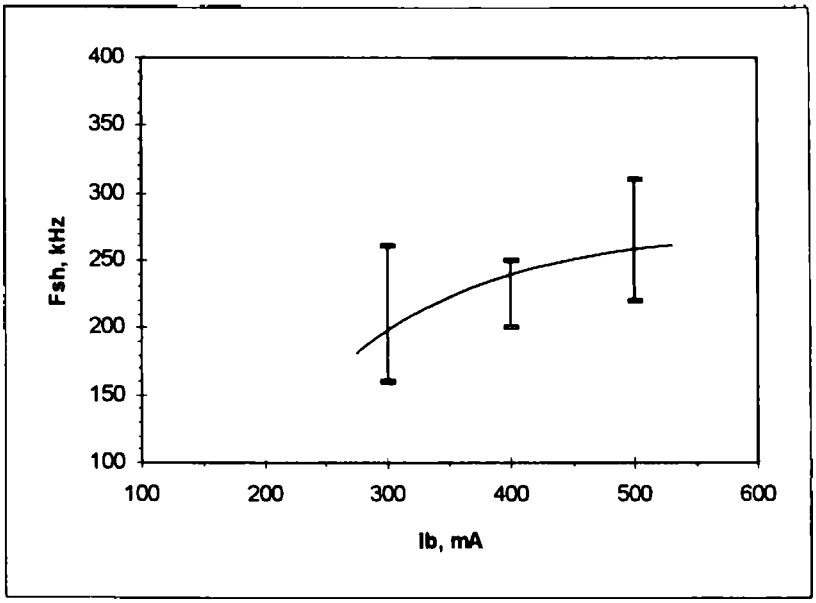

Fig. 6.7. Dependence of the optimal shaker frequency on the beam current: I - experimental data, the theoretical curve corresponds to A/Z_i = 28 in Formula (1.43).

One should underline that even in a stable state of NEB (confirmed by the pencil beam signal) the bursts of transverse coherent oscillations were observed on the PU electrodes, when the beam current exceeded 130 mA. The differential signal from two pick-up electrodes had an amplitude and frequency, which increased with the beam current (Fig. 6.7). The repetition frequency of bursts is of the order of 10-100 Hz.

6.3.3. Coherent oscillations of the NEB with the shaker in use

The NEB coherent oscillations were studied on the Test Bench at *reduced cathode heating*: I_h = 6 A and the parameters

$$\mathcal{E}_c = 2.5 \text{ keV}, I_e = 200\text{-}500 \text{ mA}, B = 500 \text{ G}.$$

When the shaker was used, the NEB remained stable at I_e = 200-470 mA, as was indicated with PB.

When *the beam is stable* (when the shaker is OFF or ON) the oscillation spectrum has a narrow width. When the shaker is OFF the spectral maximum corresponds to the ion coherent frequency at A/Z_i = 14 (Fig. 5.10), A/Z_i = *28* (Fig. 5.16a). The dependence of the maximum value on the NEB current is in good agreement with Formula (1.34), if the parameter A/Z_i is chosen properly. The examples of the spectra (Fig. 5.11d, Fig. 5.15.) prove the existence of monochromatic coherent oscillations.

When the shaker is ON, the oscillation frequency increases with the shaker voltage amplitude (Fig. 6.8), and the oscillation amplitude, after a few ripples, drops down (Fig. 6.9 a). However, the neutralisation factor does not decrease significantly (Fig.6.9 b). At the same time, the frequency dependence $F(U_{sh})$ has three plateau. The frequency value of each one corresponds to the resonant frequency for a different ratios A/Z_i (Table 6.1). Such a behaviour of the function $F(U_{sh})$ can be explained, as fast escape of ions with small Z_i, for which the space charge potential barrier is small.

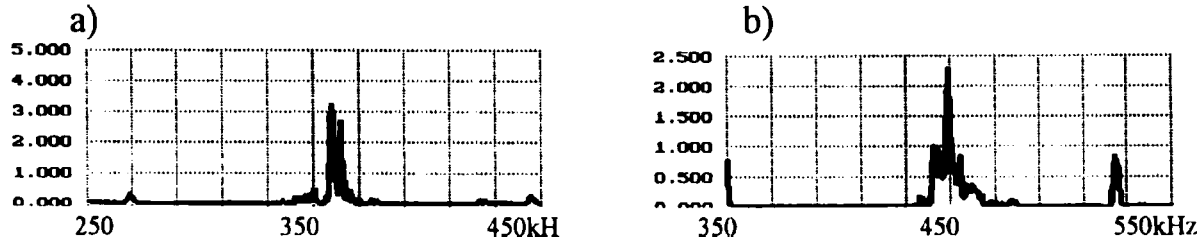

Fig. 6.8. The oscillation spectra at the Test Bench for different shaker voltage f_{sh} = 200 kHz, U_0 = 2.5 kV, I_e = 300 mA. U_{sh} = 6 V (a), 15 V (b).

One can suppose also, that such an increase leads to a significant heating of the ions, making them capable of escaping the beam potential well [see Formula 1.1], when their temperature reaches 40 eV (the typical numbers for I_e = 300 mA, β = 0.1 and η = 0.5). This hypothesis does not contradict the values of the ionisation potentials for different kinds of ions, which can participate in the process (Table 6.1).

Table 6.1. Characteristics of response to the shaker (Figs. 6.11, 6.12) for different ions

$f_{plateau}$, kHz	270		320		450		600	
A/Z_i	28	32	14	16	7	8	4	5
Ion type	N_2^+	O_2^+	N^+	O^+	N^{++}	O^{++}	N^{+++}	O^{+++}
Ionisation potential, eV	15.6	12.07	14.5	13.6	29.6	35.1	47.4	54.9

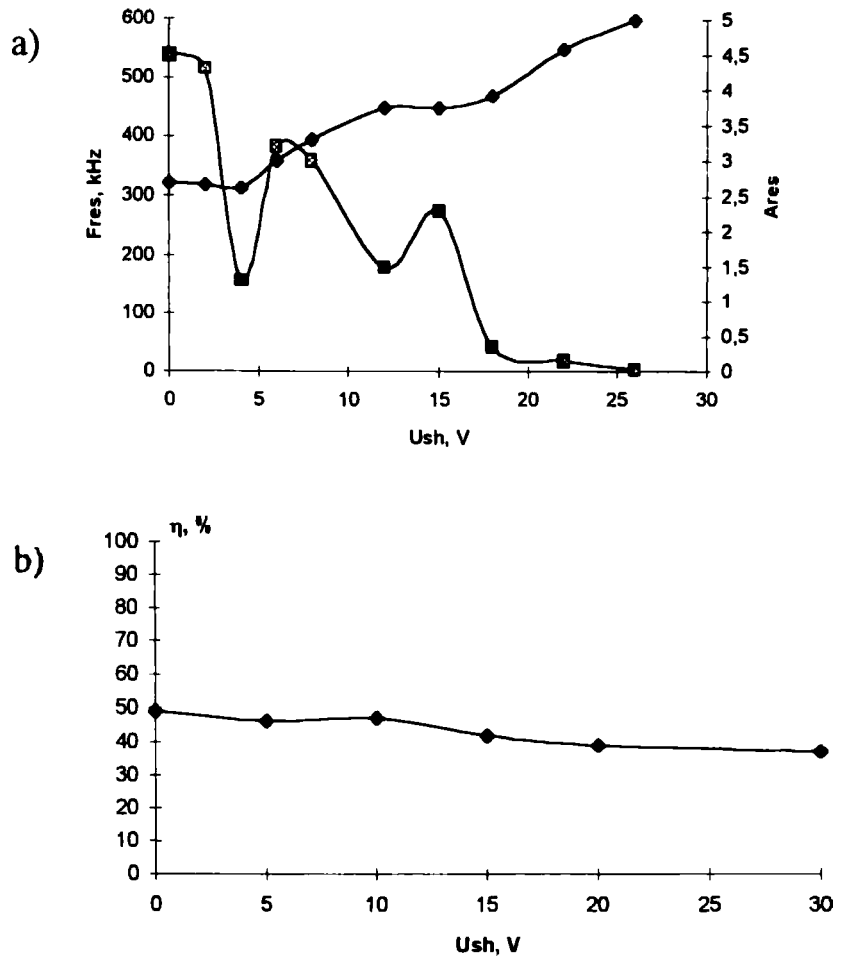

Fig. 6.9. Dependence of the maximum of the spectrum on the shaker voltage U_{sh} at the Test Bench:

a) ◆ the frequency and ■ the amplitude of the maximum of the spectrum; b) neutralisation factor

f_{sh} = 200 kHz, P = 3 nTorr, U_0 = 2.5 kV, I = 300 mA, B = 500 G.

The same explanation can be made for the dependencies of the ion oscillation spectra on the shaker frequency f_{sh} (Fig. 6.10 a,b,c). One can see that the frequency of the maximum of the spectrum has a quasi-resonant dependence on f_{sh} and this dependence reaches its maximum at the "optimal" frequency $(f_{sh})_{opt}$ ~ 200 kHz for given I_e and η. The value of this maximum increases with U_{sh} (compare curves 1-3), which agrees with the data in Table 6.1.

However, the amplitude response (Fig. 6.10b) has a minimum near $(f_{sh})_{opt}$. Perhaps this fact means efficient heating and "shaking out" of the ions from the beam near this "optimal" frequency. The spectrum width for an initially unstable state is large. It becomes smaller when the shaker is turned on, and the dependence of the spectrum characteristics on the shaker frequency in the "cured" NEB regime points to a significant "ordering" influence of the shaker. In fact, it suppresses the instability, orders the ion oscillation, but heats them at the same time, unfortunately.

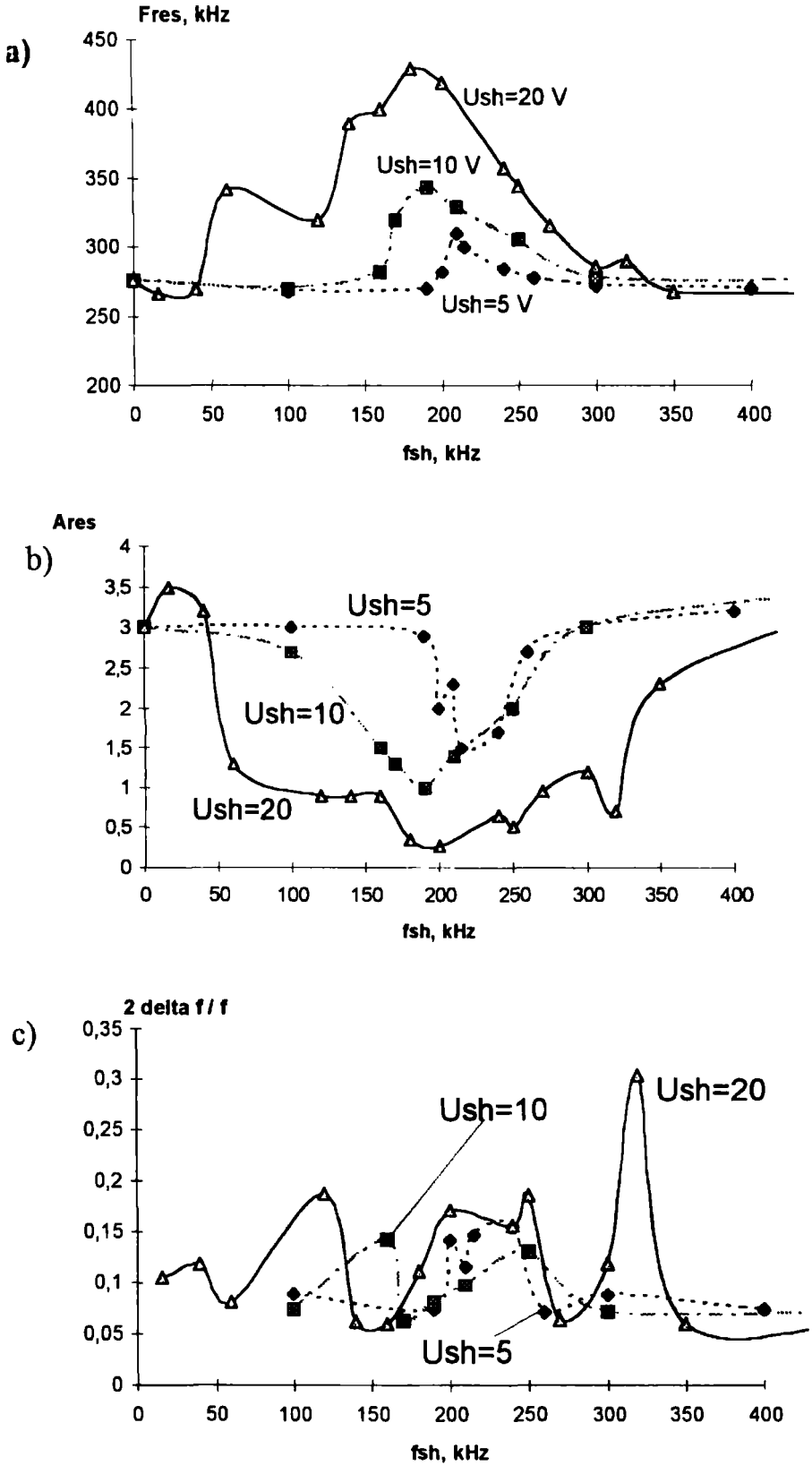

Fig. 6.10. Characteristics of the ion oscillations as a function of the shaker frequency at the Test Bench:

a) the frequency of the maximum response;

b) the value of the maximum;

c)the spectral width

$U_0 = 2.5$ kV, $I_e = 310$ mA

The beam is stable until the shaker frequency reaches that of the ion incoherent oscillations ($f_i \approx 300$ mA in this regime). Then the efficient heating leads to further ionisation (the growth of the oscillation frequency indicates this fact). At $f_{sh} \sim 400$ kHz the shaker influence vanishes and the NEB becomes unstable.

6.3.4. Heating of ions in the longitudinal direction

The same stabilisation effect as with the shaker was observed in the Test Bench experiment when the modulation of the steering electrode potential was performed [14,17]. An RF signal of 16-25 kHz frequency and 20-40 V amplitude was applied to the steering electrode. This leads to beam stabilisation (Fig. 6.11). The required modulation amplitude increases with the beam current. The beam current is of 450 mA, the stabilising amplitude is equal to 40 V. The neutralization factor obtained with longitudinal modulation is higher than with the shaker (transverse modulation), it is equal to 0.5-0.7.

The longitudinal modulation frequency is related to an excitation of longitudinal waves in the neutralised beam. When the ions interact with longitudinal waves, the longitudinal energy of the ions increases and is defined by ion motion in the wave. The reflection of an ion from a trap leads to thermalization of its energy. As a result, longitudinal energy taken by the ion in interaction with the wave transforms to transverse energy. The increase of the ion transverse energy leads to stabilisation of the beam and allows an increase of the threshold current. The resonant frequency of the modulator generator is determined by the period of ion longitudinal oscillations:

$$f_{res} = \tau_{\|}^{-1} = \frac{v_i}{L} \quad . \tag{6.11}$$

Here v_i is the ion velocity, L the distance between traps. The ion velocity is equal to the velocity of the longitudinal wave [5]:

$$v_i = v_{ph} = \frac{\omega_{pi}\eta^{1/2}a_e}{2}\left(1 + 2\ln\frac{b}{a_e}\right)^{1/2} . \tag{6.12}$$

Here ω_{pi} is the ion plasma frequency. As a result one has

$$f_{res} = \frac{\omega_{pi}}{2}\frac{a_e}{L}\eta^{1/2}\left(1 + 2\ln\frac{b}{a_e}\right)^{1/2} , \tag{6.13}$$

where $a_e = 1.5$ cm is the beam radius, $b_e = 15$ cm the radius of vacuum chamber, and $L = 1.73$ m the distance between traps.

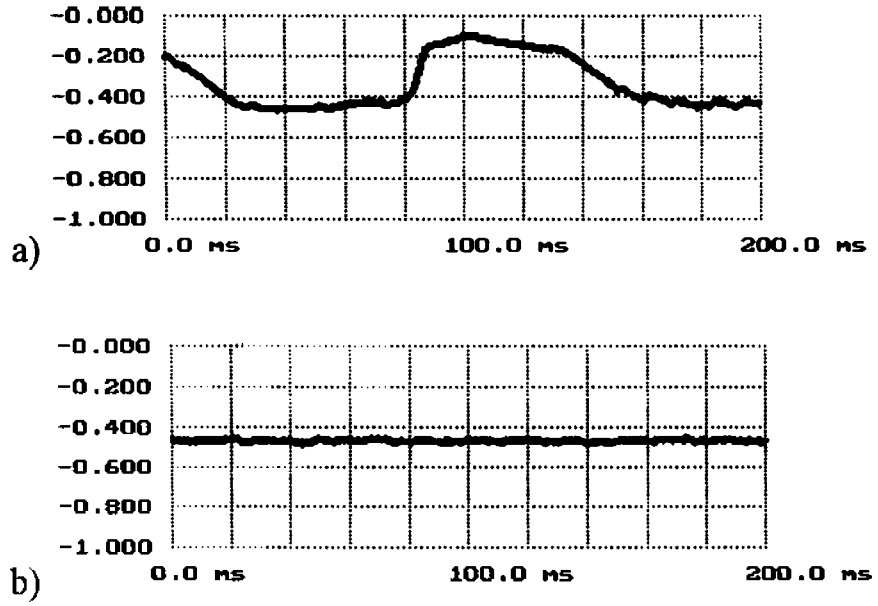

Fig. 6.11. The NEB behaviour when the steering electrode potential is modulated

$\mathcal{E}_0$ = 2.5 kV, I_e = 305 mA, P = 2-3 nTorr.

a) modulation is "OFF", b) modulation is "ON": f = 23 kHz, U = 20 V.

The results of these calculations and experimental data are compared in Fig .6.12. The agreement occurs when A/Z_i = 14.

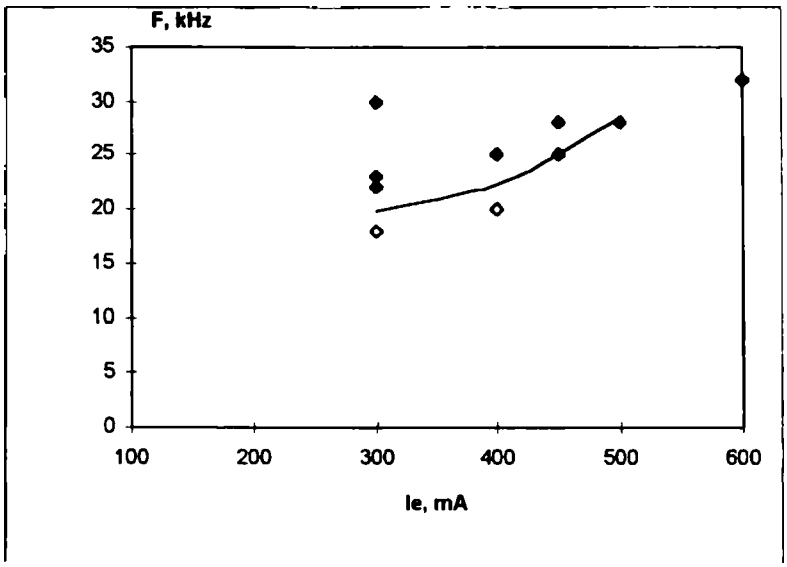

Fig. 6.12. The dependence of longitudinal modulation frequency on beam current, P = 2-5 nTorr, $U_{el1} = U_{el3}$ = 4 kV, $U_{el2} = U_{el4}$ = 0, U_{cl} = 0.
◆ - modulation on the steering electrode,
◇ - modulation on the collector trap.
Curve -calculations [Formula (6.13)], A/Z_i = 14.

In the second series of experiments the longitudinal modulation with the harmonic signal of low frequency (f = 20 kHz) was applied to one of the collector trap electrodes. The second electrode was grounded inside a vacuum chamber. At these excitation conditions both longitudinal and transverse waves occur. At a modulation frequency of about 20 kHz and an amplitude of 25÷40 V a beam current of 500 mA was stabilised. The neutralisation factor was about 0.5-0.7 at a pressure of 2÷4 nTorr. If longitudinal modulation is absent, the beam is stable only up to a current of about 130 mA.

Experiments carried out with transverse (shaker) and longitudinal modulation demonstrate the possibility of a significant increase of the stable beam current. In these modes, no "jumps" of the PB signal were observed, but the same instability bursts of the coherent oscillations were observed on the pick-up electrodes (Fig. 5.10a). The repetition frequency of the bursts is of the order of 10-100 Hz.

In a third series of experiments the influence of longitudinal modulation with frequency of 10-50 kHz applied to the collector and the repeller was studied. These experiments demonstrate that such a modulation leads to a decrease of stable beam current and to an easier development of an instability, especially with the repeller modulation.

CONCLUSION

Summarizing the results presented in the report, one can conclude the following.

1. A neutralised electron beam has been generated in a certain range of parameters *by use of the neutralisation electrodes.*

In ECOOL at a pressure P = 10 pTorr and a magnetic field of 600 G the stable neutralised electron beams have been obtained in an energy range 2.5-27 keV with the beam perveance 0.35-0.4 $\mu A / V^{3/2}$ (that gives I_e=0.13 A at ε_e =2.5 keV and a **neutralisation factor η = 0.75-0.9**.

In the Test Bench the achieved parameters were the following: ε_e =2-10 keV, perveance 1.5μA/V$^{3/2}$, P = 3 nTorr, **η = 0.6 - 0.75.**

2. The NEB current is limited by the development of the *beam-drift instability*, associated with the coherent dipole electron-ion oscillations. The threshold current density of the instability in the experiments can be described by the formula

$$J_{threshold} = \hat{k} J_0 ,$$

where

$$J_0 = \frac{\pi}{2} \cdot \varepsilon_0 \cdot \frac{v^2 B}{L}$$

is the threshold, obtained in [20]. The parameter $\hat{k}$, presented in the Table 7.1, characterizes the level achieved in different experiments ("passive regime" means no use of any of the tools, described in Section. 6, " active regime" means suppose use of the shaker, clearing electrode or similar devices).

Table 7.1. The parameter $\hat{k}$, received in different experiments

Authors	Experimental set-up	$\hat{k} = j_{threshold} / J_0$
M. Nezlin et al [20]	Lab.test bench	1.0
V. Parkhomchuk et al [4]	NAP-M cooling device	4.0
V. Parkhomchuk et al [5]	MOSOL	2.1
Present research		
Passive regime	ECOOL	0.2-0.3
Active regime	ECOOL	1.0
Passive regime	Test Bench	0.7-1.6
Active regime	Test Bench	3.0

3. The suppression of the instability on the Test Bench was performed with a few different methods (the "active regime") and brought important results: the use of the shaker, the clearing electrodes and the modulation of the steering electrode potential allow an increase in the level of the current for the stable NEB by a significant factor (see Table 7.1). The suppression of the instability on ECOOL was obtained with the shaker. The clearing electrodes on ECOOL do not

help to increase the threshold beam current. The η-factor in the situation where the instability was avoided by the shaker or the other methods had values lower 1:

$\eta = 0.4$ in ECOOL and 0.65 in Test Bench.

The mechanism of the cures was explained by the heating of stored ions (this increases the Landau damping) and the clearing of secondary electrons (reduction of the feedback introduced with them).

The use of a "conventional" feedback system did not bring any essential profit.

4. The diagnostics developed during the research allow a precise and convenient measurement of the integral (the time-of-flight and Pencil Beam methods) and local (the method of cooled particle beam) η factor value.

5. The obtainable η-factor and threshold beam current depend on the residual gas pressure: They increases for higher pressure. For instance, $j_{threshold}$ in LEAR at $P = 10$ pTorr is 3 times less, than in the Test Bench at $P = 2$ nTorr. One should point out also, that a stable beam can be obtained with $\eta \cong 1.0$ at $P = 1$ μTorr - 100 nTorr, but $\eta \cong 0.6$ at 10 nTorr. This behaviour is also dependent the beam current.

6. A reduction of the cathode heating leads to an increase of the NEB stable current. It can be related to reduction of the inhomogenity in the current density distribution across the beam. When the heating current is reduced from 10 to 6 A, the stable NEB current in the Test Bench can be increased 2-3 times. This fact needs further investigation.

7. The theoretical model, described here does clarify our understanding of the interaction of an electron beam with stored ions, and underlines the influence of secondary electrons, the mechanism of the clearing electrodes and the shaker action. However, the theory developed does not fully explain the dependence of the threshold current and the neutralization factor on the residual gas pressure.

8. The experiments on electron cooling of protons were performed with the electron energies in the rage of 2-30 keV. They established the possibility, to vary the electron current without loosing stability as long as the perveance of the NEB was in the range of $0.1\,\mu A/V^{3/2}$ to $0.6\ \mu A/V^{3/2}$

9. When it became possible to produce stable neutralization the influence of the electron beam neutralization on the cooling process could be investigated, and measurements were made on the cooling time for Pb ions as well as for protons in LEAR.

Cooling time measurements were performed varying the degree of neutralization and electron beam intensity. Up to 80% stable neutralization could be obtained for electron currents up to 150 mA at the electron energy of 2.5 keV. This was made possible due to modification of the electron cooler vacuum chamber to avoid "natural neutralization" and the introduction of the shaker electrodes.

The results of these measurements showed no appreciable gain with neutralization. In fact in many situation neutralization was detirmental to the cooling of protons and Pb ions. A marked reduction in the lifetime of Pb ions was

also observed and could be explained by charge exchange between the circulating beam and the neutralizing ions. In fact at I_e =200 mA and η=1 the density of the neutralizing ions is equivalent to a residual gas pressure P_{eq} all around the ring of 10^{-11} Torr, almost one order of magnitude higher than a "good" LEAR vacuum pressure under static condition. This explains the rapid beam decay especially since it was found that the neutralizing ions have a relatively high mass. For these reasons neutralization was not used in the subsequent lead stacking experiments.

10. The studies reported above proved to be important because even small jumps in η can lead to strong losses of the circulating beam during stacking. Therefore it is very important to control the neutralization at a constant level ($\eta \approx 0$ in the case of the lead ion experiments in LEAR). Therefore the tools described in this report are indispensable, to avoid uncontrolled (natural) neutralization leading to energy "jumps" and losses.

APPENDIX 1

A1.1. Ion motion inside the partially neutralized electron beam

We consider the ion motion between electrostatic traps inside the drift space in the field of a neutralized electron beam with radial potential distribution

$$U = \frac{I_e(1-\eta)}{4\pi\varepsilon_0 v}\begin{cases} \dfrac{r^2}{a^2}, & 0 \le r \le a \\ 1 + 2\ln\dfrac{r}{a}, & a \le r \le b, \end{cases} \qquad \text{(A1.1)}$$

Here b, and a are radius of the chamber and the beam, $\eta = Z_i n_i / n_e$ the neutralization factor, n_i, n_e the ion and electron density, I_e the beam current, v the electron velocity. This radial potential distribution is different from (1.1) by a constant value, which is equal to the potential difference between the beam centre and vacuum chamber. Assume, that the radial ion density distribution is characterized by:

$$n_i = \begin{cases} Z_i \eta n_e, & 0 \le r \le a, \\ 0, & a \le r \le b \end{cases} \qquad \text{(A1.2)}$$

The ion motion inside of a neutralized beam can be decribed by the following equations:

$$\frac{d^2 y}{dt^2} = \omega_B \frac{dx}{dt} - \omega_i^2 y, \qquad \text{(A1.3)}$$

$$\frac{d^2 x}{dt^2} = -\omega_B \frac{dy}{dt} - \omega_i^2 x,$$

where $\omega_i^2 = Ze^2 n_e(1-\eta)/2\varepsilon_0 M$ is the ion plasma frequency, $\omega_B = ZeB/M$ the cyclotron ion frequency in the longitudinal magnetic field B of the cooler, Z_i, M - the ion charge and mass. The dependence of transverse coordinates x and y on time for an ion, which is produced with initial coordinates x_0, y_0 and initial velocities v_{x0}, v_{y0} is represented by the equations

$$\begin{aligned} x = {} & \cos(\omega_{Bb} t/2)\left[x_0 \cos(\Omega t) + \left(v_{x0}/\Omega + \omega_B y_0/2\Omega\right)\sin(\Omega t)\right] - \\ & - \sin(\omega_B t/2)\left[y_0 \cos(\Omega t) + \left(v_{y0}/\Omega - \omega_B x_0/2\Omega\right)\sin(\Omega t)\right], \qquad \text{(A1.4)} \\ y = {} & \cos(\omega_B t/2)\left[y_0 \cos(\Omega t) + \left(v_{y0}/\Omega - \omega_B x_0/2\Omega\right)\sin(\Omega t)\right] + \\ & + \sin(\omega_B t/2)\left[x_0 \cos(\Omega t) + \left(v_{x0}/\Omega + \omega_B y_0/2\Omega\right)\sin(\Omega t)\right] \end{aligned}$$

where $\Omega^2 = \omega_i^2 + \omega_B^2/4$ The ion trajectory shown in Fig. A1.1.

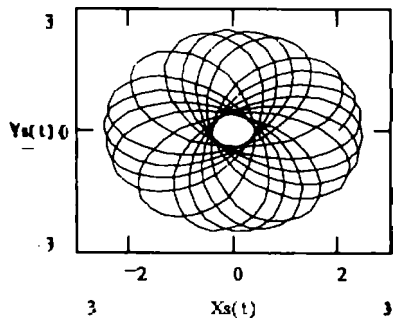

Fig. A1.1 Ion trajectory in transverse plane.

A1.2. Ion reflection from the traps

We consider the case when ion is reflected elastically from the trap. This occurs when the ion Debye radius is less than the Larmor radius

$$r_D << \rho \tag{A1.5}$$

The electrical field is normal to end face of the neutralized beam (see Fig. A1.2)

$$\vec{E} = \vec{n}E, \tag{A1.6}$$

where $\vec{n}$ is the normal vector to the trap boundary (see Fig. A1.2).

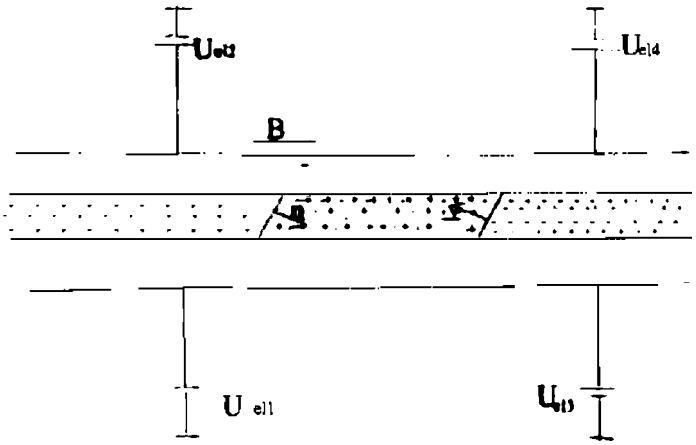

Fig. A1.2 Layout of the experiment.

The ion velocity after reflection from the trap is equal to

$$\begin{aligned} \vec{v}_1 &= \vec{v} - 2\vec{n}(\vec{v}\vec{n}), \\ |v_1| &= |v|, \end{aligned} \tag{A1.7}$$

where $\vec{v}$ is the ion velocity before collision with the trap.

The change of the ion transverse energy ε_t and the angular momentum M_φ with time is determined by the equations:

$$\begin{aligned} \frac{d\,\varepsilon_t}{dt} &= \frac{\langle \varepsilon_{t1} - \varepsilon_t \rangle}{\langle \tau_{ii} \rangle} \\ \frac{d\,M_\varphi}{dt} &= \frac{\langle M_{1\varphi} - M_\varphi \rangle}{\langle \tau_{ii} \rangle}. \end{aligned} \tag{A1.8}$$

$$M_\varphi = Mv_\varphi r + M\omega_B r^2/2,$$

where $\langle \tau_{ii} \rangle$ is average time between ion reflections from the traps. The change of the ion angular momentum and transverse energy after reflection from the trap, averaged over to the cyclotron and azimuthal motion, are given by following formula

$$\begin{aligned} \langle M_{i\varphi} - M_\varphi \rangle_{\varphi,\omega_B} &= -\langle Mv_\varphi r \rangle_{i\varphi,\omega_B} (1-(\vec{n}\vec{h})^2) \\ (\varepsilon_{it} - \varepsilon_t)_{\varphi\omega_B} &= 2M(\langle v_i^2 \rangle_{\varphi\omega_B} - \langle v_t^2 \rangle_{\varphi\omega_B}/2)(\vec{n}\vec{h})^2(1-(\vec{n}\vec{h})^2), \end{aligned} \tag{A1.9}$$

where v_l, v_t are the longitudinal and transverse components of the ion velocity, averaged over the cyclotron and azimuth circulation, $\vec{h} = \vec{B}/|B|$ is unit vector directed along the longitudinal magnetic field. The ion energy is thermalized due to collision with traps in the time

$$\tau_{ter} \approx \langle \tau_{II} \rangle / ((1-(\vec{n}\vec{h})^2)(\vec{n}\vec{h})^2). \tag{A1.10}$$

For stationary conditions after thermalization one obtains the following ion parameters

$$\begin{aligned} \langle M_* \rangle &= \langle \varepsilon_t \rangle / 2\omega_* = \frac{2\varepsilon}{5\omega_*} \\ \langle \varepsilon_t \rangle &= \left\langle \frac{M v_t^2}{2} \right\rangle = \langle \varepsilon_l \rangle / 2 = \frac{\varepsilon}{5} \\ \langle \varepsilon_l \rangle &= \left\langle \frac{M v_l^2}{2} \right\rangle + \frac{eI(1-\eta)\langle r^2 \rangle}{4\pi \varepsilon_0 v a^2} = \frac{4\varepsilon}{5}, \end{aligned} \tag{A1.11}$$

where $\langle \varepsilon_t \rangle$ and $\langle \varepsilon_l \rangle$ are the average ion transverse and longitudinal energy, $\omega_* = \omega_p^2/\omega_B$ the drift frequency, ε the initial ion energy

$$\varepsilon = \frac{M v_{lo}^2}{2} + \frac{M v_{\varphi 0}^2}{2} + \frac{M v_{r0}^2}{2} + \frac{eI(1-\eta) r_0^2}{4\pi \varepsilon_0 v a^2}, \tag{A1.12}$$

and v_{lo}, $v_{\varphi 0}$, v_{r0} are the longitudinal, azimuth and radial components of the initial ion velocity, r_0 the radius, at which the ion is produced. The maximal and minimal radii of the ion trajectory after thermalization are

$$r_{M,m}^2 = \frac{\langle \varepsilon_t \rangle}{M\omega_i^2}(1 \pm \frac{\omega_i}{\Omega}) \tag{A1.13}$$

The trajectories of ions, produced with small initial velocity, before and after thermalization are presented in the Fig. A1.3 The ion parameters before thermalization are:

$$\begin{aligned} \varepsilon &= \frac{eI_*(1-\eta) r_0^2}{4\pi \varepsilon_0 v a^2} \\ \varepsilon_t &= \varepsilon, \quad \varepsilon_l = T_{i0}, \\ r_M &= r_0, \quad r_m = \frac{\omega_B r_0}{2\Omega}, \end{aligned} \tag{A1.14}$$

where T_{i0} is the initial ion temperature. The ion parameters after thermalization due to collision with traps are

$$\varepsilon_t = \frac{4}{5}\varepsilon,\ \varepsilon_l = \frac{1}{5}\varepsilon,\ v_x = v_y = \sqrt{\varepsilon_t / 2M}$$
$$M_\varphi = \frac{2}{5}\frac{\varepsilon}{\omega_d},\quad r^2_{M,m} = \frac{2}{5} r_0^2 (1 \pm \frac{\omega_i}{\Omega}) \ . \qquad \text{(A1.15)}$$

The ions move inside the beam during the thermalization (see Fig. A1.3)

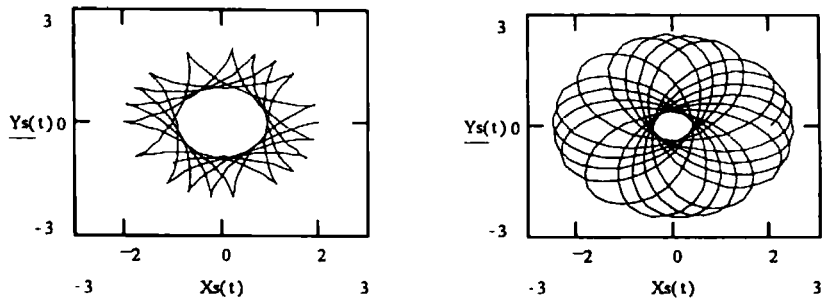

a) b)

Fig. A1.3 Ion trajectory before a) and after b) thermalization.

The ion energy increases with time owing to heating in the interaction with the electron beam. Here we examine the case, when the time of heating is larger than the time of thermalization. The ion changes its orbit, and starts to move outside of the electron beam axis. The maximal and minimal radii of the ion are determined by the relation (A1.13) with average transverse energy

$$\langle \varepsilon_{lt} \rangle = \frac{4}{5}(\varepsilon + \Delta\varepsilon) \ , \qquad \text{(A1.16)}$$

where $\Delta\varepsilon$ is the energy acquired by the ion during the heating. When the maximum ion trajectory radius is equal to the electron beam radius, the ion transverse and longitudinal energy can be represented by the following formula:

$$\varepsilon_{t*} = \frac{eI_e(1-\eta)}{2\pi\varepsilon_0 v}\frac{1}{1+\omega_i/\Omega},$$
$$\varepsilon_l = \varepsilon_{t*}/4. \qquad \text{(A1.17)}$$

A part of the ion trajectory is outside of the electron beam, when the transverse ion energy is larger than ε_{t*}.

The results, presented above, allow one to determine the ion average transverse and longitudinal energy as a function of trajectory radius for an ion which collides elastically with the traps. The ions thermalized during these collisions move on a quasistationary orbit. They escape the beam, if they obtain additional energy. One can also treat the case when the ion heating time is long compared to the thermalization time.

APPENDIX 2

A2.1. Calculations of electron trajectories inside the clearing electrodes

The potential distribution φ, radial electric field E_r and azimuthal electric field E_φ inside the clearing electrodes are given by Eq. (1.12), (1.13). The results of calculations of the potential distribution and the electric field lines are ploted in Fig. A2.1. for U_{cl1}=4 kV, U_{cl2}= -4 kV, U_0=3 kV, I_e=1 A.

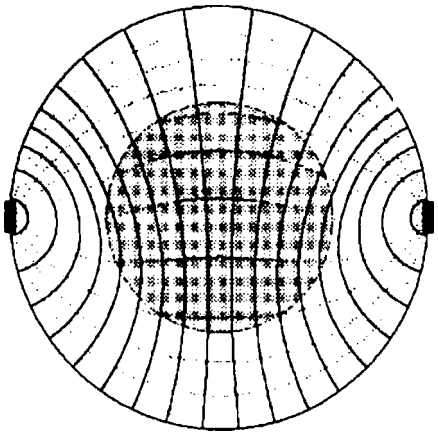

Fig.A2.1. Potential distribution and lines of electric field.

The electron movement inside the cleaning electrodes is magnetised for the magnetic field B = 600 G. The transverse velocity of the electrons is determined by the electric drift in the transverse electric field and the longitudinal magnetic field and the projection of the longitudinal velocity v on the axis e_r and e_ψ due to transverse magnetic field $B_\perp$

$$v_r = \frac{E_\psi}{B} \pm v\frac{B_\perp}{B}\sin\psi$$
$$v_\psi = \frac{E_r}{B} \pm v\frac{B_\perp}{B}\cos\psi \qquad \text{(A2.1)}$$

Here, the sign (+) is for secondary electrons and (-) for primary ones.
The electron trajectory in the (r,ψ) plane obtained from equation (A2.1) is :

$$\frac{dr}{rd\psi} = \frac{v_r}{v_\psi} = \frac{E_\psi \pm vB_\perp \sin\psi}{E_r \pm vB_\perp \cos\psi}. \qquad \text{(A2.2)}$$

The electron trajectory in the (r,z) plane is obtained from equation (A2.1.):

$$\frac{dr}{dz} = \frac{E_\psi + vB_\perp \sin\psi}{vB} \qquad \text{(A2.3)}$$

For computer calculation we used the following formula:

$$r_{n+1} = r_n + v_r \frac{dz}{v}$$
$$\psi_{n+1} = \psi_n + v_\psi \frac{dz}{v} \qquad \text{(A2.4)}$$

The results of the calculation are presented in Fig. A2.2, where U_{d1}=4 kV, U_{d2}= -4 kV, U_0=3 kV, I_e=1 A., B=500 G, $B_\perp$ =30 G is assumed. Fig 2.2 shows a primary electron motion from the gun to the collector and Fig2.2 b shows trajectories in the direction from the collector to the gun.

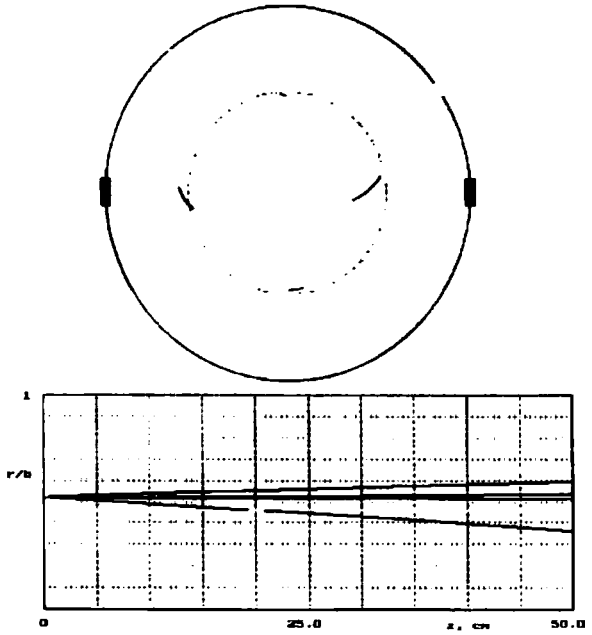

Fig. A2.2a. Primary electron trajectories.

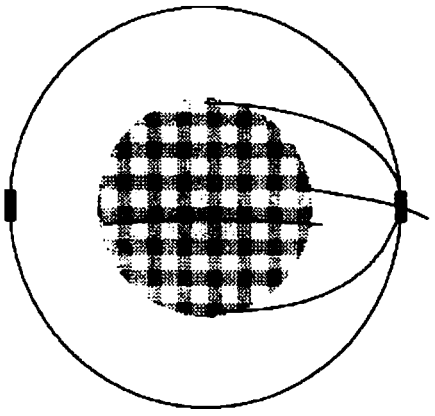

Fig. A2.2b. Secondary electron trajectories.

APPENDIX 3

A.3. Ion motion inside the shaker

In order to damp the neutralization instabilities, a shaker has been used [19]. The ion motion equation inside the shaker is represented by following formula

$$\frac{d^2y}{d^2t} = \omega_s \frac{dx}{dt} - \omega_p^2 y + \frac{Z_i e E_s \cos(\omega_s t)}{M}, \qquad \frac{d^2x}{d^2t} = -\omega_s \frac{dy}{dt} - \omega_p^2 x \tag{A.3.1}$$

where E_s is the electric field of the shaker, ω_s the shaker frequency, $\omega_p = \omega_i\sqrt{1-\eta}$ the plasma frequency and ω_i (see Eq.1.24) the plasma frequency for η=0. The dependence of the transverse coordinates x and y on time is given by equations

$$\begin{aligned} y &= \tilde{y}_0 + \frac{Z_i e E_s k_1}{2M(\omega_s+\omega_2)}\left(\sin\frac{(\omega_s+\omega_1)t}{2}\frac{\sin(t(\omega_s-\omega_1)/2)}{(\omega_s-\omega_1)/2} - \frac{\sin(\Omega t)}{\Omega}\sin\frac{\omega_B t}{2}\right) \\ &+ \frac{Z_i e E_s k_2}{2M(\omega_s+\omega_1)}\left(\sin\frac{(\omega_s+\omega_2)t}{2}\frac{\sin(t(\omega_s-\omega_2)/2)}{(\omega_s-\omega_2)/2} - \frac{\sin(\Omega t)}{\Omega}\sin\frac{\omega_B t}{2}\right) \\ x &= \tilde{x}_0 - \frac{Z_i e E_s k_1}{2M(\omega_s+\omega_2)}\left(\cos\frac{(\omega_s+\omega_1)t}{2}\frac{\sin(t(\omega_s-\omega_1)/2)}{(\omega_s-\omega_1)/2} - \frac{\sin(\Omega t)}{\Omega}\cos\frac{\omega_B t}{2}\right) \\ &- \frac{Z_i e E_s k_2}{2M(\omega_s+\omega_1)}\left(\cos\frac{(\omega_s+\omega_2)t}{2}\frac{\sin(t(\omega_s-\omega_2)/2)}{(\omega_s-\omega_2)/2} - \frac{\sin(\Omega t)}{\Omega}\cos\frac{\omega_B t}{2}\right) \end{aligned} \tag{A3.2}$$

where x_0, y_0 are the ion coordinates without the shaker (see A1.4)), k_1=k_2=1 and ω_1, ω_2 are the incoherent ion frequencises [see Eq.(1.43)]

$$\omega_{1,2} = \Omega \pm \frac{\omega_B}{2}$$

The ion motion inside the shaker with a circular polarized electrical field (see Fig. A3.1) is given by the following formula

$$\frac{d^2y}{d^2t} = \omega_s \frac{dx}{dt} - \omega_p^2 y + \frac{ZeE_s \cos(\omega_s t)}{M}, \qquad \frac{d^2x}{d^2t} = -\omega_s \frac{dy}{dt} - \omega_p^2 x \pm \frac{ZeE_s \sin(\omega_s t)}{M} \tag{A3.3}$$

The solution of equations (A.4.3) can be represented by equations (A.3.2) with numerical coefficients k_1=2, k_2=0 for the sign ''-'' in equation (A.3.3), and k_1=0, k_2=2 for the sign ''+''. The ion behaviour inside the shaker depends on the shaker frequency. When the shaker frequency is equal to the incoherent ion frequency, the ions escape from the beam in 20 - 30 micro seconds(see Fig. A. 3.2). This time corresponds to the time that ions with low energy $\varepsilon_i \approx 0.1$-$0.3$ eV take to pass through shaker. When the shaker is used on the resonance frequency of the ions it can shake out the ion during one pass through it.

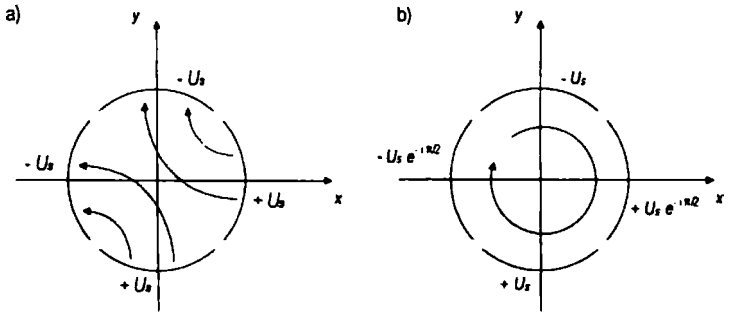

Fig. A. 3.1 a) Shaker electrodes with transverse electric field.
b) Dipole shaker electrodes with circular polarized electric field

The dependence of the ion coordinates on time at the resonance frequency $\omega_s=\omega_2$ for the shaker with circular polarized electric field is given by the following formula

$$y = \tilde{y}_0 + \frac{Ze\,E_s}{2M\Omega}\left(\sin(\omega_2 t)t - \sin\left(\frac{\omega_s t}{2}\right)\frac{\sin(\Omega t)}{\Omega}\right)$$
$$x = \tilde{x}_0 + \frac{Ze\,E_s}{2M\Omega}\left(\cos(\omega_2 t)t - \cos\left(\frac{\omega_s t}{2}\right)\frac{\sin(\Omega t)}{\Omega}\right) \qquad \text{(A.3.4)}$$

The amplitude of ion displacements due to the shaker is less than the beam size, when the shaker frequency does not coincide with resonance frequency (shaker electric field E_s= 200 V/m the ion trajectory inside the dipole shaker with circular polarized electrical field is shown in Fig A. 3.2). In this case ions are shaken out from the beam during many passes through the shaker. This is due to the random phase of the ions at the entrance of the shaker after reflection from the trap boundary or potential barrier.

The "diffusion" of the ions during many passes in the shaker with circular polarized transverse electric field is given by the following formula

$$r^2 = \tilde{r}_0^2 + \frac{1}{2}\left(\frac{Z_i e\,E_s}{M\,\Omega\,(\omega_1+\omega_2)}\right)^2\left(\left(\frac{2\Omega}{\omega_s-\omega_2}\right)^2+1\right)\frac{t}{\tau_{//}}, \qquad \text{(A.3.5)}$$

where $\tau_{//}$ is the ion period of oscillations, $\tau_{//}=L/v_l$, $v_l=\sqrt{2\varepsilon/5M}$. Here L = 3.2 m is the distance between two traps, v_l the longitudinal ion velocity after thermalization due to reflections from the traps [see (A1.14], $\tilde{r}_0$ is the average ion radial coordinate without shaker. The ion time of escape is equal to

$$\tau_{es} \approx \tau_{//}\left(\frac{M\Omega(\omega_1+\omega_2)a}{Z_i e\,E_s}\right)^2 \frac{1}{1+\left(2\Omega/(\omega_s-\omega_2)\right)^2}. \qquad \text{(A3.6)}$$

For typical LEAR parameters a) U_0 = 2.7 kV, I = 0.3 A, or b) Uo = 27 kV, I_e = 1 A, Es = 200 V/m, $M = M_p$ (proton mass) the time of ion escape from the beam is estimated as a) τ_{es} = 0.02 s, or b) τ_{es} = 0.027 s. The density of stored ions in the system with shaker is estimated as

$$n_i = n_b\frac{\tau_{es}}{\tau_{ion}} \approx 10^{-2}\,n_b \qquad \text{(A3.7)}$$

where n_b is the beam density, τ_{ion} = 3 s the time of ionization. It is the typical regime of the LEAR experiments, when the shaker is used for fast ion expulsion

escape. When the electrical field of the shaker is reduced to 20-40 V/m the ion density may be essentially increased .

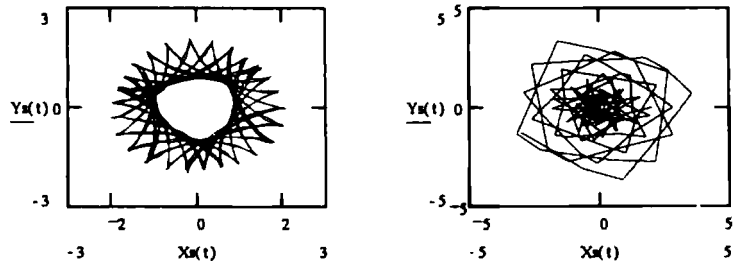

a) b)

Fig. A. 3.2 Ion trajectory inside the dipole shaker electrodes with circular polarization.

I_e = 1 A, Uo = 27 kV, B = 600 Gs, η= 0, Es = 200 V/m, t = 30 μsec, x_0 = 2sm, y_0 = 0, a) f_s = 160 kHz b) $f_s = f_2$ = 532 kHz

REFERENCES

1. J.Bosser, D. Möhl, G. Tranquille,I. Meshkov, E. Syresin and V. Parkhomchuk, Neutralization of the LEAR-ECOOL Electron Beam Space Charge, CERN/PS 93-08 (AR).

2. A. Lavrentjev, I. Meshkov The Computation of Electron Cooling Process in a Storage Ring, JINR Preprint E9 - 95-317, Dubna, 1995.

3. I. Meshkov "Electron Cooling", Proc. Workshop on "Crystal Beams", Erice, Italy, 1995, World Scientific Publish., A.G. Ruggiero (edd), p.129

4. V. Kudelainen, V. Parkhomchuk and D. Pestrikov, The Experimental Study of Compensated Electron Beam Stability Sov. ZhETF, v. 53, No.5, 870, 1983.

5. A. Burov, V. Kudelainen, V. Lebedev, V. Parkhomchuk, A. Sery and V. Shiltsev, Experimental Investigation of an Electron Beam in Compensated State, Preprint INP 89-116, Novosibirsk Engl. Transl. CERN/PS 93-03 (AR).

6. J. Bosser, S. Maury, I. Meshkov, D. Möhl, E. Mustafin, E. Syresin, F. Varenne and P. Zenkevich, Stability Conditions for a Neutralized Electron Beam, Proceeding of the 1995 Particle Accelerator Conference (PAC), Dallas, USA, (1995), p. 2940

7. E. Mustafin and P. Zenkevich, Dipole Oscillations of the Beam in a Neutralized Electron Cooling System, CERN/PS/AR/Note 95-19.

8. E. Syresin, The Secondary Electron in the Electron Cooling System, CERN/PS/AR Note 95-14.

9. E. Syresin, The Parameters of the Secondary Electrons in the Electron Cooling System, Nucl. Instrum. and Methods, A391(1), (1997), 114.

10. I. Meshkov, E. Mustafin, E. Syresin and P. Zenkevich, Stationary Parameters of Neutralized Electron Cooling System. Nucl. Instrum. and Methods, A391(1), (1997), 107.

11. F. Varenne, Neutralization of the Electron Beam Space Charge in the Electron Cooling System of LEAR, Doctoral Thesis University of Clermont – Ferrand (1995), preprint CERN-PS/AR Note 96-02.

12. R. Lapik, I. Meshkov, V. Polyakov, A. Smirnov,I. Selesnev, E. Syresin, M. Zavrazhnov, J. Bosser, R. Ley and G. Tranquille, The Variable Current Gun: the Parameter Test and Results of the First Electron Cooling Experiment at LEAR, Nucl. Instrum. and Methods, A355, (1995), 208.

13. F. Caspers, Y. Korotaev, I. Meshkov, A. Petrov, Y. Rao, A. Smirnov, E. Syresin, V. Varenne, X. Yang Diagnostic of a Neutralized electron beam on the JINR Test Bench Nucl. Instrum. and Methods, A391(1), (1997), 128.

14. J. Bosser, Y. Korotaev, R. Ley, R. Maccaferri, I. Meshkov, D. Möhl, G. Molinary, A. Smirnov, E. Syresin, G. Tranquille and F. Varenne, The Active Methods of Instability Suppression in a Neutralised Electron Beam, Nucl. Instrum. and Methods, A391(1), (1997), 110.

15. J. Bosser, R. Ley, G. Tranquille, V. Bikovsky,V. Funtikov, I. Meshkov, V. Polyakov, A. Rogosin, V. Sinitsky, I. Selesnev, A. Smirnov and E. Syresin,

The New Collector for the Electron Cooling at LEAR, Nucl. Instrum. and Methods, A311, (1992), 465.

16. J. Bosser, Y. Korotaev, R. Ley, R. Maccaferri, I. Meshkov, G. Molinary, A. Smirnov, E. Syresin, G. Tranquille and F. Varrene The Experimental Study of the Electron Beam Neutralization, Nucl. Instrum. and Methods, A391(1), (1997), 103,.

17. J. Bosser, Y. Korotaev, R. Ley, R. Maccaferri, I. Meshkov, G. Molinary, A. Smirnov, E. Syresin, G. Tranquille and F. Varrene The Experimental Study of the Neutralized Electron Beam for Electron Cooling, 5th EPAC, Barcelona, Spain, (1996), p. 1193.

18. J. Bosser, R. Ley, G. Molinary, G. Tranquille, F. Varrene, I. Meshkov, V. Polyakov, A. Smirnov and E. Syresin, Electron Cooling with Neutralized Electron Beams, Fourth European Particle Accelerator Conference (EPAC), London, England, (1994), p.1211.

19. J. Bosser, F. Caspers, M. Chanel, R. Ley, R. Maccaferi, S. Maury, I. Meshkov, G. Molinary, V. Polyakov, A. Smirnov, O. Stepashkin, E. Syresin, G. Tranquille and F. Varenne, Neutralization of the LEAR Electron Cooling Beam: Experimental Results, Proceedings of the 1995 Particle Accelerator Conference (PAC), Dallas, USA, (1995) p. 2943

20. M. V. Neslin, A. M. Solntsev, Limiting Threshold Currents and Electron Beam Oscillation, Sov. ZhETF, v.53, (1967), 437.